SKB

TECHNICAL REPORT 88-13

Validation of the rock mechanics HNFEMP code against Colorado school of mines block test data

Ove Stephansson, Tomas Savilahti
University of Luleå, Luleå

May 1988

SVENSK KÄRNBRÄNSLEHANTERING AB
SWEDISH NUCLEAR FUEL AND WASTE MANAGEMENT CO

BOX 5864 S-102 48 STOCKHOLM
TEL 08-665 28 00 TELEX 13108-SKB

VALIDATION OF THE ROCK MECHANICS HNFEMP CODE AGAINST COLORADO SCHOOL OF MINES BLOCK TEST DATA

Ove Stephansson, Tomas Savilahti

University of Luleå, Luleå

May 1988

Information on KBS technical reports from 1977-1978 (TR 121), 1979 (TR 79-28), 1980 (TR 80-26), 1981 (TR 81-17), 1982 (TR 82-28), 1983 (TR 83-77), 1984 (TR 85-01), 1985 (TR 85-20), 1986 (TR 86-31) and 1987 (TR87-33) is available through SKB.

VALIDATION OF THE ROCK MECHANICS HNFEMP CODE AGAINST COLORADO SCHOOL OF MINES BLOCK TEST DATA

Ove Stephansson
Tomas Savilahti

1988-05-01

TABLE OF CONTENTS

ABSTRACT

In the determination of crustal response and farfield stability of a vault for radioactive waste, the rock mass may be modelled either as a discontinuous or as a continuous medium. In this report, we emphazise the "continuum" approach, where discontinuities like joints and faults are smeared out in the rock mass.

The purpose of this report is to validate the non-linear finite element code HNFEMP against the Colorado School of Mines (CSM) block test data at Edgar Mine, Idaho Springs, Colorado. Results from mapping field tests and successive analyseis were used to define three different material models with different normal and shear stiffnesses. Altogether, 18 models of a block consisting of three sets of joints under uni-axial and bi-axial loading conditions were considered. The results from the numerical modelling were subsequently compared with the measured displacements, strains and stresses obtained from five field tests on the CSM block.

There is fair agreement in the orientations and magnitudes of the displacement vectors between the field test conducted by Richardson (1986), and the HNFEMP-modelling. Good quantitative agreement between the experimental and numerical results were obtained in the modulus of deformation from four corner measuring stations in the block. Using the stiffness values suggested by the Terra Tek research group, the overall block deformation modulus has been calculated and the numerical results are in close agreement with the data obtained from the block test. Monitoring of the principal horizontal stress by the USBM borehole deformation gage gave the best agreement with the applied loading and the numerical results.

Field test results have shown that the CSM block is larger than the critical size needed for an equivalent continuum approach. Modelling with the smeared out method and HNFEMP is therefore valid. The fair to good agreement between the field data and the modelling results at low stresses means that the model with

three intersecting joints and a linear joint stiffnesses is a good representation of the CSM block.

SUMMARY

The problem of long term stability and geodynamic processes of the Baltic Shield has been addressed in the research plan for the coming six years, 1987-1992, of the Swedish Nuclear Fuel and Waste Management Company. The aims of the research activities are to quantify and delimit effects of earthquakes, glaciation, and glacial rebound. This analysis must rely heavily on numerical models.

The process of validation seeks to determine whether a proposed model will accurately simulate the phenomenon for which it has been designed. In general, such confidence can best be acquired by designing experiments to test the models and their basic assumptions. In rock mechanics, the validation and calibration of numerical models entered the scene at a late stage, and the opposite procedure must be applied, meaning that the field experiments (block tests) are first designed conducted and evaluated. The results obtained from these experiments are then used to test results from subsequent numerical models.

A key issue in the numerical modelling of rock masses is how to predict the effects of joints, faults, shear zones, etc. on deformability and stability. The crustal response and far field stability of a vault for radioactive waste, can in principle be considered to either in a discontinuous or continuous rock mass. In this report we emphasize on the continuum approach, where the discontinuities are smeared out in the rock mass. A parallel study is conducted by the Norwegian Geotechnical Institute using a discrete approach (Barton and Chryssanthakis, 1988).

The purpose of this study is to validate the non-linear finite element code HNFEMP against the Colorado School of Mines (CSM) block test at the Edgar Mine, Idaho Springs, Colorado, USA. The CSM block test was chosen because of extensive studies has been conducted and it is possibile to apply a discontinuous and a continuous modelling techniques to one and the same problem.

In Chapter 2 of this report, geological and mechanical data on the CSM block is presented. From extensive laboratory tests on the rocks, the elastic modulus of the intact rocks is assumed to be isotropic and is taken to be E = 60 GPa and v = 0.25. Three tests have been performed on the mechanical properties of joints in the block. Two of these are based on results from tests on the block under uni-axial and bi-axial loading conditions. The stiffness data are presented in Table 2-1. The method by which they were derived are presented in Chapter 2.

By using a fixed reference frame, a subsurface instrumentation system and an automated data acquisition system, Richardson (1986) developed a new method to measure displacements in a block test. From fixed displacement instrumentation stations in the block displacements, strains and deformability were determined. These data, together with overall displacement measurements made by the research team of Terra Tek and borehole dilatometer tests and stress measurements, form the basis for comparison of the results between the experiments and the modelling.

A brief description of the joint model and the numerical code HNFEMP is presented in Chapter 4. The continuum model of the CSM block containing the three intersecting sets of joints is presented in Chapter 5. Six different model materials have been tested under three different loading conditions, making a total of 18 models. Results are presented as a set of graphical plots of stresses and displacements (Figures 5-3, 5-4) and tabulated values of maximum stress and displacement at specific instrumentation locations in the block. A sensitivity analysis of displacement as a function of stiffness has been conducted. Changes in shear stiffness at constant normal stiffness is found to have a minor effect on the displacement , while changes in normal stiffness (and under bi-axial conditions in particular) affect the displacement data significantly.

Results from different field tests have been used to demonstrate the applicability of the smeared out approach to rock mass modelling. In principle, there is a fair agreement in the displacement vector orientations and magnitudes obtained from

the field tests and the HNFEMP- modelling. Modelling results always give smaller displacement magnitudes than those obtained from the field data. An equivalent Youngs modulus of 12.4 GPa for the CSM block was determined from calculated overall strains between four block corners and from discontinous deformation calculated by the DDA. This is found to be in close agreement with the finite element modelling result of 12.0 GPa.

Two stress measurement techniques were applied in the CSM block tests. The direction of the principal horizontal stress for the three loading situations was in fair agreement with the modelling results. The magnitude of the average maximum horizontal stress from the monitoring with the USBM borehole deformation gage agreed best with the results of the modelling and the applied loading from the flatjacks.

Field test results have shown that the CSM block is larger than the critical size needed for an equivalent continuum approach (cf. Figure 6-2). Modelling with the smeared out approach using HNFEMP is therefore valid. The fair to good agreement between the field data and the modelling results at low stress levels means that the model with three intersectiong sets of joints and linear joint stiffnesses is a good representation of the CSM block.

1 INTRODUCTION

The Swedish Nuclear Fuel and Waste Management Company is studying the concept of nuclear fuel waste disposal in a vault deep within granitic rock. An extensive research program is now being undertaken as a continuation of the work presented in the KBS I, KBS II, and KBS III reports (Swedish Nuclear Fuel and Waste Management Co., 1986). An essential part of the Earth science program is devoted to the stability of large rock masses, i.e. neotectonic structures, glacial rebound, seismicity. A special program is set up for modelling large scale rock masses and the farfield stability of vaults for radioactive waste disposal.

In modelling crustal mechanical processes and the far field stability of vaults, we are faced with new problems. Geometry, structures, and the geomechanical parameters of large rock masses and the boundary conditions which might be applied to the models must be known. Here there are a limited number of studies performed, in which the behaviour of very large jointed rock masses are simulated. One example is the modelling of compaction and subsidence of the Ekofisk oil and gas field in the North Sea (Barton et al., 1986). Generic, two-dimensional models are now proposed for vertical and planar sections of a traverse having a direction NW-SE in Northern Fennoscandia (Stephansson, 1987). The influence of glaciation, deglaciation and glacial rebound on hydrology and stability will be studied in the modelling work.

However, a minimum requirement modelling of any crustal mechanical problems is that mathematical models for simulation of stresses and displacements of rock under various coupled and uncoupled processes are verified and validated must be done. The Swedish Nuclear Fuel and Waste Management Co. is now sponsoring validation of two numerical approaches against a well controlled in-situ block test. A group at the Norwegian Geotechnical Institute is validating the discrete element codes, μDEC-linear and μDEC with the Barton-Bandis joint model,

against the CSM block test (Barton et al., 1988), and the group at Luleå University of Technology is validating the non-linear finite element code HNFEMP against the same block.

This report first describes briefly the CSM block and the rock mechanics and hydrology studies and major results obtained since the tests started 1979. Secondly it describes the non-linear model for the mechanical behaviour of continuous rock joints and the computer code HNFEMP, and the tests performed to check the code results against published analytical and experimental data. Thirdly, the results of a major code validation exercise involving the prediction of the stress, strain and displacement of the CSM block under uni-axial and bi-axial loading are presented. Finally, results from the modelling of the block are compared with data from five different field tests reported in the literature. Agreement in the results obtained is also discussed here.

2 BRIEF DESCRIPTION OF MECHANICAL DATA FROM THE CSM BLOCK

A series of mechanical and hydrological experiments is being conducted with an in-situ block of fractured gneissic rocks at the Colorado School of Mines (CSM) Experimental Mine at Idaho Springs, Colorado. In recent years the project has included studies of applied stresses versus deformation, stress and fracture conductivity, together with studies of fracture deformation versus fracture conductivity. The block and the specially-excavated drift (the block location) have been the sites for several rock mechanics and hydrology studies, see for example the theses of El Rabaa (1981), and the papers by Montazer et al. (1982), Jakubick (1983), Brown et al. (1985), Richardson et al. (1985), Sour et al. (1987).

2.1 General description of the block

The test block is a two-meter cube of Precambrian gneiss that was excavated by Terra Tek, Inc. in 1979. They subjected the block to bi-axial and uni-axial loading at ambient and elevated temperatures, using flatjacks and a line of borehole heaters for measuring hydro-thermal-mechanical properties of the rock mass. Joint permeability, static modulus, dynamic modulus, joint normal and shear stiffness, coefficient of thermal expansion, thermal conductivity and diffusivity were investigated under various conditions of stress (0 - 6.9 MPa, uni-axial and bi-axial) and temperature (12 - 74^{o} C mean block temperature). 24 boreholes - 17 of EX size (3.8 cm diameter) and 7 of NX size (7.6 cm diameter) - were drilled in the block, and another 10 EX holes were drilled outside the block. A full description of the test series are presented by Hardin et al. (1981). A summary of the most important results of the rock mechanical characterization and tests are presented by Barton et al. (1988) in their validation of μDEC against the CSM block. After Terra Tek completed their program, CSM began a second series of experiments with the block, with W. Hustrulid as principal investigator.

The block is defined by line-drilled slots which contain hydraulic flatjacks so that loading can be controlled independently in two directions. Due to leakage, the original flat-flatjacks installed by Terra Tek had to be replaced, Richardson (1986), and the new slots were wider and permitted geological mapping of the outside of the four slots. The top of the block is a free surface, while the bottom joins continuously with the surrounding rock mass.

2.2 Geology of the block

The geology of the test block has been mapped several times. Mapping efforts have included detailed surface mapping, borehole logging with TV equipment and detailed photography and mapping of flatjack slots (Richardson, 1986). Two rock types appear to dominate in the block; a banded quartz-biotite gneiss and a light-coloured pegmatite, interfingered throughout the test block and forming a migmatite rock type.

A very detailed geological characterization of the entire test drift and the vicinity of the CSM block was conducted by Rosasco (1985) and of the block surface by Hardin et al. (1981), and Sour et al. (1987a, b). The results of four mapping efforts of the surface geology of the block are shown in Figure 2-1. According to Richardson (1986), the difference in interpretation by different geologists can be attributed to variations in measurement techniques, the level of interpretation possible in characterizing the geology, and also the effort denoted to the mapping. From all the geological information available, Richardson (op. cit) applied a kriging algorithm for interpolating contours between the two dominant rock types and the results confirmed the complex geology of the block.

In this study, where we use a "smeared out" approach in characterizing the jointed block, the mapping of the joint sets in the vicinity of the block is of great importance. The dominant strike and dip of foliation joints in the block are 45° and 88° respectively. Most of these joints appear to be continuous

over 1-2 m, and their average spacing is 60 cm, Hardin (1981). The major set of mineralized joints crossing the block diagonally have an orientation of $106^{o}/89^{o}$ an average spacing of 75 of and are continuous over distances of at least 2-3 meters. The third set of joints is oriented at $134^{o}/85^{o}$ with an average spacing of about 1 meter, and continuity over distances of 0.5-1.5 m. A schematic block diagram of the average joint structure in the block is shown in Figure 2-2. This model will be applied to the non-linear finite element modelling by means of the HNFEMP.

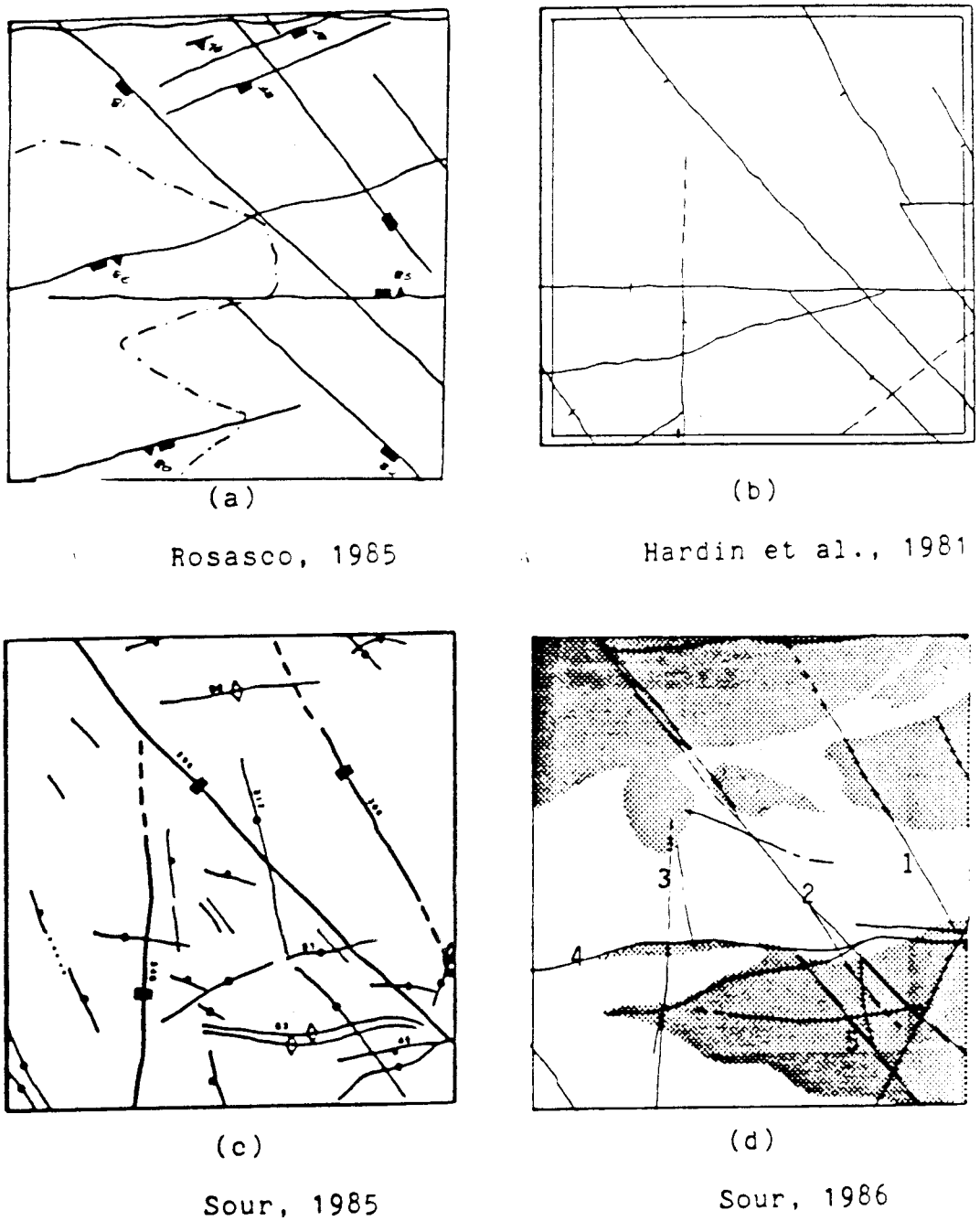

Figure 2-1 Surface geology of the CSM block after Richardson (1986).

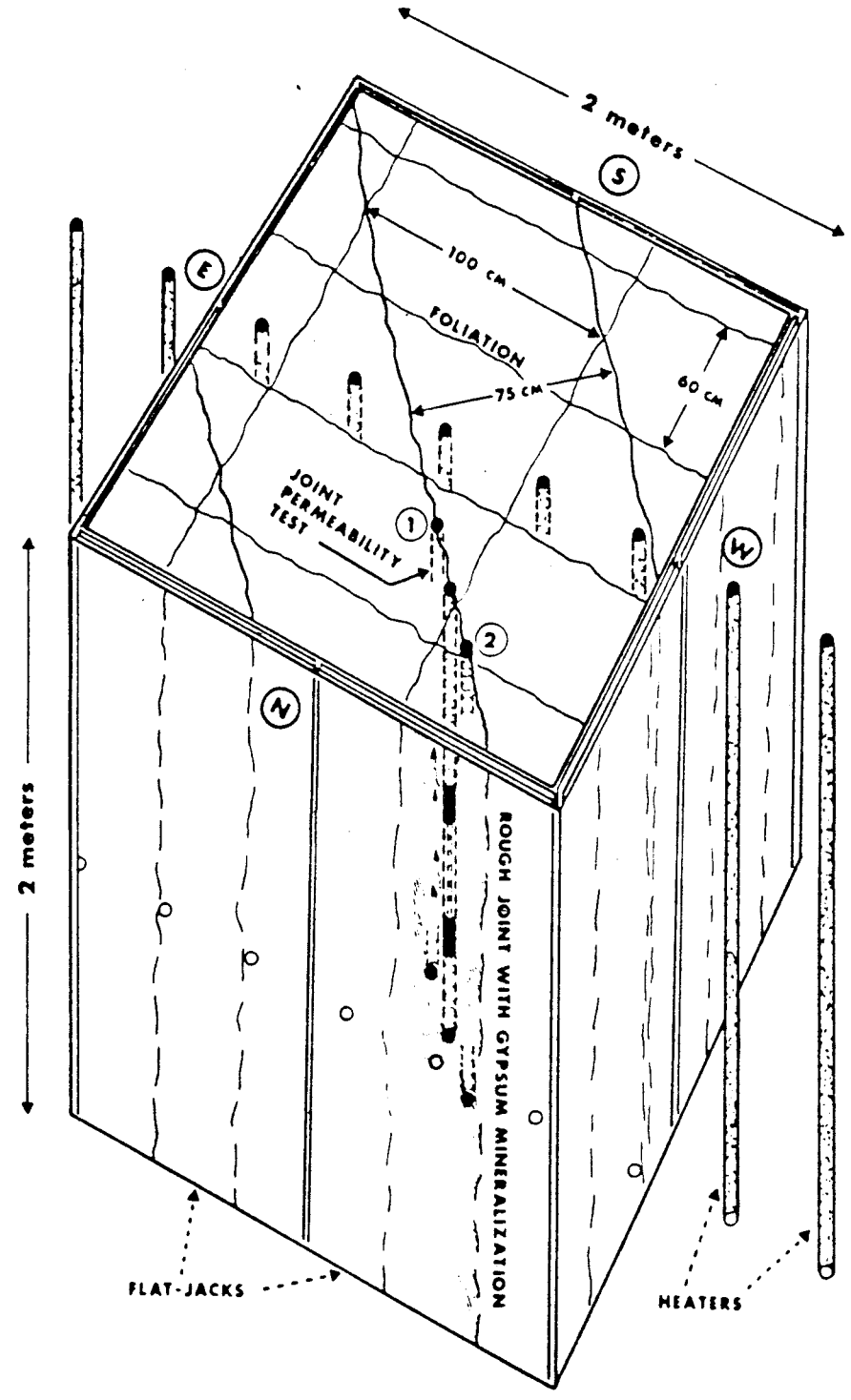

Figure 2-2 Schematic block diagram showing the relationship of the average joint structure to the flatjacks, the line of borehole heaters and the joint permeability test. After Hardin et al. (1981).

2.3 Mechanical properties of intact rock

All hard crystalline rocks are jointed over some scale. It is the joints, rather than the rock matrix material that determine the strength and the deformability of the rock mass at engineering levels of loading. In modelling the CSM test block by HNFEMP, an equivalent material is defined in which the properties of the joint system is smeared out over a unit volume of the rock mass. This requires knowledge of the mechanical properties of the intact rock matrix material and the joints.

Extensive laboratory tests on intact rocks from the experimental mine have been conducted. From the test results reported by four different researchers on rocks from the so-called CSM/OCRD room, Richardson (1986) made a compilation. He recommended the following values for the elastic constants of the intact rock matrix:

E_R = 58.6 GPa for all rock types, all directions

ν = 0.25

E_R^P = 55.2 GPa for pegmatite, no anisotropy

E_R^G = 62.1 GPa for gneiss, average

$E_{R\perp}^G$ = 51.7 GPa for gneiss perpendicular to foliation

$E_{R//}^G$ = 79.3 GPa for gneiss parallel with foliation

As demonstrated by Richardson (op. cit.) for the CSM block and also a number of studies on elastic modelling of rock mass structures, minor variations in elastic constants have little effect on the final results for stresses and displacements in the structure. For the HNFEMP modelling of the block the following values for the (isotropic) elastic constants of the intact rock were used

E_R = 60 GPa

ν = 0.25

The Young's modulus is about 2 percent larger than the value for all rock types and all directions as is suggested by Richardson (1986). The Poisson's ratio is identical with Richardson's value.

2.4 Joint stiffnesses according to Barton & Bandis

Careful recording of joint roughness profiles and measurement of the joint wall strengths using a Schmidt hammer on available joint surfaces in the vicinity of the block, together with tilt tests on jointed drill cores, enabled the two parameters, JRC (Joint Roughness Coefficient) and JCR (Joint Wall Compression Strength) to be estimated Hardin et al. (1981). These two parameters for the Barton system of joint characterization are known to control the normal closure of joints. They can be used for prediction of the dilation path during shearing, the joint aperture and the permeability. Based on the joint parameters recorded in the field (Hardin et al., 1981) and the known hydro-mechanical coupled joint behaviour, as described by Barton et al. (1985), the input data assumed to best represent the joint sets in the block are presented as stress-deformation conductivity diagrams. These illustrate the non-linear behaviour of the rock investigated (Barton et al., 1988, Tables 1-4). The calculated average natural values for the foliation joint set and the diagonal joint set were as follows:

$JRC_n = 8.2$

$JCS_n = 62.2$ MPa

$\Phi_r = 26.5^o$

The cohesion and the friction angle at a representative normal stress level was calculated from to the equations

$$\tau = \sigma_n' \tan \Phi' \qquad (2.1)$$

$$\Phi' = JRC \log (JCS/\sigma_n') + \Phi_r \qquad (2.2)$$

where τ = peak shear strength

σ'_n = effective normal stress

Φ' = peak friction angle at representative normal stress

Φ_r = residual friction angle

For a representative normal stress level of 3.5 MPa, the cohesion and friction angle is found to be

$c = 0.4$ MPa

$\Phi = 32^o$

Tilt tests on jointed drill core run perpendicular to the foliation gave a mean value for the friction angle of $\Phi_b = 32.5^o$. Parallel to the foliation, it was found that $\Phi_b = 30.5^o$ (Hardin et al., 1981).

The peak dilation angle, $d_n(peak)$, was calculated from the empirical formula (Barton et al., 1988)

$$d_n(peak) = \frac{1}{2} JRC \cdot \log \left(\frac{JCS}{\sigma'_n}\right)$$

For the normal stress interval 0.5-3.5 MPa, the calculated $d_n(peak) = 6.7^o$, and this value is also obtained from the stress-deformation diagrams presented by Barton et al. (1988).

The parameters associated with the joint-shear and normal stiffness properties will be described next. Figure 2-3A shows shear stress versus shear displacement for the diagonal joint set in the block computed from the joint input parameters and at three normal stresses, σ_n = 0.5, 3.5 and 7.0 MPa. The shape of the curves are defined by Barton. These emphasize first the mobilization of friction in the joint, is followed by the mobilization of the roughness of the joint. The peak quantity shown in Figure 2-3B is the normalized maximum shear strength for the given applied normal stress. Shear stiffness values were derived from tangent gradients of the linear portion of the curves. The average shear stiffness of the foliation and diagonal joint sets for the representative normal stress is

found to be K_S^{av} = 2.7 MPa/mm. The degree of joint closure depends primarily upon the initial mechanical aperture (E_o) and secondarily upon the roughness (JRC_o) and wall strength of the (JCS_o). Unloading is inelastic. A large hysteresis look and a permanent set is obtained. The constitutive equations for loading and unloading, and the empirical constitutive relationship for maximum closure and initial joint stiffness is described in a report by Barton et al. (1988). The cyclic joint behaviour for the diagonal joint set is shown in Figure 2-3B. The non-linear behaviour of the joint closure is apparent and the initial stiffness increases with the number of cycles of loading. Average normal joint stiffness of the foliation and diagonal joint set for representative normal stresses in the range 0-7 MPa is estimated to be k_n^{av} = 67.2 MPa/mm.

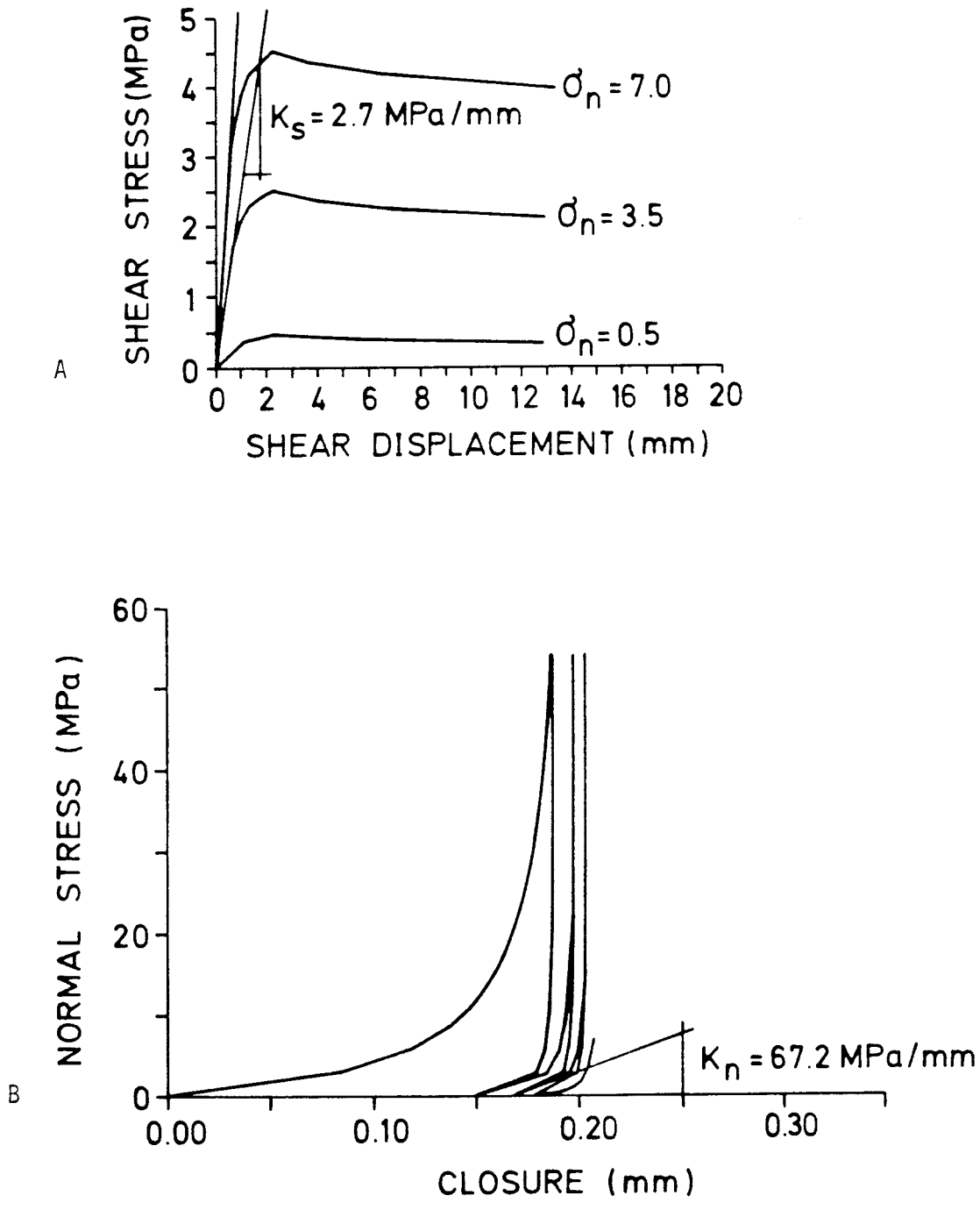

Figure 2-3 Predicted average joint stiffness of diagonal joint set for CSM block. A, Shear stress versus shear displacement for different normal stress. B, Normal stress versus closure stress for four loading cycles. After Barton et al. (1988).

2.5 Joint stiffnesses form Terra Tek tests

During the first testing phase conducted by Terra Tek the surface of the block was instrumented with some thirty pairs of Whittmore pins. Several of these were located across visible joints intersecting the block. Several gauges provided closure data for the diagonal and foliation joints. By subtraction of the deformation of the intervening intact rock from the overall gauge response, the net joint deformation was obtained. The average normal stiffnesses of the diagonal and foliation joints for the first loading cycle (bi-axial) over the stress range 0-6.9 MPa were 117 MPa/mm and 57.5 MPa/mm respectively (Hardin et al., 1981). Following the bi-axial load cycle, the block was sub-jected to two uni-axial load cycles and again a bi-axial cycle which indicated a normal stiffness of 150 MPa/mm. This stiffness is larger than that obtained for the first load cycle. The initial shear stiffness of the diagonal joint for an N-S uni-axial loading cycle was k_s = 4.8 MPa/mm, but above 1 1 MPa this increased to 84.6 MPa/mm. If a secant value, from 0 to peak load is used, the shear stiffness is found to be 16.7 MPa/mm and almost the same secant value was also recorded during the successive E-W uni-axial loading cycle.

2.6 Joint stiffnesses from CSM tests

Joint normal and shear displacement curves were also construc-ted for the tests run by CSM using a field measuring system and an evaluation technique described by Richardson (1986). In principle, tests were selected for which there were two dis-placement measuring stations on each side of a joint. This yielded four possible triangular rosettes. These were averaged to give a single joint normal curve and a single joint shear curve. Based on measurements of joint stiffness data for the four major joints in the block conducted at three levels in the block, Richardson (op. cit.), obtained an average normal stif-fness of k_n = 42.7 MPa/mm for the diagonal joint and k_n = 28.0 MPa/mm for the dominant foliation joint. The average normal stiffness then becomes k_n^{av} = 35.4 MPa/mm. The shear stiffness

for the major diagonal joints were 9.1 and 38.8 MPa/mm, respectively, which gives an average value of k_s^{av} = 24.0 MPa/mm.

The normal and shear stiffnesses obtained by applying different sampling methods and field measurements are summarized in Table 2-1.

Table 2-1 Stiffness data obtained for the CSM block.

Stiffness	Barton System Linear MPa/mm	Terra Tek Field Measurements* MPa/mm	CSM Field Measurements† MPa/mm
Normal	67.2	117.3	35.4
Shear	2.7	16.7	24.0

* Whittmores pins (Hardin et al., 1981)

† Triangulation array (Richardson, 1986)

The triangulation of the upper horizon tests of diagonal and foliation joint sets conducted by CSM yielded the least normal stiffness. If we consider all normal stiffness data for all tested joints in the block, the value will increase. It becomes k_n = 48 MPa/mm. This value is based on a linear regression for the entire upload curve for each test. If the secant load up to peak load of the stress versus displacement recordings are used, the normal stiffness will increase and becomes 68.8 MPa/mm. This is slightly larger than the value obtained from the Barton system. Richardson (1986) believes that the difference between the CSM results and the Terra Tek results presented in Table 2-1 indicate the following: (i) possible surface decoupling in the Terra Tek results, (ii) the lower peak stress level (5 MPa versus 7 MPa) used in the CSM test,

and (iii) broader array spacing for the deformation measurements in the CSM test.

The difference between the stiffness results presented in Table 2-1 may also be due to increased stiffness resulting from the attached bottom (Hardin et al., 1981). This becomes most apparent when field measured data for shear stiffness is compared with calculated values according to the Barton system. The situation is illustrated in Figure 2-4 (Barton and Bandis, 1982), where results from the block test are plotted together with data of shear stiffness versus block length for different values of normal stress.

The shear stiffness according to the Barton system is located in the expected region of the diagram, whereas the large shear stiffnesses from the field measurements are more relevant for a normal stress around 100 MPa. The effect of this on the stresses and displacements in the block will be demonstrated from the results of the modelling.

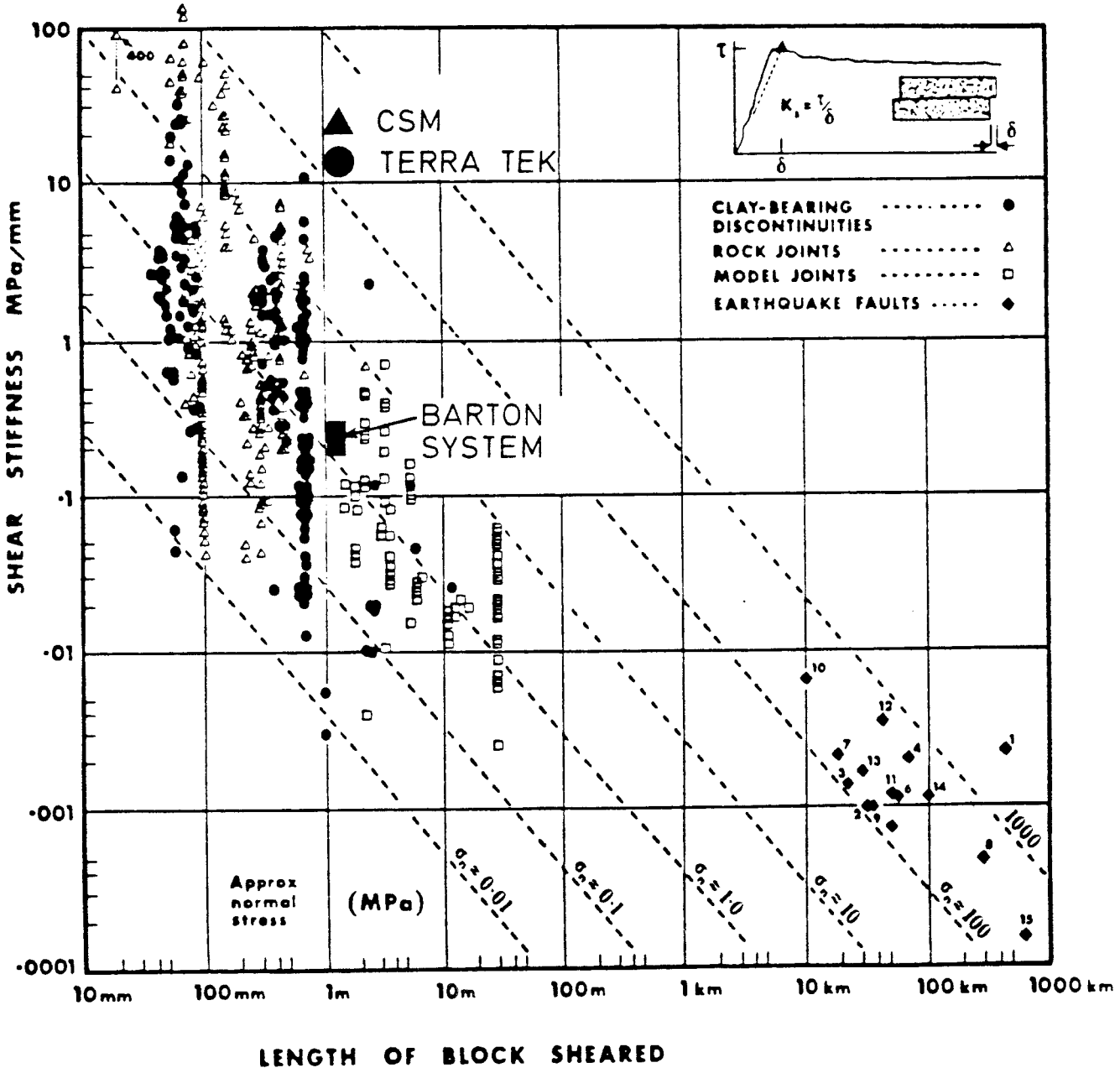

Figure 2-4 Shear stiffness data for the CSM block plotted in the diagram of shear stiffness versus length of block sheared. Modified after Barton and Bandis (1982).

3 MECHANICAL TESTING OF THE BLOCK

The heated flatjack test series conducted by Terra Tek to measure the thermomechanical and transport properties of in-situ rock masses included several rock mechanical tests. Of the many rock mechanics instruments installed in the block, only the rod extensometers and the Whittemore pins provided useful data. Results from these measurements have been applied to the stiffness determination presented in Table 2-1.

The ambient temperature block test conducted by CSM incorporates a number of new features and new methods of data interpretation. For this study, the investigation of applied stress versus deformation of fractured rock and applied stress versus measured stress within the block is of outmost interest.

3.1 Block displacement tests

Richardson (1985, 1986) developed a new method to measure displacements in block tests through the use of a fixed external reference frame, automated data acquisition system, and a subsurface instrumentation system, Figure 3-1. The fixed external reference frame permits the measurements of absolute displacement rather than just that of relative displacement. By subsurface instrumentation, displacement monitoring could be conducted in the central portion of the block, away from the decoupled surface and attached bottom. The electronic monitoring system with inductive proximity transducers attached to free-standing rods anchored in the borehole enabled three-dimensional displacement recordings to be made.

Displacement measurements were made in ten boreholes and at three horizons within the block. The principal joints in the block and the displacement instrumentation stations are shown in Figure 3-2. Three load configurations, equal bi-axial, N-S uni-axial and E-W uni-axial where applied to a maximum pressure of 5.2 MPa. The test series conducted by Richardson (1986)

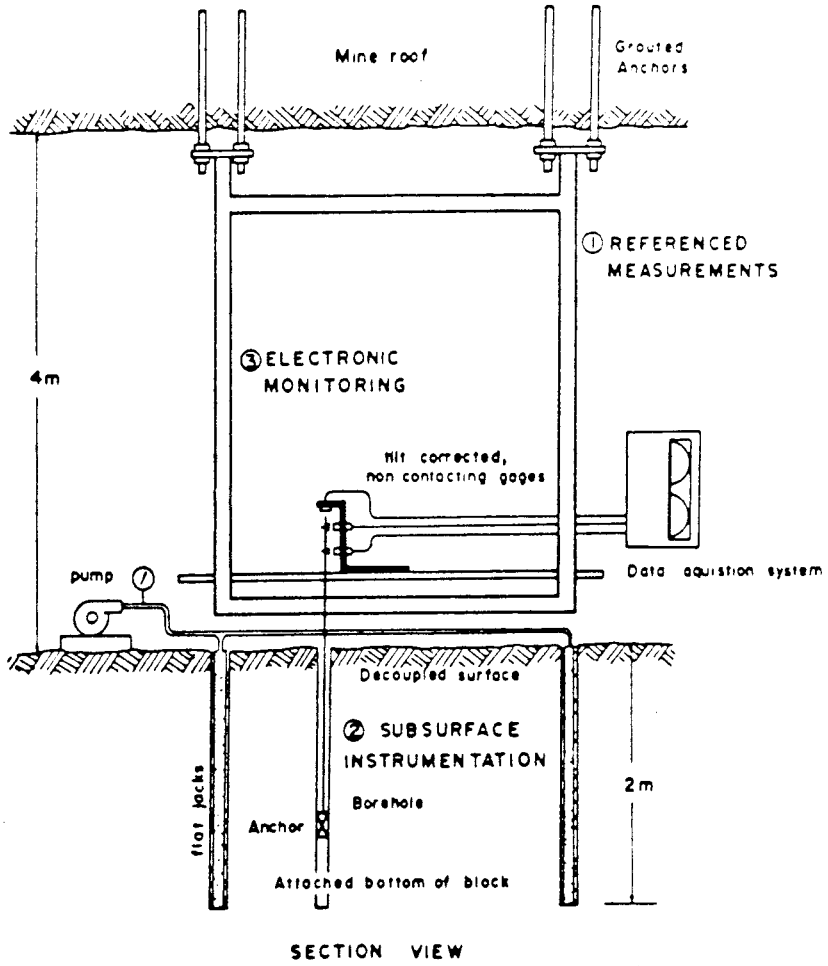

Figure 3-1 Schematic illustration of the CSM block test and instrumentation system. After Richardson (1986).

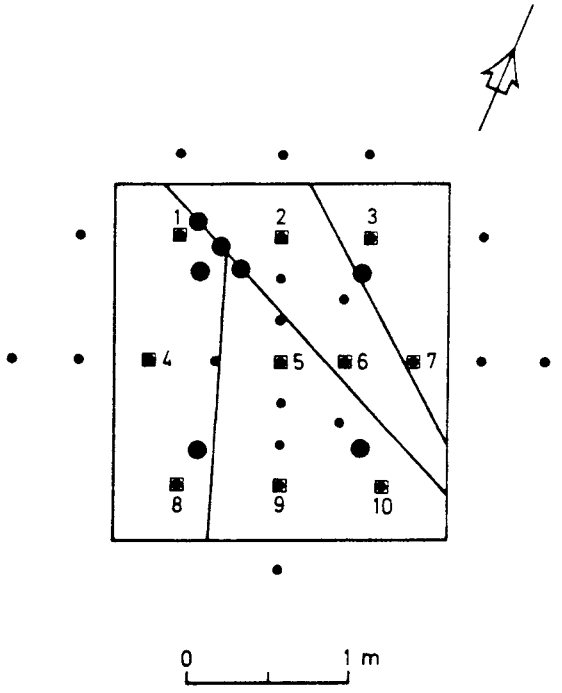

Fig. 3.2 Major joints in the CSM block and instrumentation for displacement tests. After Richardson (1986).

involved 13 loading tests where each test yielded approximately 2500 displacement data points for a total of 32,500 readings.

From this large data base we select the vector plots for the upper horizon showing the incremental displacements resulting from each scan at every 0.5 MPa increment of loading, Figure 3-3. When the block is loaded at equal flatjack pressure on all sides, the displacements are fairly symmetrical and point towards the center of the block, cf. Figure 3-3A. The minor "kinks" in the displacement vectors could indicate slip-stick behaviour along the joints. Results from N-S and E-W uni- axial tests show smooth displacements and the final directions for most vectors differ little from the initial directions. The magnitude of the maximum recorded displacement vector is slightly more than 0.4 mm. Tilt vectors, representing the incremental tilt of the anchor rod during the test sequence were shown to behave in an unpredictable manner. The tilt vectors were randomly distributed.

Vertical displacements were monitored by using a transducer mounted vertically at each measuring station, cf. Figure 3-1. As anticipated, the block bulged vertically during the flatjack loading. The average vertical displacement for the equal bi-axial loding was 104 microns (0.104 mm), while the average for the N-S uni-axial was 50 microns and for the E-W uni-axial 66 microns (Richardson, 1986).

For comparisons between the model calculations and the field measurements presented by Richardson (op. cit.), peak load displacement vectors, secant values of deformation modulii to peak load and secant values at peak stress calculated from discontinuous deformation analysis (DDA) are presented and evaluated in chapter 6 of this report.

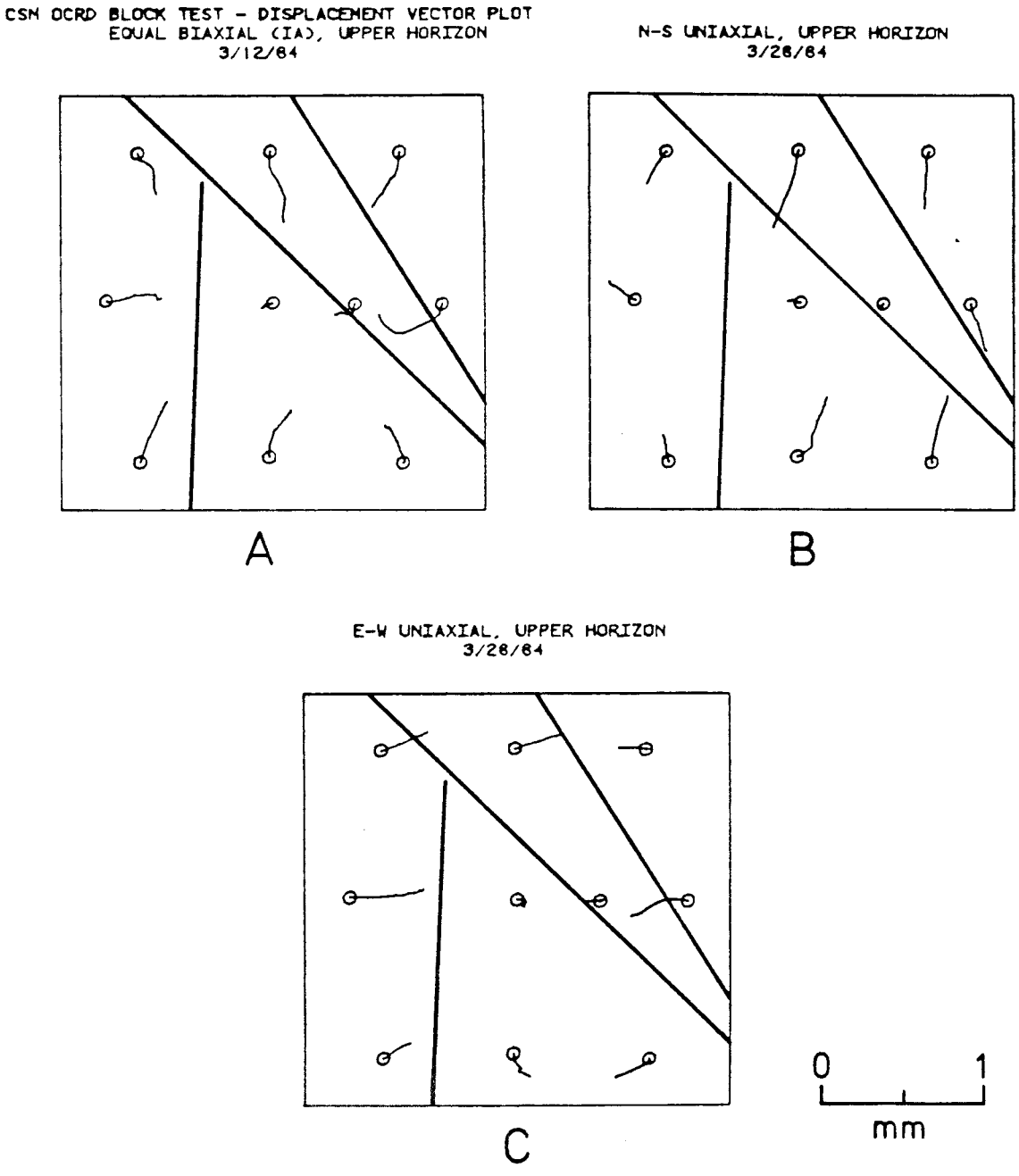

Figure 3-3 Incremental displacement vector plots for tests on upper horizon in CSM block. A) Bi-axial loading to 5.17 MPa, B) N-S uni-axial loading to 5.12 MPa, and C) E-W uni-axial loading to 5.16 MPa. After Richardson (1986).

3.2 Rock stress monitoring

Flatjacks surrounding the block enabled the application of a uniform stress field along the block boundary. Assessment of stress redistribution in the block is possible by measurement of borehole deformations within the block. The stress distribution can be determined together with an accurate measure of the borehole deformability. Brown (1986) conducted a series of rock deformability tests in 23 boreholes and 7 levels of the CSM block. The CSM dilatometer system was used. Youngs modulus (E) at the mid-plane of the block varied from 8 GPa to 68 GPa, Figure 3-4. Boreholes in the midstrip (H3-H7) of the block were used as sites for heaters used by Terra Tek during the first phase of the test program. These points also have the smallest deformability moduli. This is probably caused by near-hole heat damage to the rock (Sour et al., 1987).

The borehole strains induced by changes in the surrounding stress field were measured alternately with the USBM borehole deformation gauge and the Luleå University of Technology cell, LuT-cell (Brown et al., 1986). From the displacements recorded by the cells major and minor principal strains in the mid-plane of the block were determined, cf. Figure 3-5. Results showed a rather non-uniform strain distribution. Some of these are eliminated as principal stress are calculated at each hole and normalized by that hole's deformation modulus.

In section 6.5 of this report, the comparison between numerical model calculations and the field measurements presented by Brown (1986) and Brown et al. (1986) for the magnitudes and directions of mid-plane stresses are presented and evaluated.

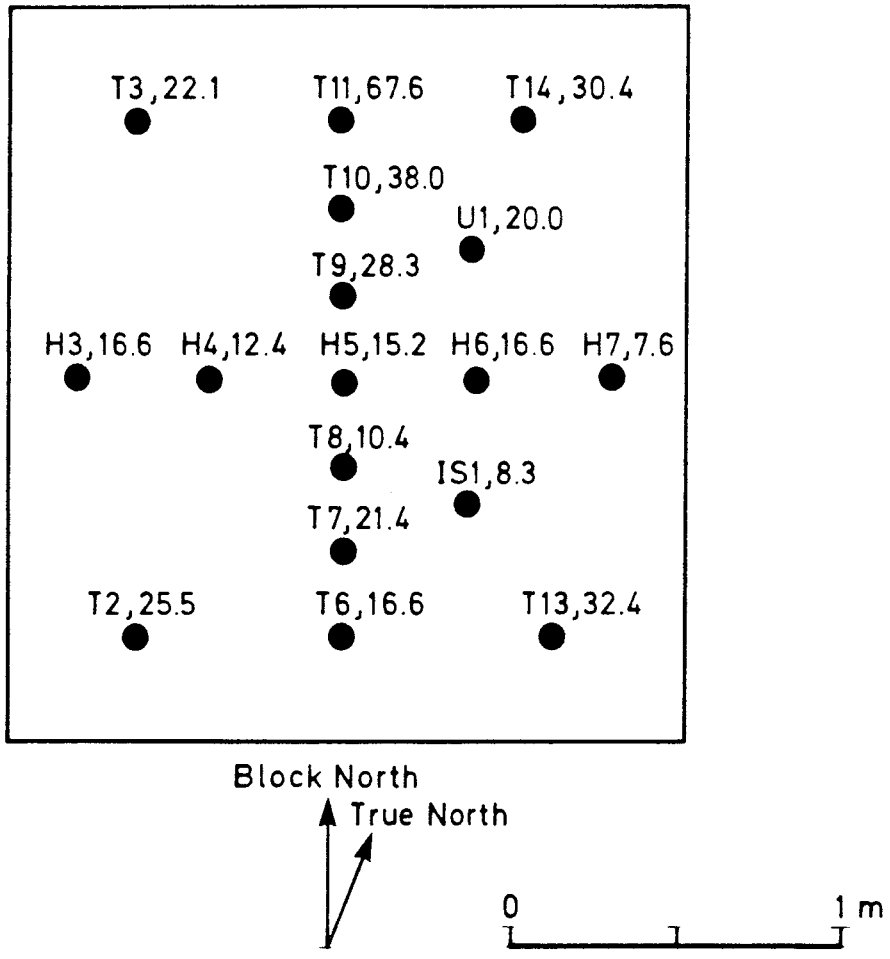

Figure 3-4 Deformability modulus at the mid-plane of the CSM block. The borehole number and the modulus in (GPa) are shown. Modified after Brown (1986).

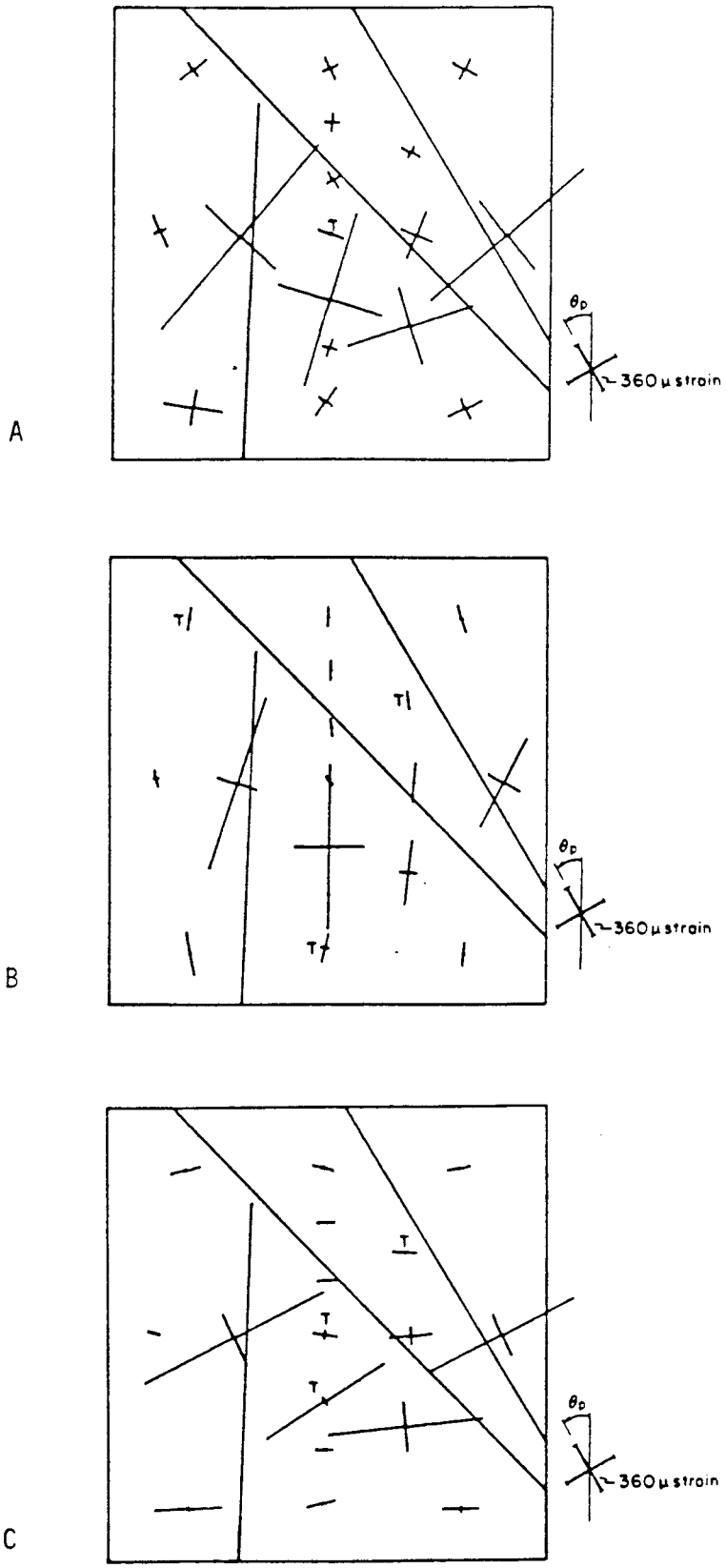

Figure 3-5 Major and minor principal strains at the mid-plane of the CSM block determined from USBM borehole deformation gauge. A) Bi- axial, uploading to ~ 5.2 MPa, B) N-S uni-axial upload to 5.3 MPa, and C) E-W uni-axial upload to 5.2 MPa. After Brown (1986).

4 JOINTED ROCK MODELS

In principle, two approaches can be used in modelling jointed rock masses: continuum or discontinuum. The first approach uses a material constitutive model that accounts for the properties of the intact rock and the joints without including the joints as separate entities. The joints are assumed to be planar and the mechanical properties of the intact rock and joints are averaged, and distributed throughout the rock mass in proportion to the spacing of the defined joint sets. Since the joint system consisting of one or several sets of joints are smeared out in a unit volume of rock, the method is sometimes called the "smeared out" approach or the "equivalent material approach", Zienkiewicz and Pande (1977), Pande (1985), Olofsson (1985) and Zimmerman and Blanford (1985). In a recent paper by Costin and Chen (1988), they evaluated the validity of the continuum approach for jointed rock masses from the G-Tunnel Heated Block Experiment at the Nevada Test Site. Despite extremely high shear stiffness and low cohesion, they obtained good quantitative agreement between the experimental and numerical results.

The discontinuum approach implies that jointed rock masses is modelled by describing the response of every joint separately. Goodman (1976) developed a special joint element for rocks and implemented it in a finite element program. The distinct element method (Cundall, 1980) is another technique for analysing problems in which fracturing or jointing controls the rock mass response. This method models the rock mass as a series of blocks which are separated by intervening joint planes. The MUDEC code is based on the distinct element method and has been applied to both loading tests on a large basalt block (Hart et al., 1985) and to the CSM block, cf. Barton et al. (1988).

4.1 Jointed rock continuum model, HNFEMP

A jointed non-linear rock continuum model has been formulated by Olofsson (1985a,b) for use in modelling jointed rock mechan-

ical response in continuum-based numerical codes. The joint model has been implemented in a finite element code called HNFEMP and applied to the CSM block. The recoverable normal and shear joint deformations are assumed to depend linearly on the applied stresses so that the joint elastic compliance is regarded as a constant property. The intact rock is considered to be a linear elastic material and for an elastically isotropic material the compliance matrix may be determined from the Youngs modulus and the Poisson's ratio.

In the model of Olofsson (op. cit.) a joint has two failure modes (i) shear failure, and (ii) normal failure. Shear failure is initiated when the shear stress exceeds the frictional forces in the joint plane. Normal failure can either be tensile or compressive. The viscoplastic yield function, F, for a single joint in the rock mass is illustrated in Figure 4-1. This function depends on the following parameters:

- cohesion, c_o
- angle of dilation, Φ_i
- basic friction angle, Φ_b
- asperity angle, Φ_s
- normal compressive strength of asperity, N

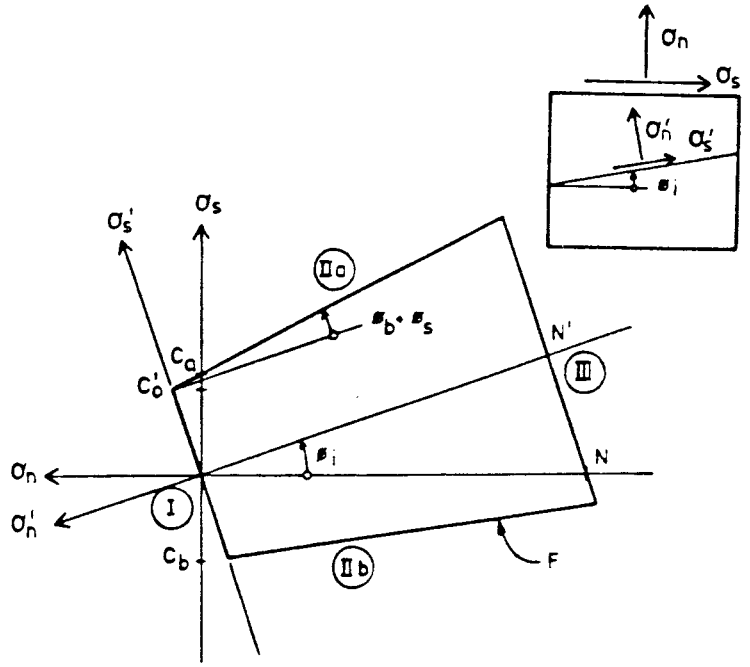

Figure 4-1 Viscoplastic yield function, F, for a single joint. After Olofsson (1985).

The fundamental Mohr-Coulomb failure criterion in the σ_n - σ_s co-ordinate system is transformed to the joint plane to obtain the equations for the final yield function, for details see Olofsson (1985). Figure 4-2 shows the viscoplastic potential Q for a single joint. Differentiation of the viscoplastic potential gives the viscoplastic flow tensor that contains the unknown dilation angle, Φ_i. Olofsson (op. cit.) presents equations to relate the dilation angle and other unknowns to the well-known empirical formulations of joint shear and normal behaviour by Barton and Bandis (1982) and Barton's parameters JRC, JCS and joint length, L. He also made a comparison of the joint model with shear-box experiments and found that the calculated total peak friction angles were in close agreement with the measured values.

The equivalent rock mass model for the mechanical behaviour of continuous rock joints have been implemented in a finite element code called FEMP (Nilsson and Oldenburg, 1983) and the special version containing the non-linear model of the rock joints is called HNFEMP. This version also is capable of modelling rock bolts installed in the rock mass structure (Larsson et al., 1985).

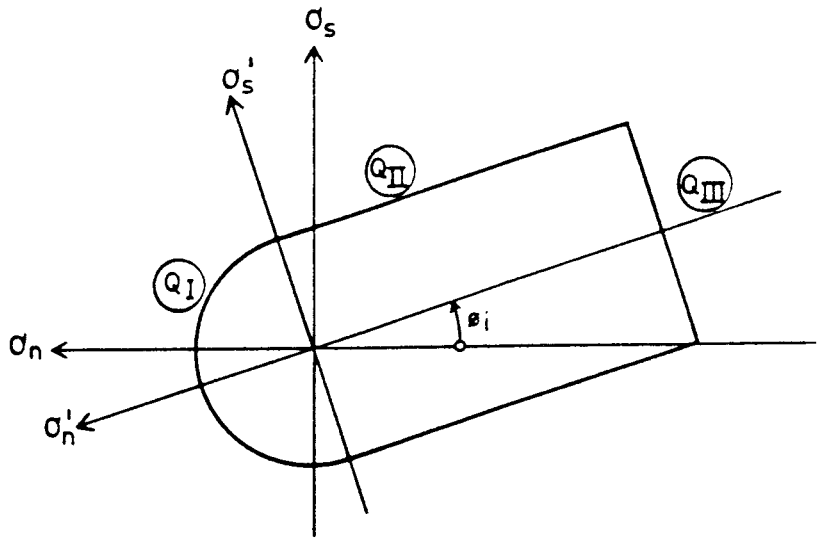

Figure 4-2 Viscoplastic potential Q for a single joint. After Olofsson (1985).

5 MODELLING OF CSM BLOCK WITH HNFEMP

A continuum model of the CSM block was constructed using the code HNFEMP. The dimensions of the block, its orientation and the three sets of continuous joints and their average spacing are shown in Figure 5-1.

Based on the geological investigations presented in section 2.2, the rock block size index is approximately 75 cm, the volumetric joint count approximately 4.8 joints m^3 (medium size block), and the rock quality designation (RQD) is 90-100 % (Hardin et al., 1981).

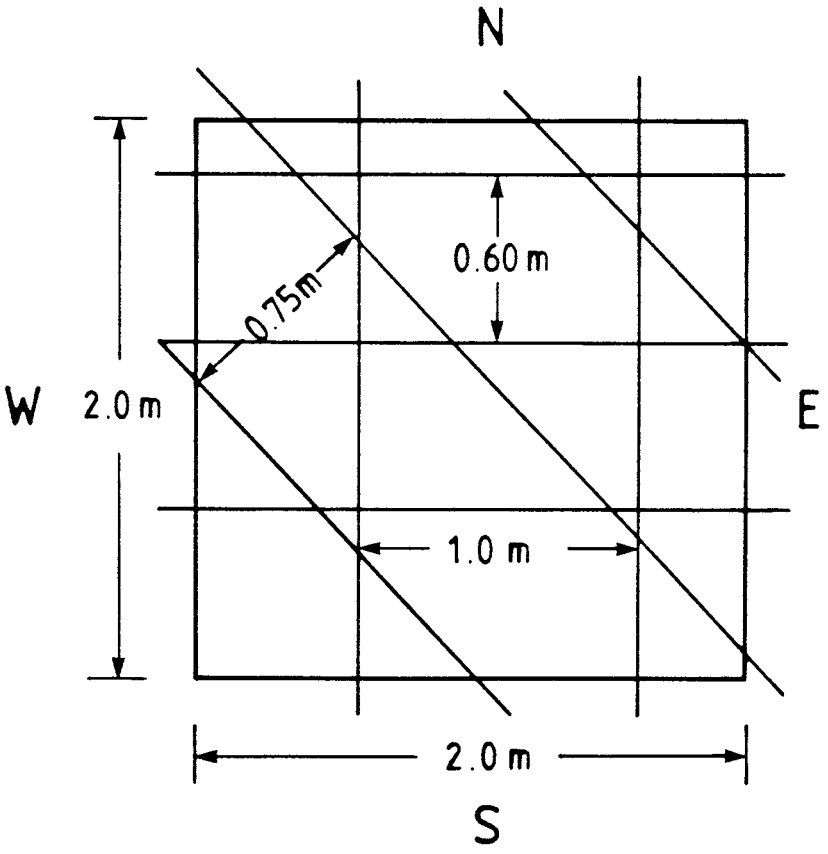

Figure 5-1 Geometrical model for the CSM block containing three intersecting sets of continuous joints.

5.1 Material properties

The following six different material models were tested in the HNFEMP modelling: 1, isotropic linear elastic solid; 2, joint model according to Barton's system; 3, joint model with stiffness properties determined from the Terra Tek field measurements; 4, joint model with stiffness properties determined from the CSM field measurements; 5 and 6, joint models with given stiffness properties for sensitivity analysis.

The intact rock properties for all models are as follows:

density: 2500 kg/m^3

Young's modulus: 60 GPa

Poisson's ratio: 0.25

Following the description of the joint properties as presented in section 2.4, the average characteristics for the three sets of joints are as follows:

Joint roughness coefficient, JRC: 8.2

Joint compressive strength, JCS: 62.2 MPa

Residual friction angle, Φ_r: 26.5^o

Dilation angle, d_n: 6.7^o

Tensile strength, τ_s: 0 MPa

Cohesion, c: 0.4 MPa

From the Barton's classification of joint characteristics, the joint stiffnesses for the linear joint model are k_n = 67.2 MPa/mm and k_s = 2.72 MPa/mm, model 2. These data were derived from tangent gradients of the linear portions of the normal stress versus closure displacement and shear stress versus shear displacement in Figure 2-3. Evaluation of the field measurements gave other average stiffness data for the joints in the block. These have also been modeled in models 3 and 4. Finally, two models with the same normal stiffness and extreme shear stiffness were tested, models 5 and 6. The six different models and their material properties are presented in Table 5-1.

Table 5-1 Material models tested with HNFEMP.

	Material Model					
Joint Stiffness MPa/mm	1 Isotropic Linear Elastic	2 Field Data Barton System	3 Block Test Terra Tek	4 Block Test CSM	5 Sensitivity Analysis	6 Sensitivity Analysis
Normal	∞	67.2	117.3	35.4	117.3	117.3
Shear	∞	2.7	16.7	24.0	2.7	100.0

5.2 Boundary conditions

Boundary conditions in this type of modelling is a difficult problem, since there is no fixed point in the block. Furthermore, exact plane strain or plane stress conditions do not exist. One way to handle these problems would be to fix the centre point in the model and apply normal stresses to all four edges of the block. This is a possibility in HNFEMP modelling, but it would not allow correct comparison of the results those from MUDEC modelling, where fixed boundaries are used at the outer edges of the flatjack blocks, cf. Barton et al. (1988). For future modelling a fixed centre point approch will be used.

East-West uni-axial loading (1), N-S uni-axial loading (2) and bi-axial loading (3) directions were modelled and the peak stresses were as shown in Figure 5-2. Each model tested is assigned a two-digit number where the first digit stands for the material number (1-6), and the second for the loading conditions (1-3).

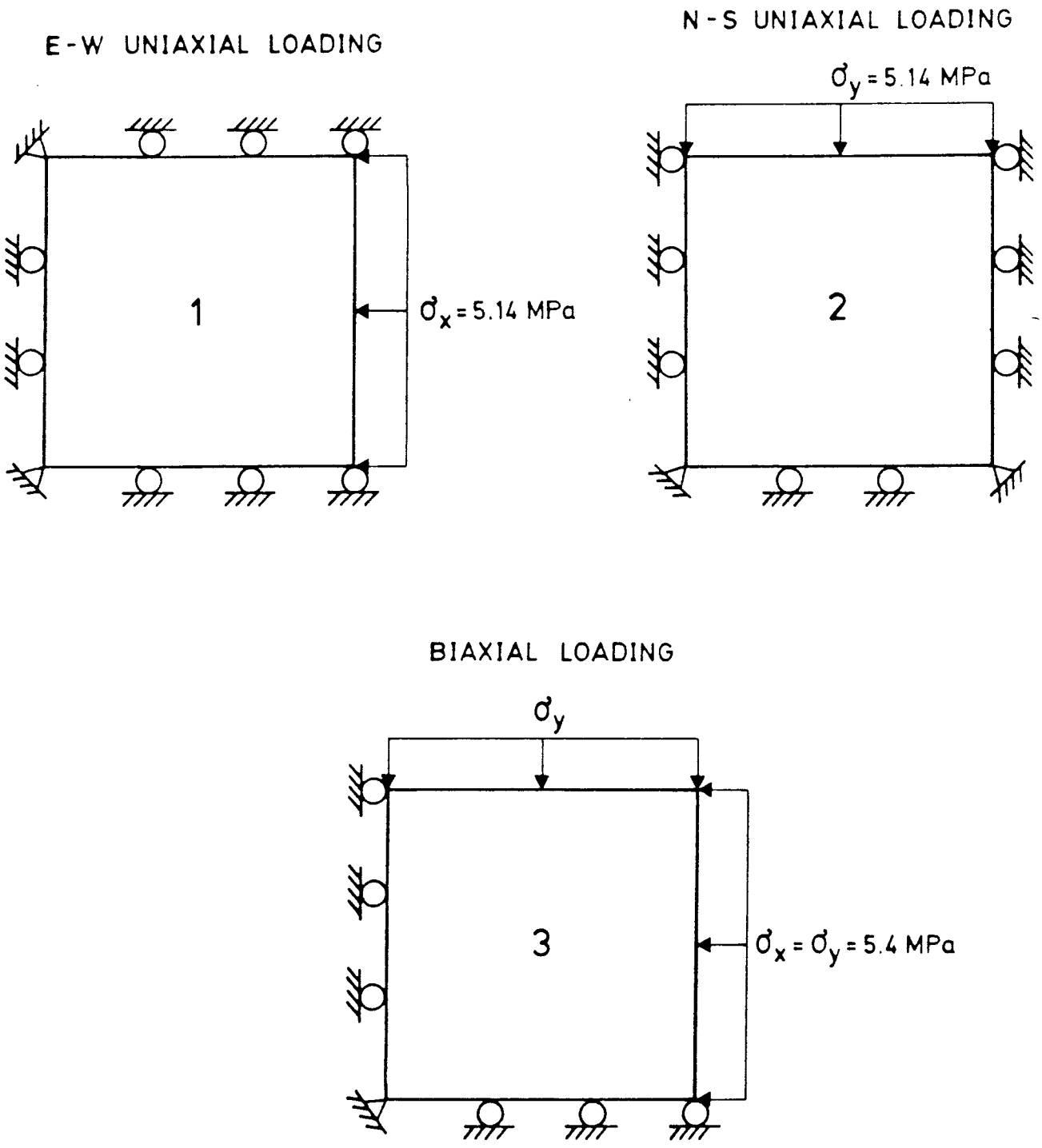

Figure 5-2 Loading configurations (1-3), applied peak loads and boundary conditions for finite element modelling.

5.3 Results

A total of 6 x 3 models of the CSM block were analysed. Complete graphical output for each model consists of the following iterms:

- principal stress vectors
- displacement vectors
- contour plot of x-stress, y-stress, x-y shear stress
- contour plot of x- and y-displacement

A selection of plots are presented in Appendices 1-4, starting with results from the elastic modelling and followed by jointed models.

Principal stress vectors and iso-curves for the x-stress of Model 2.3 (Barton's joint system and bi-axial loading) are shown in Figure 5-3. Due to the anisotropy caused by the sets of joints, the stresses are re-oriented (A) and the stress magnitudes diminish in a direction towards the fixed, bottom left corner (B).

The displacements in the x- and y-directions for Model 2.3 are shown in Figure 5-4. Iso-curves for the displacement are slightly distorted compared with the straight isolines for the elastic models, cf. Appendix 1. The anisotropic displacement, with an excess in the y-direction, is due to a larger volume density of E-W striking set of joints, cf. Figure 5-1.

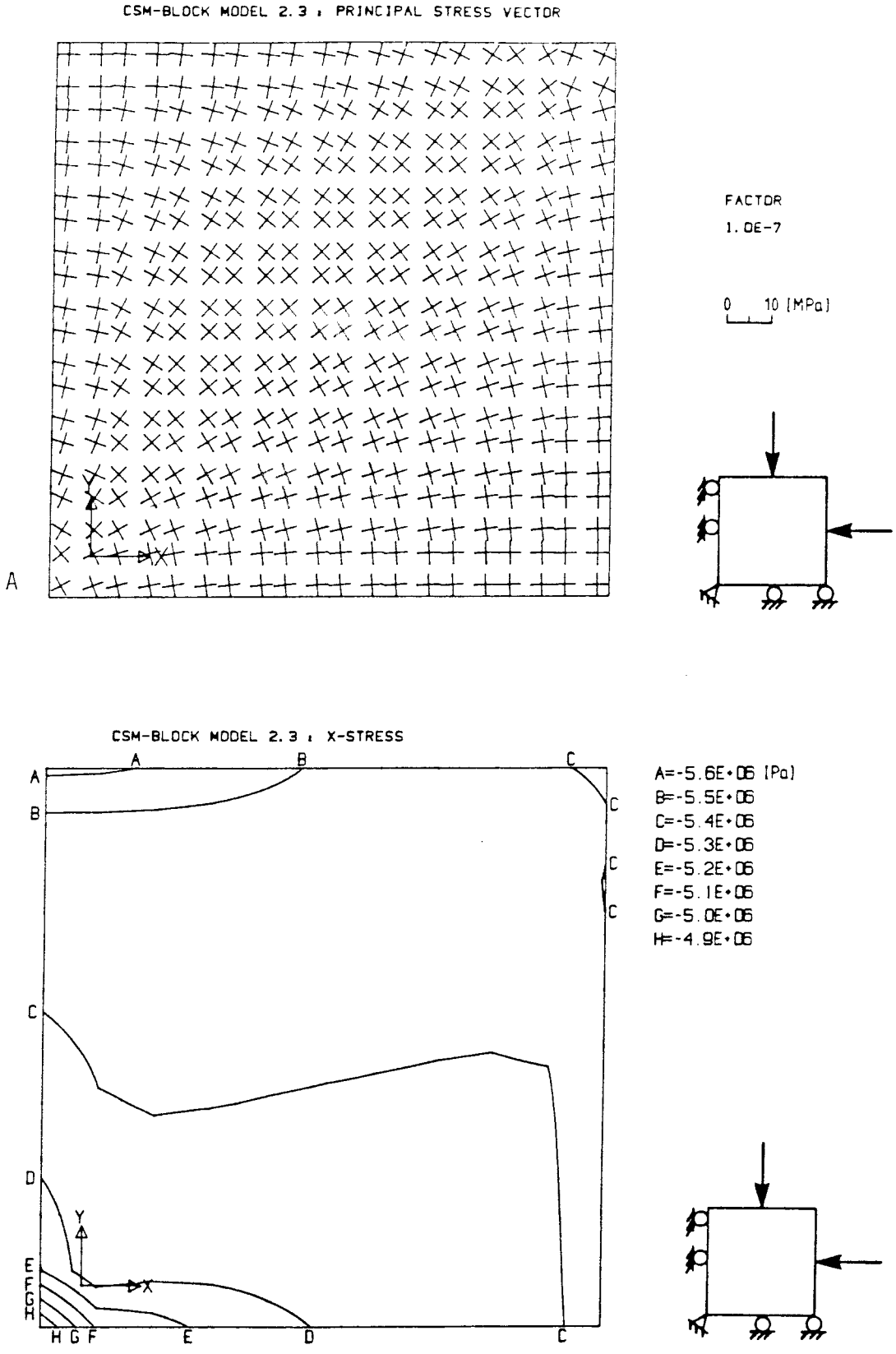

Figure 5-3 HNFEMP model of CSM block, Model 2.3, Barton's joint system and uni-axial loading 5,14 MPa. A) Principal stress vectors. B) Normal stress, x-direction. Notice the re-orientation of stress vectors and decrease in magnitude of stress towards the bottom left corner.

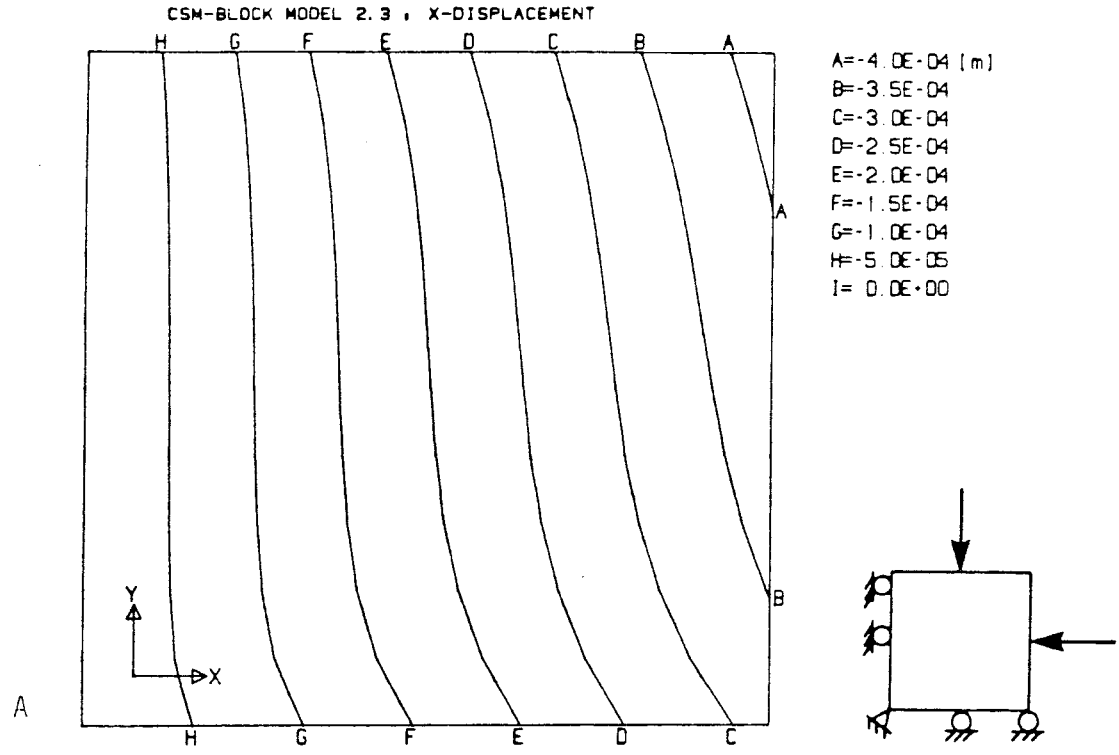

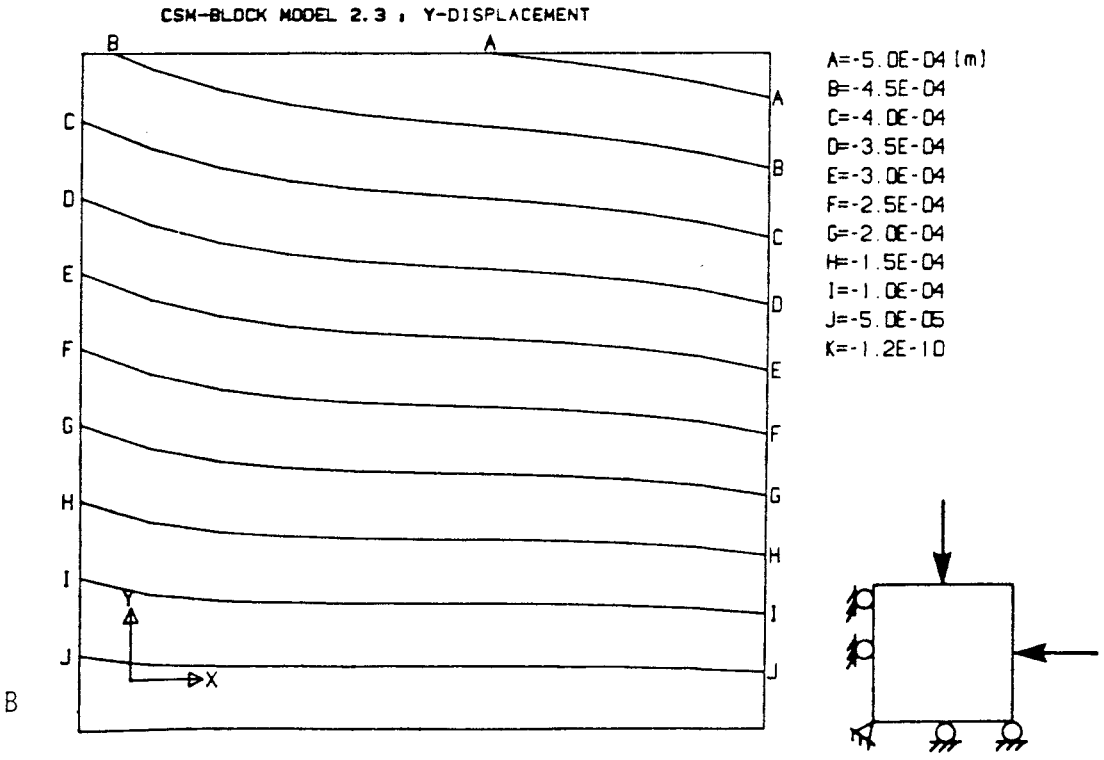

Figure 5-4 HNFEMP model of CSM block, Model 2.3. A) x-displacement. B) y-displacement. The larger y-displacement is due to smaller spacing of E-W striking set of joints.

Ten instrumentation locations were used in the CSM tests for studies of load versus displacement and load versus stress, Figure 5-5. Displacements at the ten locations for the three loading conditions and the Barton's joint system (Models 2.1, 2.2, 2.3) are shown in Figure 5-6. Maximum x-displacement, 0.7 mm, is obtained for location point 7 at the eastern part of the block (A), and since this point is located closest to the edge of the block, it gives larger displacements than those at points 1, 2 and 3.

Introduction of joints into the block model reduces its stiffness. This is illustrated in Figure 5-7, where x- and y-displacements for ten ten instthe ntation locations in Model 1.3 (elastic) and Model 2.3 (Barton's joint system) are shown. The modelling results for the maximum stress and displacement at the instrumentation locations of the CSM block are presented in Table 5-2. In the most cases, the maximum values for each loading mode appear at the same location for the same joint model. Models with a low shear stiffness (Models 2.1, 3.1, 5.1 and 2.2, 3.2, 5.2) tend to give large stresses perpendicular to the direction of loading. This is an effect of the given boundary conditions.

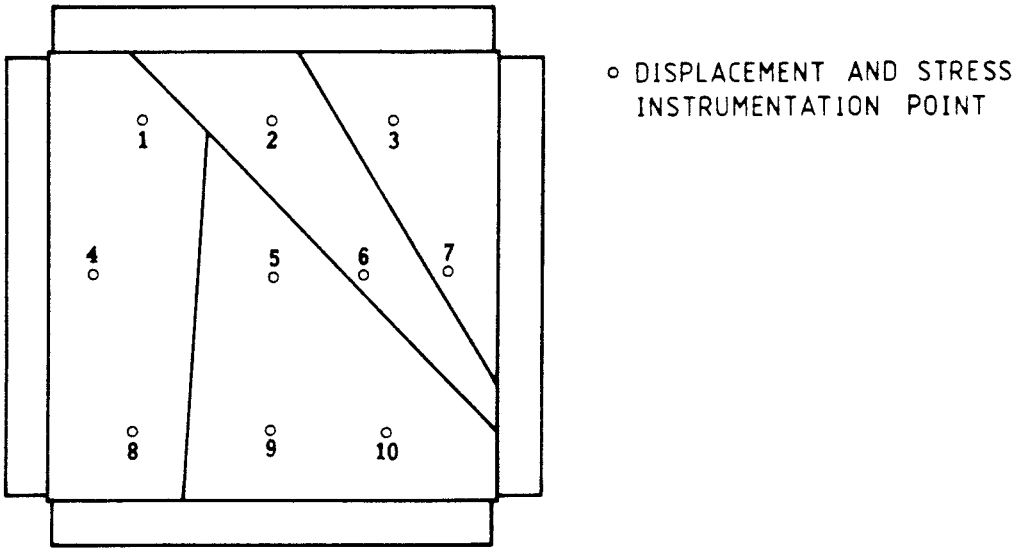

Figure 5-5 Instrumentation locations for load-displacement and load-stress studies.

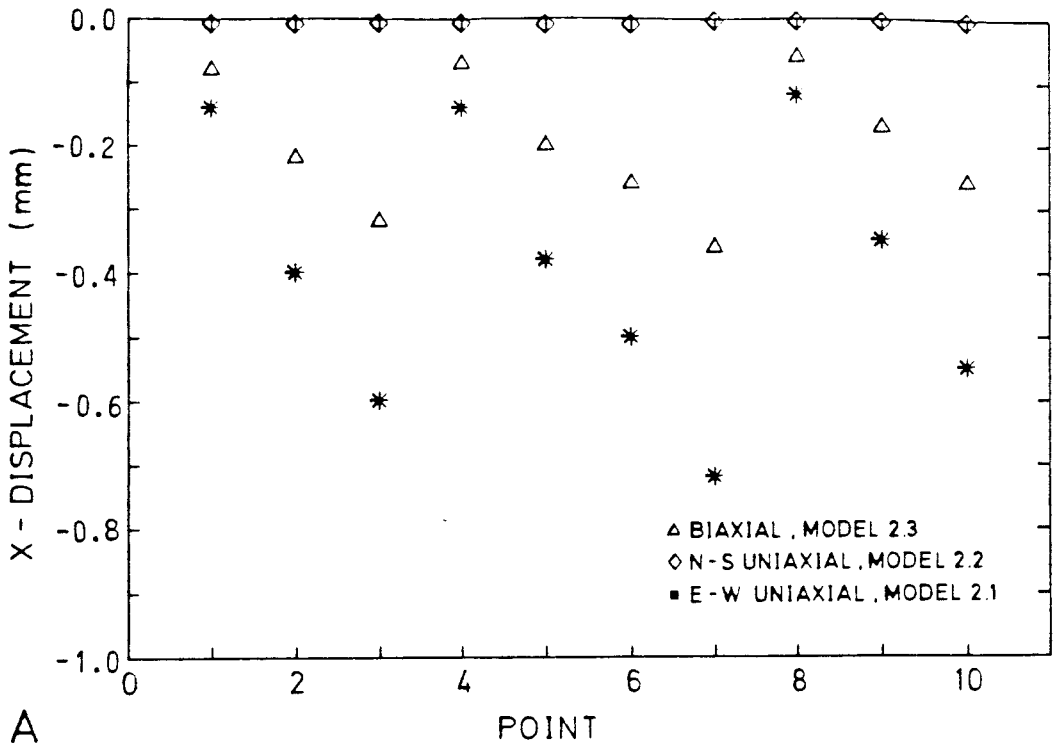

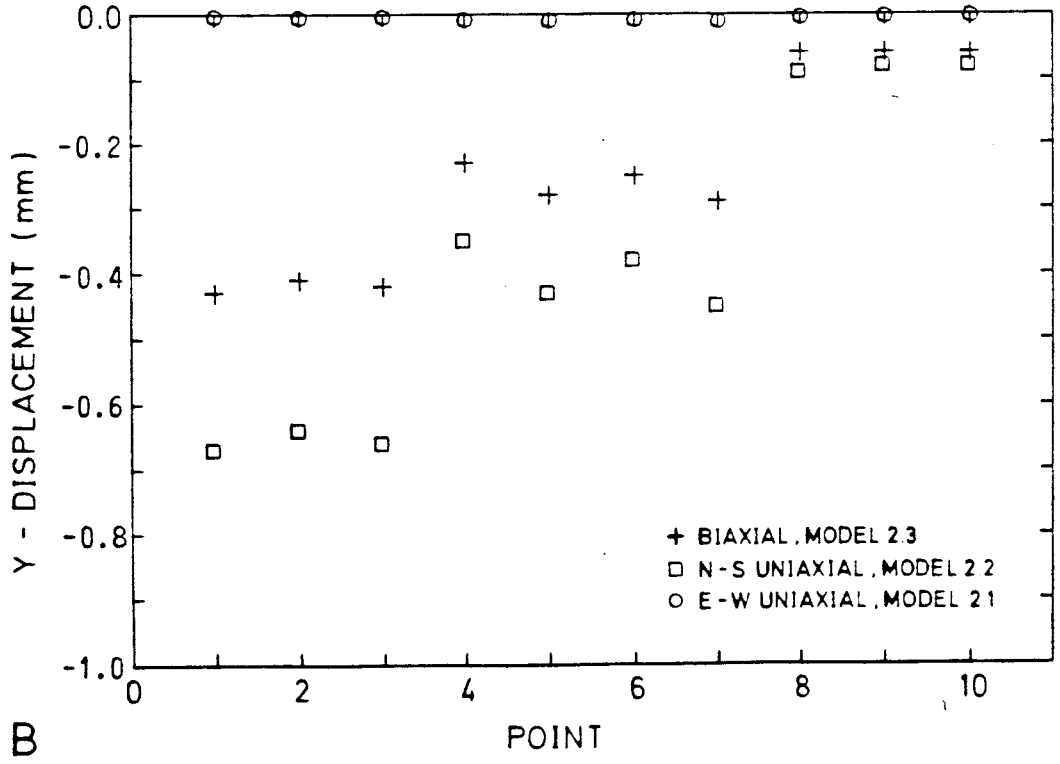

Figure 5-6 HNFEMP model of CSM block, Models 2.1, 2.2 and 2.3. Displacement of ten points in the block. A) x-displacement. B) y-displacement.

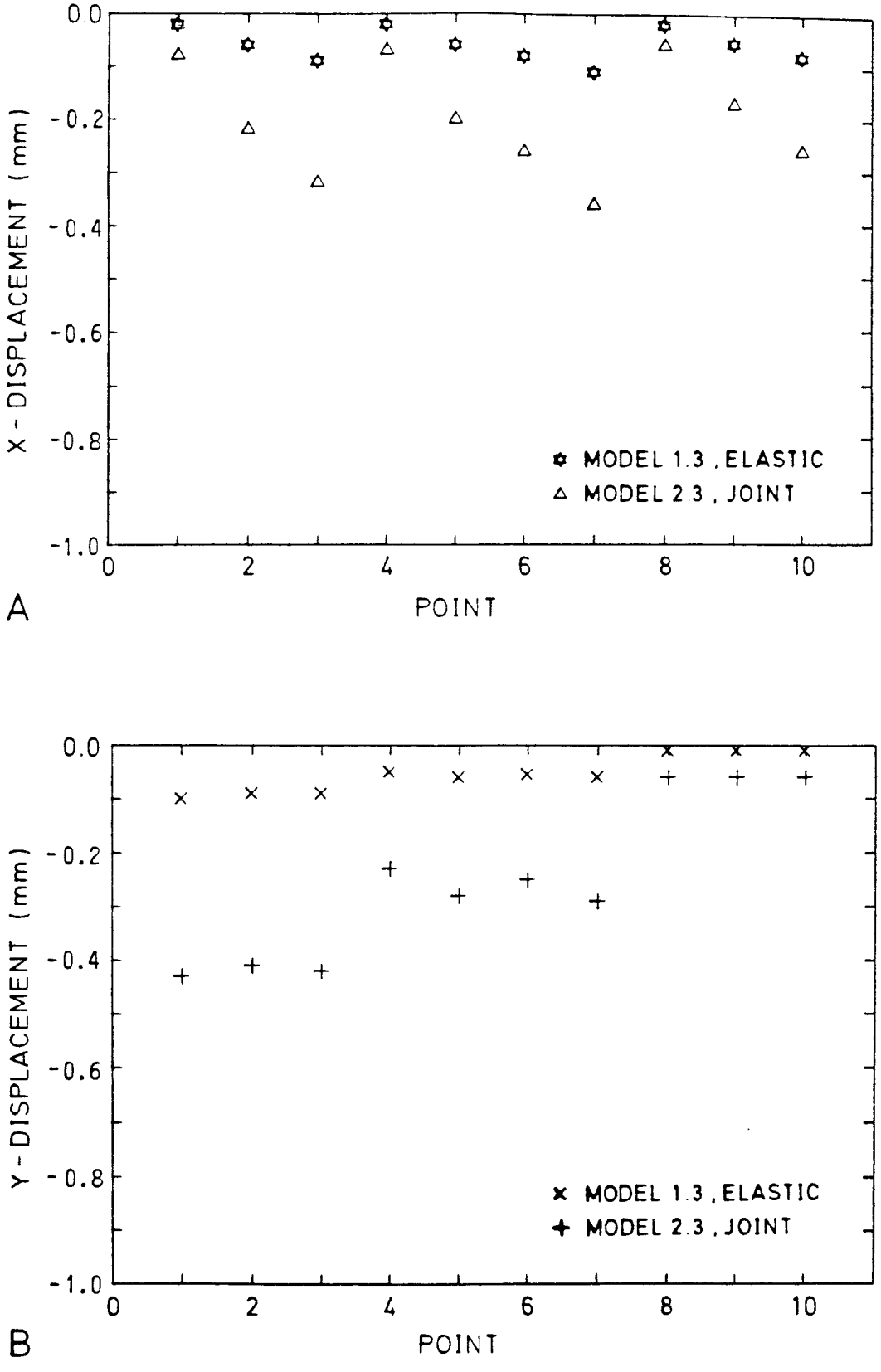

Figure 5-7 Deformation of instrumentation locations for Model 1.3 (elastic) and Model 2.3 (joints according to Barton's system). A) x-displacements. B) y-displacements.

Table 5-2 HNFEMP modelling of maximum stress and displacement at the instrumentation locations of the CSM block.

Loading Mode	Stress [MPa] Displacement [mm]	Material Model					
		Elastic	Joint				
		1	2	3	4	5	6
1 E-W	x-stress	5.16 (8)	5.20 (1)	5.30 (1)	5.70 (1)	5.20 (1)	5.60 (1)
	y-stress	1.77 (8)	4.40 (1)	3.05 (1)	1.40 (1)	4.65 (1)	1.35 (1)
	x-y-stress	0.002 (6)	0.03 (5)	0.08 (5)	0.25 (5)	0.02 (5)	0.20 (5)
	x-displacement	0.13 (7)	0.72 (7)	0.42 (7)	0.74 (7)	0.50 (7)	0.31 (7)
	y-displacement	0.0002(5)	0.011 (7)	0.006 (7)	0.02 (7)	0.007 (7)	0.006 (7)
2 N-S	x-stress	1.78 (8)	4.55 (1)	3.40 (1)	1.83 (1)	4.73 (10)	1.63 (10)
	y-stress	5.22 (8)	5.25 (7)	5.60 (10)	5.60 (10)	5.27 (10)	5.50 (10)
	x-y-stress	0.002 (3)	0.05 (5)	0.12 (5)	0.27 (5)	0.03 (5)	0.21 (5)
	x-displacement	0.0001(5)	0.01 (2)	0.005 (2)	0.01 (2)	0.006 (2)	0.004 (2)
	y-displacement	0.13 (3)	0.67 (3)	0.41 (3)	0.80 (3)	0.47 (3)	0.33 (3)
3 Bi-axial	x-stress	5.40 (8)	5.50 (1)	5.65 (1)	6.10 (1)	5.50 (1)	5.95 (1)
	y-stress	5.40 (8)	5.50 (10)	5.55 (10)	5.90 (10)	5.53 (10)	5.80 (10)
	x-y-stress	0.001 (6)	0.04 (5)	0.11 (5)	0.33 (5)	0.02 (5)	0.26 (5)
	x-displacement	0.105 (7)	0.36 (7)	0.26 (7)	0.60 (7)	0.25 (7)	0.26 (7)
	y-displacement	0.105 (3)	0.43 (3)	0.28 (3)	0.71 (3)	0.29 (3)	0.28 (3)

( ) instrumentation location, cf. Figure 5-5

In the modelling performed, the sensitivity of displacement to changes in stiffness can be studied. Plots of the y-displacement for instrumentation location 3 (close to the NE corner of the block) for the different material models under bi-axial and N-S uni-axial loading show that changes in shear stiffness at constant normal stiffness has only a small effect on the magnitude of displacement, Figure 5-8A. This is expected due to the confinement from the fixed boundaries. Changes in normal stiffness have a greater effect on displacements, particularly for bi-axial loading, cf. Figure 5-8B.

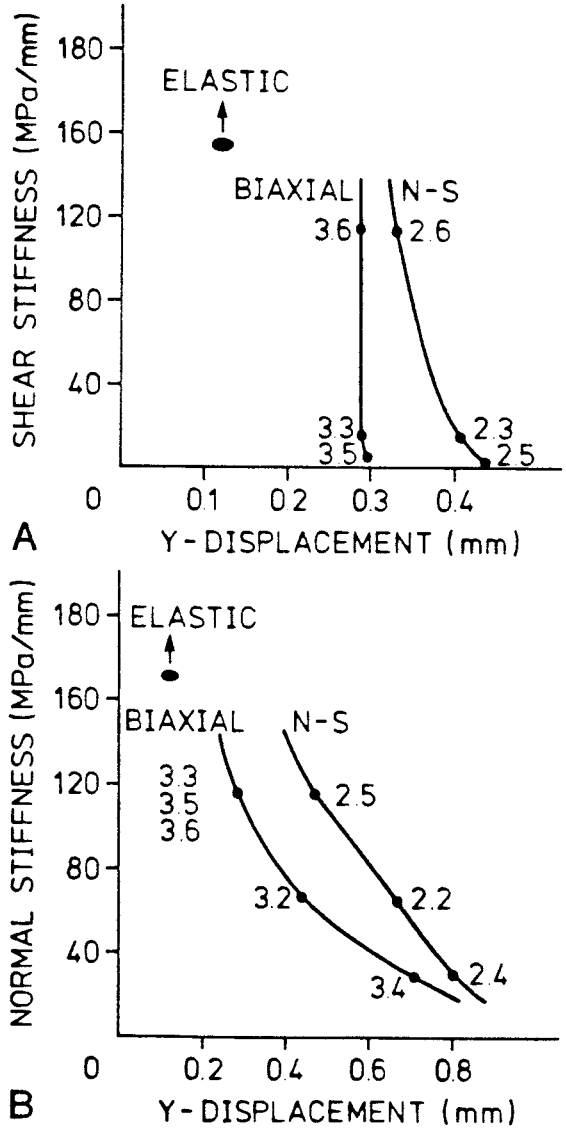

Figure 5-8 Stiffness versus y-displacement for instrumentation location No. 3 (NE corner) of the CSM block. Bi-axial and N-S uni-axial modelling. A) Shear stiffness vs. y-displacement. B) Normal stiffness vs. y-displacement.

5.4 Calculation of the effective Young's moduli

In the modelling of the CSM block with HNFEMP, the jointed rock mass behaves like an equivalent "continuum" material. From calculated displacements corresponding to the overall block deformation, the strains can be determined and from these strains and the applied loading, the effectiv Young's modulus can be calculated. To compare the results from the finite element modelling with results from the field tests and also to evaluate of these tests by alternative analytical methods, the four corner displacement stations (stations 1, 3, 8 and 10) suggested by Richardson were used, cf. Figure 5-5.

The method used for calculating the effective Young's modulus was as follows:

(1) The co-ordinates of the four corner stations were applied to the calculated x- and y-displacement records from the HNFEMP analysis and the strain was calculated, Figure 5-9.

(2) Due to the non-uniform strain distribution in the models, average strains between the four corners in the x- and y-directions were determined.

(3) From known loading conditions, σ_1, and the application of the theory of elasticity, assuming plane stress conditions, the Young's modulus was calculated as follows:

E-W uni-axial test

$$E_x = \frac{\sigma_x}{\varepsilon_x}$$

N-S Uni-axial test

$$E_y = \frac{\sigma_y}{\varepsilon_y}$$

Equal bi-axial test

$$E_x = \frac{\sigma_x}{\varepsilon_x}(1 - \nu_{xy})$$

$$E_y = \frac{\sigma_y}{\varepsilon_y}(1 - \nu_{yx})$$

where, ε_x and ε_y are the average strains in x- and y-directions and $\nu_{yx} = \nu_{xy} = 0.25$, for Poisson's ratio.

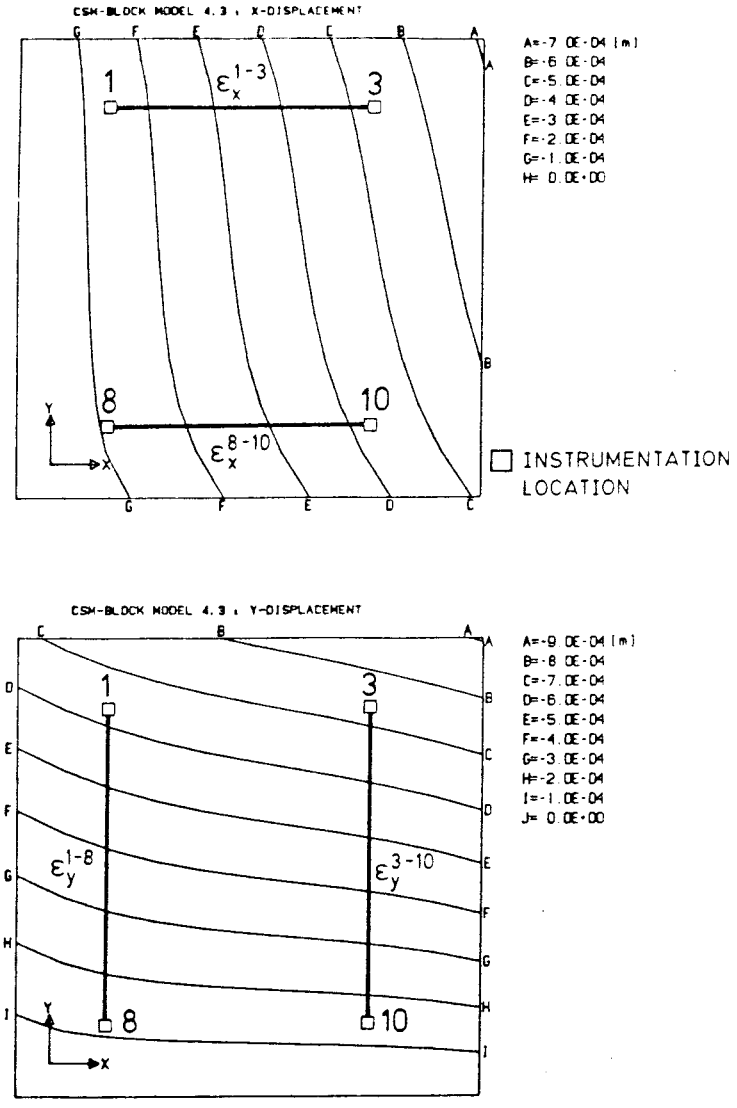

Figure 5-9 Determination of strains from calculated displacements of corner points. A) Strain in x-direction, ε_x. B) Strain in y-direction, ε_y.

More precise calculations of the effective Young's moduli may be performed, e.g. the rosette-analysis method applied to four triangles determined by the four corner array and its diagonals, see Richardson (1986). The calculated effective Young's moduli in the x- and y-directions for the rock mass defined by the four corner displacement stations in the CSM block are shown in Table 5-3. Elastic anisotrpy is apparent, and models having large stiffness parameters give large effectiv Young's moduli.

Table 5-3 Calculated effective Young's moduli for the rock mass defined by the four corner displacement stations 1, 3, 8 and 10 in the CSM block.

	Effective Young's moduli, E [GPa]									
Material Model	2 k_n = 67.2 k_s = 2.7		3 k_n = 117.3 k_s = 16.7		4 k_n = 35.4 k_s = 24.0		5 k_n = 117.3 k_s = 2.7		6 k_n = 117.3 k_s = 100.0	
Loading	E_x	E_y	E_x	E_y	E_x	E_y	E_x	E_y	E_x	E_y
1, E-W	13.6	--	23.7	--	13.1	--	19.7	--	31.9	--
2, N-S	--	13.4	--	22.7	--	10.9	--	18.9	--	28.2
3, Bi-axial	21.2	16.7	30.0	25.2	12.9	10.2	32.1	24.6	31.0	26.4
Av. E_x, E_y	17.4	15.0	26.8	24.0	13.0	10.6	25.9	21.8	31.4	27.3
Av. E	16.2		25.4		11.8		23.8		29.4	

6 COMPARISON OF NUMERICAL AND FIELD TEST RESULTS

For comparison of numerical results with data recorded in the field, and results from field data by techniques other than finite element analysis, the following tests are used. The principal investigator has also been cited:

1) Peak-load displacement vectors, CSM test (Richardson, 1986)
2) Effective Young's modulus, CSM test (Richardson, 1986)
3) Young's modulus for block, Terra Tek test (Hardin, 1981)
4) Young's modulus for rock, CSM tests (Brown, 1986)
5) Rock stresses, CSM tests (Brown et al., 1986)

6.1 Peak load displacement vectors, CSM test

With the fixed frame anchored into the mine back, absolute displacements of station points at various depths within the block during loading could be measured (Richardson, 1986), cf. section 3.1. Upper horizon test results are considered to be the most accurate and the least likely to be influenced by the attached bottom of the block. Peak load displacement vector plots for the three loading conditions are shown in Figure 6-1. To compare the calculated displacements with the measured absolute vectors for tests with model material 4, the calculated values were re-referenced with respect to a fixed point at the center of the block. The E-W and N-S uni-axial vectors show the results expected with displacement in the direction of the loading and lateral expansion. Vectors from equal-bi-axial tests show a general trend towards the centre of the block. The calculated vectors are valid for material model 4 based on parameters from the CSM block tests by Richardson (1986). In principle, there is fair agreement in vector orientation and length for the field tests and the HNFEMP modelling. Station No. 7 at the eastern end of the block showed greater tilting and a more erratic behaviour than most other stations.

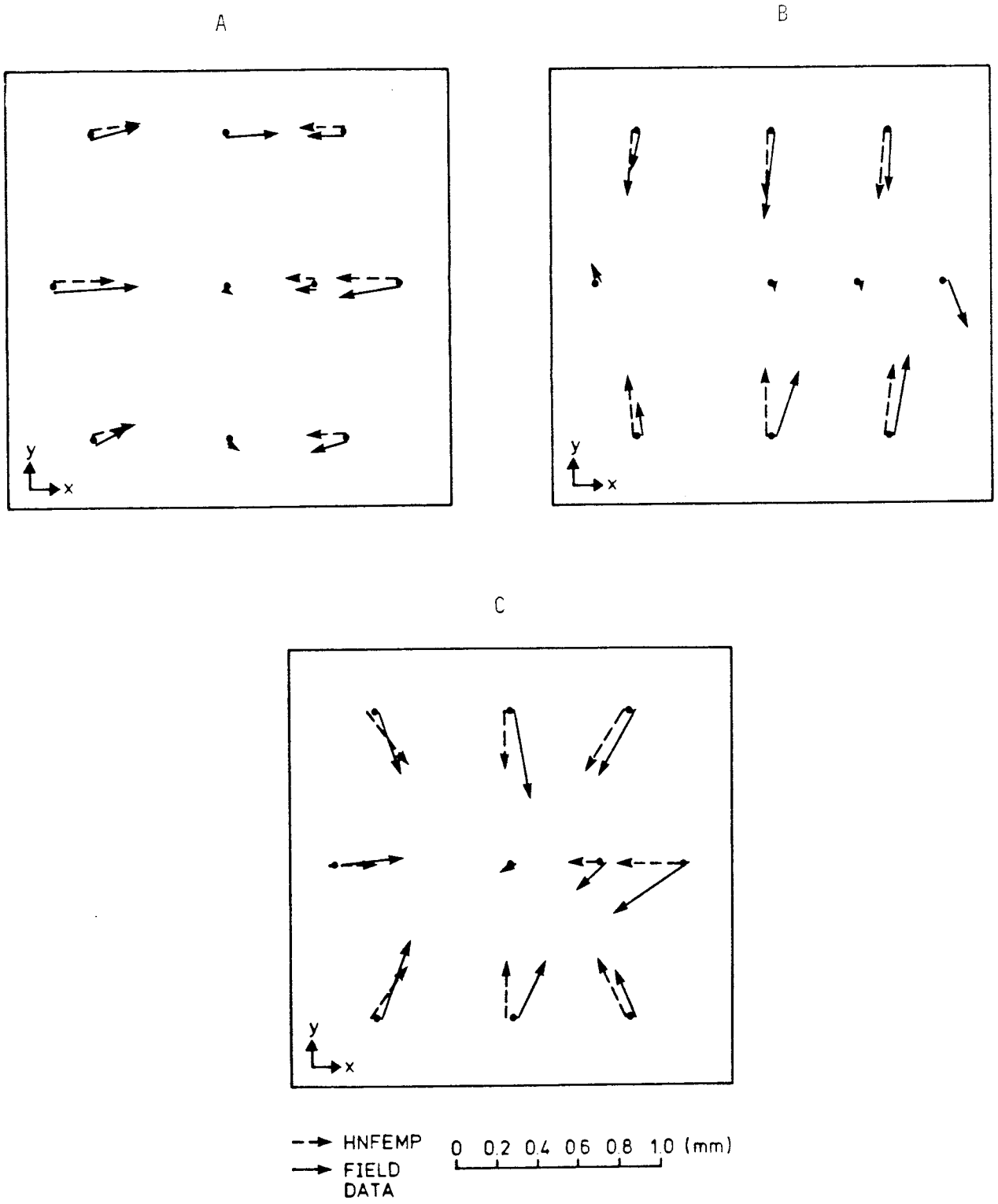

Figure 6-1 Displacement vectors at peak loads from field tests and modelling with material model 4, CSM test. A) E-W loading. B) Uni-axial N-S loading. C) Bi-axial loading.

According to Richardson (op. cit.) this is believed to reflect intense fracturing of this borehole. The maximum horizontal displacement at peak-load and the location of the corresponding instrumentation station are listed in Table 6-1. Modelling results always give smaller displacements than those obtained from the field tests. The discrepancies for the uni-axial loading cases are due to boundary constrains. Other material models give smaller displacement magnitudes, although vector orientations are similar for all models tested.

Table 6-1 Maximum peak-load horizontal displacements (mm).

Loading	CSM Block* Upper Level		Modelling HNFEMP, Material 4	
	x-displacement	y-displacement	x-displacement	y-displacement
1, E-W	0.34 (7)	0.14 (9)	0.33 (7)	0.02 (7)
2, N-S	0.16 (9)	0.46 (2)	0.01 (9)	0.37 (1)
3, Bi-axial	0.38 (7)	0.43 (2)	0.29 (7)	0.31 (1)

* After Richardson (1986)

( ) Instrumentation location

6.2 Effective Young's moduli, CSM test

The deformation of the block is composed of an elastic and inelastic parts. Due to the stiff rock material, the low applied stresses and the recording of very small permanent deformations after each loading cycle, it is believed that linearly elastic behaviour dominates. The four corner displacement stations 1, 3, 8 and 10 were selected for computation of the overall strains in the block. This first was done for the CSM block test and later the discontinuous deformation analysis (Richardson, 1986) and also for the finite element analysis. Values for the effective Young's moduli for the CSM test were

determined from a linear regression of the entire upload portion of the stress-strain curve and secant values at peak-load. These values compare favourably and average values of E_x and E_y have been calculated for each of the loading sequences, cf. Table 6-2.

Table 6-2 Calculated effective Young's moduli from strain analysis, DDA and HNFEMP analysis.

	Effective Young's Moduli, E [GPa]									
	Strain Analysis From Block Corner Stations*						Discontinuous Deformation Analysis* (DDA)		Finite Element Analysis Model Material 4 (HNFEMP)	
	Linear Regression Upload Portion		Secant Value at Peak Load		Average Value					
Test	E_x	E_y	E_x	E_y	E_x	E_y	E_x	E_y	E_x	E_y
1, E-W	15.9	--	16.4	--	16.2	--	12.0	--	13.1	--
2, N-S	--	13.9	--	14.1	--	14.0	--	13.2	--	10.9
3, EB I(a) EB II	21.9	12.0	23.7	11.8	22.8	11.9	14.3	10.2	12.9	10.2
Av. E_x, E_y	18.9	13.0	20.1	13.0	19.5	13.0	13.2	11.7	13.0	10.6
Av. E	15.9		16.5		16.2		12.4		11.8	

* After Richardson (1986)

An application of the Discontinuous Deformation Analysis method (DDA) offers an alternative approach where all the available displacement data from the measuring stations are used. The single-block DDA model represents the unique, best-fit equivalent continuum model and the calculated properties are pre-

sented in Table 6-2. Results from the DDA analysis are considered to be the most reliable equivalent rock mass properties obtained by Richardson (1986). The average Young's modulus of 12.0 GPa and the moduli for bi-axial loading with the finite element analysis agrees very closely with the results of the DDA. This gives considerable confidence in the modelling of regularly jointed rock masses with the smeared out approach.

If we assume the CSM block contained only the two orthogonal sets of joints, the effective Young's moduli may be determined by the following relations:

$$E_x^* = \frac{1}{\frac{1}{E} + \frac{1}{k_n s_x}} = \frac{1}{\frac{1}{60} + \frac{1}{35.4 \times 1.0}} = 22.3 \text{ GPa} \qquad (6.1)$$

$$E_y^* = \frac{1}{\frac{1}{E} + \frac{1}{k_n s_y}} = \frac{1}{\frac{1}{60} + \frac{1}{35.4 \times 0.6}} = 15.7 \text{ GPa} \qquad (6.2)$$

where E is the Young's modulus of intact rock, k_n is the normal stiffness and s is the spacing. The values of the parameters are those for model material 4. If we compare the results in Eqs. (6.1) and (6.2) with data from the HNFEMP modelling, Table 6-2, the introduction of the third diagonal set of joints will reduce the effective Young's moduli of the block by E_x/E_x^* = 13.3/22.3 = 0.6 and E_y/E_y^* = 10.9/15.7 = 0.7 respectively. Hence, diagonal joints have a significant effect on the overall deformability of the block.

At present there is no analytical solution to the 2-dimensional problem of three intersecting sets of joints in an elastic rock mass. However, if it were solved, the constitutive equation will contain some 13 independent elastic constants (Amadei, personal communication).

6.3 Young's moduli for the block, Terra Tek

In an attempt to measure the Young's moduli for the block, the Terra Tek research group measured the aperture of the boundary

crack in the grout above the flatjacks when the block was loaded. Several Whittemore pins were located across these boundaries for monitoring the aperture. A solution for the elastic deformation of a vertical rectangle subjected to a uniform horizontal stress, and the expression for the Young's modulus of the block was presented by Hardin (1981). Values of the Young's modulus for the block, included corrections for a deformation of about 25 cm of intact rock in each gauge, assuming E (intact rock) = 50 GPa, are tabulated in Table 6-3. Although there is obviously large scatter in the data, depending upon loading level, loading and unloading, the average moduli for each loading direction and for all recorded data have been calculated. The data is very consistent with that from other field tests in that loading in the N-S direction gives the least value for Young's modulus.

Results from HNFEMP modelling using a model material and strain determination for the overall block are tabulated in Table 6-3. The values are found to be in close agreement with the data from the field tests conducted by Terra Tek. The stiffness values that were used in the modelling are determined from measurements of Whittemore pins located across visible joints intersecting the block, cf. Table 5-1. Although the measuring technique with the Whittemore pins is crude it proved to give the most reliable field data of all the rock mechanics instruments installed by Terra Tek.

In the validation of HNFEMP against field test results the most reliable data from Terra Tek field tests were used. The calculated Young's modulus for the block from overall block displacement data obtained by modelling with HNFEMP was almost idential to that derived from the analysis of boundary crack aperture. The discrepancy in magnitudes between the Young's modulus for the block (Table 6-3) and the effective Young's (Table 6-2) could reflect some surface decoupling in the measurements at one stage.

Table 6-3 Young's modulus for the block obtained from monitoring boundary crack aperture and HNFEMP modelling.

Loading	Young's modulus (GPa) for the block					
	Terra Tek Boundary Crack Monitoring†					Finite Element Analysis Model Material 3 (HNFEMP)
	Loading (MPa)		Unloading (MPa)		Average	
	0-3.45	3.45-6.9	6.9-3.45	3.45-0		
1, E-W	14.9	35.6	28.8	17.1	24.1	23.7
2, N-S	19.2	20.6	26.1	18.3	21.1	22.7
3, Bi-axial	39.2*	18.6	34.7	17.8	27.6	25.6
				Average	24.2	24.0

* Av. of two tests

† After Hardin (1981)

6.4 Rock deformation modulus, CSM tests

As part of the rock stress measurement program for the CSM block tests, detailed definition of the rock deformability was conducted (Brown, 1986). Dilatometer tests using the CSM-cell were performed at the block midplane in each borehole to determine the rock deformability and the relative stiffness of different zones in the block. The results of these tests are shown in Figure 3-4. Young's modulus for the rock varied from 8 GPa to 68 GPa with an average value of 20.9 GPa. Only material models with fairly large stiffness values can give an effective Young's modulus in the range of 20 GPa, cf. materials 2, 3 and 5 in Table 5-3. But here we also have to consider volume effects on Young's modulus for the rock. Figure 6-2 summarizes

results from the CSM tests on the block where laboratory tests on intact rock core samples give the largest modulus, cf. section 2.3, followed by borehole dilatometer data recorded by Brown (1986). In the diagram Young's modulus from borehole tests on migmatitic gneiss with a large dilatometer of diameter 45 cm (El Raaba, 1981) is also presented. The jump between the laboratory test results and the dilatometer results represents the change from intact rock modulus to rock mass modulus. The step from dilatometer results to the overall block results given by corner strain analysis, DDA and finite element modelling indicates a change in the volume of the block. Data points for relative strain from an array of 45 extensometers given by the 10 monitoring stations (Figure 5-5) made it possible to calculate Young's moduli for stations with different lengths and these data points and the results presented in Figure 6-2 enabled Richardson (1986) to draw the curve shown in the same figure. These results suggest that the critical size for an equivalent continuum approach of the block has been reached.

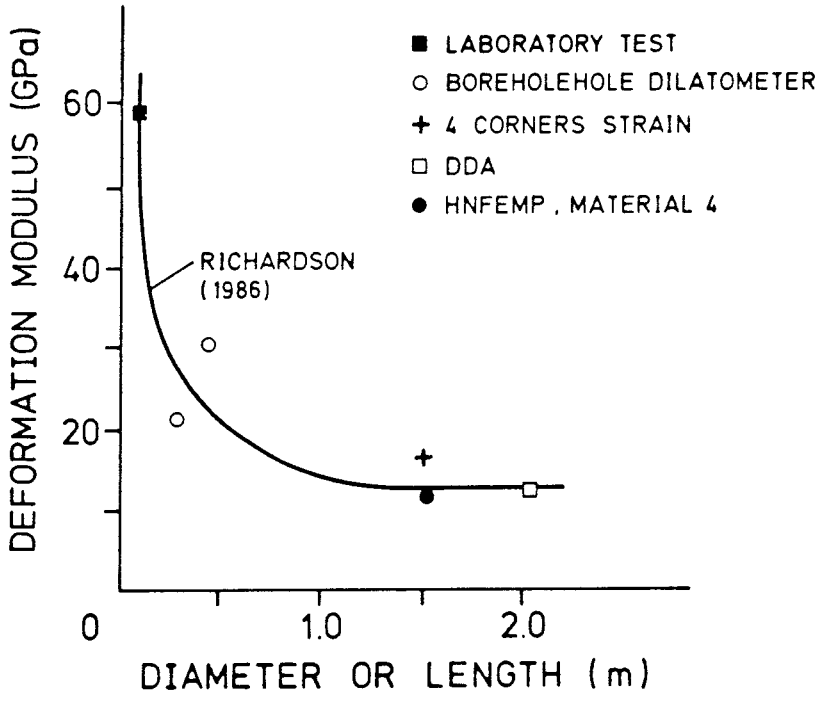

Figure 6-2 Measured and calculated Young's modulus versus diameter/length for the CSM block test. Modelling results agree with data presented by Richardson (1986).

6.5 Rock stresses

An extensive effort was made to measure the stress distribution in the CSM block tests using point measurements (Brown, 1986, Brown et al., 1986). Although the tests were successful and the USBM Borehole Deformation Gage (BDG) and the Luleå University of Technology gauge (LuT) operated satisfactorily, the results exhibited large scatter. Incorporation of rock mass anisotropy due to the major foliation and different rock mass modulus due to variation in rock types into the analysis of stresses did not affect the results significantly (Brown, 1986).

Peak-load principal stress in the horizontal plane from measurements by the BDG and LuT method respectively are shown in Figures 6-3A, B. Excluding the two measuring points in the centre of the block (encircled), the directions obtained are in fair agreement, while the BDG-tests gave stresses that were about 20 % higher on average than those obtained with the LuT gauge.

Simultaneous plotting permits direct comparison of the two field methods and the results from the HNFEMP modelling, Figure 6-3A-C. Modelling the jointed block as an equivalent material gives an uniform stress distribution and a very consistent direction of stresses for the uni-axial loading cases. The most striking difference between the monitored and the modelled stresses is the low stresses recorded in the central portion of the block. The origin of this variation is not fully understood, although it is believed that decoupling effects caused by discontinuities and highly localized variations of Young's modulus are the most important contributing factors (Brown et al., 1986).

To asses the modelling of the stresses in the CSM block the recorded average maximum horizontal stress have been calculated for the 13 (LuT) and 17 (BDG) borehole locations respectively, Table 6-4. The results show that the average stress calculated for the borehole deformation gauge (including the high values in the centre) is in close agreement with the applied load. The

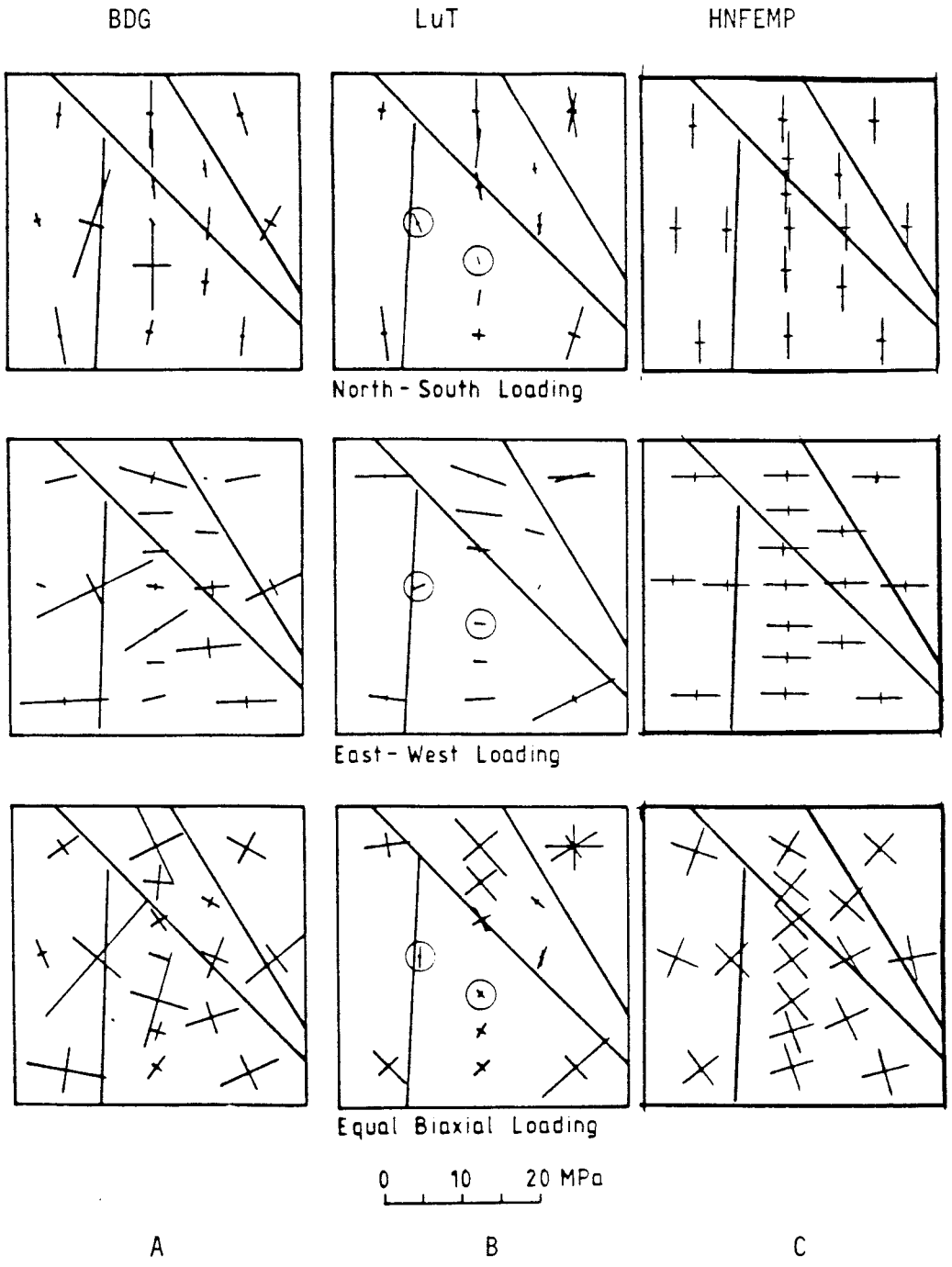

Fig. 6.3 Horizontal principal stresses in the mid-plane of the CSM block. A) Monitoring by USBM Borehole Deformation Gauge (BDG). B) Monitoring by Luleå University of Technology Gauge (LuT). C) Modelling by HNFEMP, model material 4.

average stresses for the LuT measurements are about 20 % less. The stress magnitudes for HNFEMP model were determined at locations where corresponding field measurement were taken. The average maximum horizontal principal stress slightly exceeded the applied stress, cf. Table 6-4. This is due to a Poisson's effect from the fixed boundaries in the cases of uni-axial loading.

Brown et al. (1986) concluded that pointwise measurements of the BDG and LuT types might not provide useful results when they are used for stress monitoring in jointed rock masses subjected to low stresses. This statement is supported from a recent study by Leijon (1988), where he states that the measuring error for the LuT method produces a standard deviation of 2 MPa for the mean stress independently of the stress level. He also found that the Young's modulus does not have a significant effect on the stress state in the rock mass when the LuT overcoring technique is used. For pointwise measurements with the LuT gauge, the three-dimensional stress state was recorded and the magnitudes of the least principal stress, σ_3, were much lower than the almost horizontal maximum and intermediate principal stresses. Further-more, the sign of σ_3 changed non-systematically between compression and tension. Hence, at present, it is believed that stress monitoring with the USBM borehole deformation gauge in the CSM block gave more reliable results, and these should be used in a comparison with the modelling results.

Leijon (1988), in a recent study, showed that a large data set of stress measurements from individual locations (boreholes) fitted normal distributions closely. This enables the application of locationwise averaging of stress tensor components, and it supports the method of averaging the maximum stresses used in presenting data for the CSM block, cf. Table 6-4.

It can be concluded that the BDG gauge provides the most reliable stress monitoring method. The CSM block is sufficiently large to be representative of the rock mass (cf. Fig. 6.2), and stresses are therefore assumed to be normally distributed and

Table 6.4 Applied stress and recorded average maximum horizontal stress in mid-plane of CSM block.

Test	USBM Borehole Deformation Gauge (BDG)*		Luleå University of Technology Gauge (LuT)**		HNFEMP Material Model 4	
	Applied Load [MPa]	Av. max. Horizon. Stress [MPa]	Applied Load [MPa]	Av. max. Horizon. Stress [MPa]	Applied Load [MPa]	Av. max. Horizon. Stress [MPa]
1, E-W	5.2	5.5	5.2	3.5	5.1	5.4
2, N-S	5.3	4.9	5.3	3.9	5.1	5.4
3, Bi-axial	5.4	5.7	5.4	4.2	5.4	5.5

* After Brown (1986)

** After Brown et al. (1986)

the arithmetric means of maximum horizontal stress can be calculated. Average maximum horizontal stresses from BDG measurements are in fair agreement with applied loads as are those from the HNFEMP modelling.

7 CONCLUSIONS

1. A series of mechanical and hydrological experiments is being conducted on an in-situ block of fractured gneissic rock at the Colorado School of Mines Experimental Mine at Idaho Colorado - the CSM block. This block was selected for the following reasons:
   i) numerous studies and careful documentation of results have been performeed, ii) superior three-dimensional mechanical (displacements and stresses) monitoring of any block test, and iii) a joint structure that allows modelling of the block by an equivalent continuum approach, where the joints are smeared out in the rock mass, and also by a discontinuum approach where discrete joints are simulated. In this report, we use the continuum approach to simulate the response of the CSM block subjected to mechanical loading.

2. The mechanical properties of the CSM block and their method of determination form an important task of this study. Based on numerous laboratory tests, the values of the elastic properties of the intact rock for the modelling are taken to be $E = 60$ GPa and $\nu = 0.25$. Joint strengths are taken from the determination by Barton and reported by Hardin (1981). The average parameters for the three sets of joints are as follows:

Joint roughness coefficient, JRC	8.2
Joint compressive strength, JCS	62.2 MPa
Residual friction angle, Φ_r	26.5^o
Dilation angle, d_n	6.7^o
Tensile strength, τ_s	0 MPa
Cohesion, c	0.4 MPa

   These values were assumed constant throughout the study of the equivalent continuum models.

3. Six material models were tested. One of these is a linearly elastic solid. The others are equivalent continuum models

Joint Stiffness MPa/mm	Material Models					
	1 Isotropic Linear Elastic	2 Field Data Bartons System	3 Block Test Terra Tek	4 Block Test CSM	5 Sensitivity Analysis	6 Sensitivity Analysis
Normal	∞	67.2	117.3	35.4	117.3	117.3
Shear	∞	2.7	16.7	24.0	2.7	100.0

with different stiffnesses, as presented above.

Material model 2 has stiffnesses obtained from the linear portion of the shear stress versus shear displacement curves and the normal stress versus closure respectively, according to the Barton and Bandis joint modelling system, cf. section 2.4. Results from block tests by Terra Tek and CSM form the basis for stiffnesses of material models 3 and 4. To conduct a sensitivity analysis, two additional models were added to this study, models 5 and 6.

4. In Chapter 4 the two principal approaches applied in modelling jointed rock masses are discussed. A jointed non-linear rock continuum model formulated by Olofsson (1985) has been used in this study. This model describes a representative two-dimensional element of a jointed rock mass containing any number of continuous sets of joints with any orientation. Any set of joints can fail in shear or normal failure, and the parameters governing the yield function are extracted from the classical parameters of Barton (JCS, JRC, L). The joint model itself is tested against simple shear-box experiments results are obtained. The equivalent rock mass model for the mechanical behaviour of continuous sets of joints have been implemented into a finite element code called FEMP, and the version containing the non-linear model of the rock joints is called HNFEMP (Hans Non-linear FEMP) after the late Hans Larsson.

5. A continuum model consisting of two orthogonal joint sets with joint spacings of 0.6 m and 1.0 m and one diagonal set with a joint spacing 0.75 m has been applied to the CSM block. The six different material models were tested for east-west uni-axial loading, north-south uni-axial loading and bi-axial loading at peak-load. Three-sides rigid boundary were applied to the uni-axial loadings and two-sides to the bi-axial, cf. Figure 5-2. In future modelling we would suggest that a symmetry point is fixed inside the model and appropriate boundary conditions are applied.

6. Results from a total of 18 different models are presented as graphical output in following forms:

   - principal stress vectors
   - displacement vectors
   - contour plots of x-stress, y-stress and x-y-shear stress
   - contour plots of x-, and y-displacement

   Plots for selected models are shown in Appendix 1. Anisotropy in displacements due to different joint spacing is clearly shown. Displacements at discrete points corresponding to instrumentation locations in the CSM test are presented. A model with Barton joint properties (model 2) show displacement magnitudes double those for the linearly elastic model.

7. A sensitivity analysis of displacement as a function of stiffness has been conducted. For models under N-S uni-axial loading and bi-axial loading, changes in shear stiffness at constant normal stiffness is found to have only a small effect on the y-displacement. Changes in the normal stiffness have a significant effect on he displacement data especially for bi-axial loading, cf. Figure 5-8.

8. From displacements modelled by HNFEMP, strains from four corner instrumentation stations have been calculated. The effective Young's modulus is determined from the known applied stresses. The Young's modulus in the N-S direction

of the block is 20-30 % less than the Young's modulus in the E-W direction. The average Young's modulus, $(E_x + E)/2$, varies between 29.2 GPa (model material 6) and 12.0 GPa (model material 4), cf. Table 5-3.

9. To demonstrate the applicability of the smeared out approach to rock mass modelling, comparison between model predictions of the block behaviour and the recorded and analysed field data is essential. The following tests are used for the validation. The principal investigators are also cited:

   Peak-load displacement vectors, CSM test (Richardson, 1986)

   Equivalent modulus of deformation, CSM test (Richardson, 1986)

   Block deformation modulus, Terra Tek test (Hardin, 1981)

   Rock deformation modulus, CSM tests (Brown, 1986)

   Rock stresses, CSM tests (Brown et al., 1986)

10. In principle there is a fair agreement in the magnitude and orientation of the displacement vector obtained from the field tests and the HNFEMP modelling. Modelling results always give smaller magnitudes in displacement than those obtained from the field data. Maximum displacement at peak-load for the upper horizon in the block was 0.46 mm. This was recorded for instrumentation station NO. 2 during N-S loading. Maximum displacement from HNFEMP modelling was 0.37 mm and appeared at instrumentation station No. 1, cf. Table 6-1 and Figure 5-5.

11. The effective Young's modulus of the CSM block was determined from the calculated overall strains between four block corners and discontinuous deformation analysis (DDA). The average Young's modulus of 12.4 GPa calculated from DDA is found to be in good agreement with the result (12.0 GPa) of the finite element modelling with the stiffness parameters suggested by Richardson (1986), material model 4.

12. Closed form expressions for the effective elastic moduli of a rock mass containing two sets of orthogonal joints can be

found. At present, there is no analytical solution to the corresponding problem for a rock mass with three intersecting joints sets. From the modelling results, it is demonstrated that the introduction of a third, diagonal set of joints to the CSM block will cause a reduction in the effectiv modulii of by a factor of 0.6 in the x-direction and 0.7 in the y-direction respectively.

13. The Terra Tek reserch group measured the aperture of the boundary crack in the grout above the flatjacks. They calculated the effectiv elastic modulus of the block. Using the stiffness values suggested gested by Terra Tek, material model 3, the modulus was calculated and the results are in close agreement with the field data, cf. Table 6-3.

14. The effectiv elastic modulus of the rock is known to depend on the volume of the rock considered. Elastic modulus versus diameter/length from different tests on the CSM block were collected and plotted. The result suggest that the critical size for an equivalent continuum approach of the block had been exceeded and the modelling approach applied in this work is therefore valid.

15. Stress monitoring during flatjack loading of the CSM block was conducted with two instrumentation systems - the USBM Borehole Deformation Gauge (BDG) and the Luleå University of Technology gauge (LuT). Excluding a few measuring stations at the centre of the block, the monitored directions of the principal horizontal stress were in fair agreement with the modelled results. Further, the magnitude of the average maximum horizontal stress from the BDG monitoring agreed best with the results of the modelling and the applied loading from the flatjacks.

8 ACKNOWLEDGEMENTS

U. Singh and T. Olofsson made important improvements of the code HNFEMP and offered valuable suggestions for the completion of this report.

Parts of this study were conducted during a sabbatical leave of O. Stephansson to the Colorado School of Mines. The helpful attitude and stimulating discussions with W. Hustrulid and his students are gratefully acknowledged.

G. Bäckblom made valuable comments and suggestions for improvements to the first draft of this report. G. Olofsson typed the manuscript, M. Leijon made the drawings and P. Digby corrected the English. The authors are grateful for their help.

9 REFERENCES

Barton, N.R. and Bandis, S.C. 1982. Effect of block size on the shear behaviour of jointed rock. Proc. 23rd U.S. Symposium on Rock Mechanics, Berkeley, California, pp. 739-760.

Barton, N.R., Bandis, S.C. and Bakhtar, K. 1985. Strength, deformation and conductivity coupling of rock joints. Int. J. Rock Mech. Min. Sci. & Geomech. Abstr., 22 (3), pp. 121-140.

Barton, N.R., Harvik, L., Christianson, M., Bandis, S.C., Makurat, A., Chryssanthakis, P. and Vik, G. 1986. Rock Mechanics modelling of the Ekofisk reservoir subsidence. Proc. 27th U.S. Symposium on Rock Mechanics. Univ. of Alabama, Tuscaloosa, June 23-25, 1986, pp. 267-274.

Barton, N.R., Monsen, K. and Chryssanthakis, P. 1988. Validation of μDEC against Colorado School of Mines block test data. Technical Report. Swedish Nuclear Fuel and Waste Management Co., Stockholm.

Brown, S.M. 1986. Stress fields in jointed rock. M.S. thesis T-3152, Colorado School of Mines, Golden, Colorado. 251 p.

Brown, S.M., Hustrulid, W.A. and Richardson, A.M. 1985. A study of the validity of stress measurements in jointed crystalline rock. Proc. 26th U.S. Symposium on Rock Mechanics, Rapid City, S. Dakota, pp. 1247-1254.

Brown, S.M., Leijon, B.A. and Hustrulid, W.A. 1986. Stress distribution within an artificially loaded, jointed block. Proc. Int. Symposium on Rock Stress and Rock Stress Measurements, Stockholm, September 1-3, 1986, pp. 429-439.

Costin, L.S. and Chen, E.P. 1988. An analysis of the G-Tunnel heated block experiment using a compliant-joint rock-mass model. Proc. 29th U.S. Symposium on Rock Mechanics, Minneapolis, Minnesota, June 13-15, 1988. (Preprint)

Cundall, P.A. 1980. UDEC - A generalized distinct element program for modelling jointed rock. Report PCAR-1-80, Peter Cundall Associate; Contract DAJA 37-79-C-0548, European Research Office, U.S. Army, March 1980.

El Raba, A.W.M.A. 1981. Measurements and modelling of rock mass response to underground excavation. M.S. thesis T-2470, Colorado School of Mines, Golden, Colorado, U.S.A.

Goodman, R.E. 1976. Methods of geological engineering in discontinuous rocks. West Publ. Co., St Paul.

Hardin, E.L., Barton, N.R., Lingle, R., Board, M.P. and Voegele, M.D., (1982). A heated flatjack test to measure the thermomechanical and transport properties of rock masses. Office of Nuclear Waste Isolation, Columbus, OH, ONWI - 260, p. 1983.

Hart, R.D., Cundall, P.A. and Cramer, M.L. 1985. Analysis of a loading test on a large basalt block. Proc. 26th U.S. Symposium on Rock Mechanics, Rapid City, S. Dakota, June 1985, pp. 759-768.

Jakubick, A.T. 1983. Vacuum logging for measurement of the integrity of the near-excavation zone. Proc. Int. Symposium on Field Measurements in Geomechanics, Vol. 1, pp. 166-178.

Larsson, H., Olofsson, T. and Stephansson, O.1985. Reinforcement of jointed rock mass - non-linear continuum approach. Proc. Int. Symposium on Fundamentals of Rock Joints, Björkliden, September 15-20, 1985, pp. 567-577.

Leijon, B. 1988. Relevance of pointwise rock stress measurements - an analysis of overcoring data. Int. J. Rock Mech. Min. Sci. & Geomech. Abstr. (Manuscript)

Montazer, P., Chitombo, G., King, R. and Ubbes, W. 1982. Spatial distribution of permeability around CSM/ONWI Room, Edgar Mine, Idaho Springs, Colorado. Proc. 23rd U.S. Symposium on Rock Mechanics, Berkeley, California, pp. 47-56.

Nilsson, L. and Oldenburg, M. 1983. FEMP - An interactive, graphic finite element program for small and large computer system. Technical Report 1983:07 T, Luleå University of Technology, Luleå, Sweden.

Pande, G.N. 1985. A constitutive model of rock joints. Proc. Int. Symposium on Fundamentsls of Rock Joints, Björkliden, September 15-20, 1985, pp. 429-439.

Richardson, A.M. 1986. In-situ mechanical characterization of jointed crystalline rock. Ph.D. thesis T-3256, Colorado School of Mines, Golden, Colorado. 543 p.

Richardson, A.M., Hustrulid, W.A., Shi, G. and Lindner, E. 1985. A mechanical study of the influence of joints on block test results. Proc. Int. Symposium on Fundamentals of Rock Joints, Björkliden, September 15-20, 1985, pp. 143-152.

Rosasco, . 1985. Geometric continuity and physical characteristics of structural descontinuities at the ONWI test site, CSM Experimental Mine, Idaho Springs, Colorado. M.S. thesis ER-2453, Colorado School of Mines. 201 p.

Sour, L.E. and Ubbes, W. 1987a. Fracture flow response to applied stress: A field study. Proc. 28th U.S. Symposium on Rock Mechanics, Tucson, Arizona, pp. 501-508.

Sour, L.E., Richardson, A.M., Brown, S.M., Hustrulid, W.A. and Lindner, E.N. 1987b. A field study of coupled mechanical-hydrological processes in fractured crystalline rock. In: Tsang (Ed) Coupled Processes Associated with Nuclear Waste Repositories. Academic Press, New York, pp. 699-710.

Stephansson, O. 1987. Modelling of crustal rock mechanics for radioactive waste storage in Fennoscandia - Problem definition. Technical Report 87-11, Swedish Nuclear Fuel and Waste Management Co., Stockholm, May 1987. 79 p.

Swedish Nuclear Fuel and Waste Management Company. 1986. Final Storage of Nuclear Fuel Research and Development Program 1987-1992. SKB R & D Program 86. Swedish Nuclear Fuel and Waste Management Co., Stockholm, September 1986. 84 p.

Zienkiewics, O.C. and Pande, G.N. 1977. Time-dependent multilaminate model of rocks - A numerical study of deformation and failure of rock masses. Int. J. Numerical and Analytical Meth. in Geomech., Vol. 1, pp. 219-247.

Zimmerman, R.M. and Blanford, M.L. 1985. Evaluation of the accuracy of continuum-based computational models in relation to field measurements in welded tuff. Proc. Int. Symposium on Fundamentals of Rock Joints, Björkliden, September 15-20, 1985, 233-245.

LIST OF APPENDICES

ELASTIC CSM-BLOCK MODEL WITHOUT FAULTS 1.3 : INITIAL STRESS VECTOR

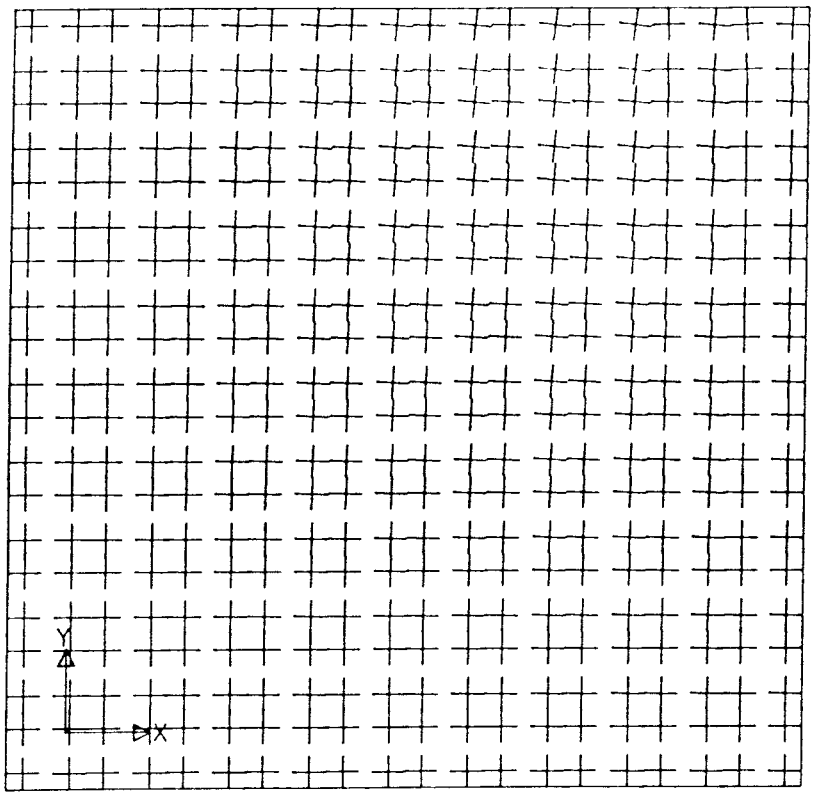

FACTOR
1.0E-7

0 10[MPa]

ELASTIC CSM-BLOCK MODEL WITHOUT FAULTS 1.3 : INITIAL X-STRESS

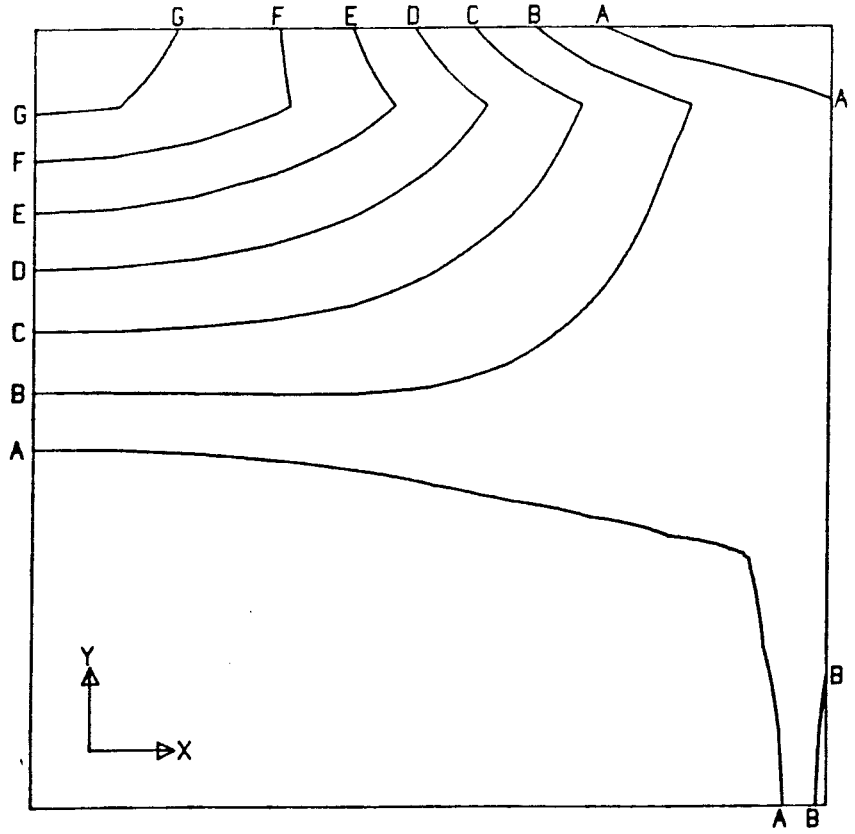

A=-5.4E+06 [Pa]
B=-5.4E+06
C=-5.4E+06
D=-5.4E+06
E=-5.4E+06
F=-5.4E+06
G=-5.4E+06

ELASTIC CSM-BLOCK MODEL WITHOUT FAULTS 1.3 : INITIAL Y-STRESS

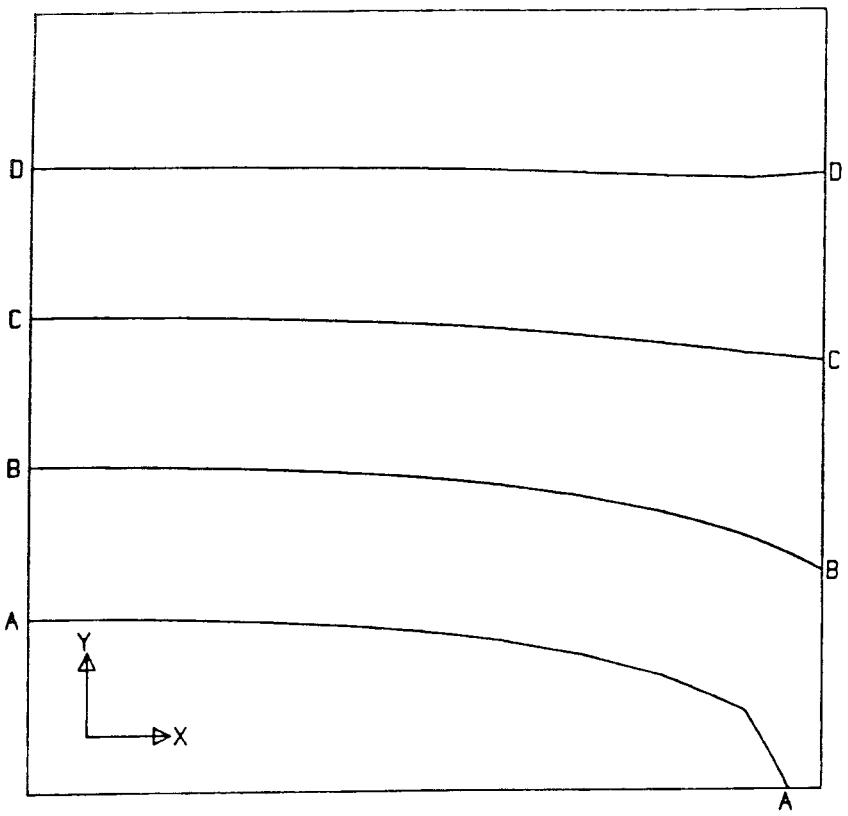

ELASTIC CSM-BLOCK MODEL WITHOUT FAULTS 1.3 : INITIAL SHEAR STRESS

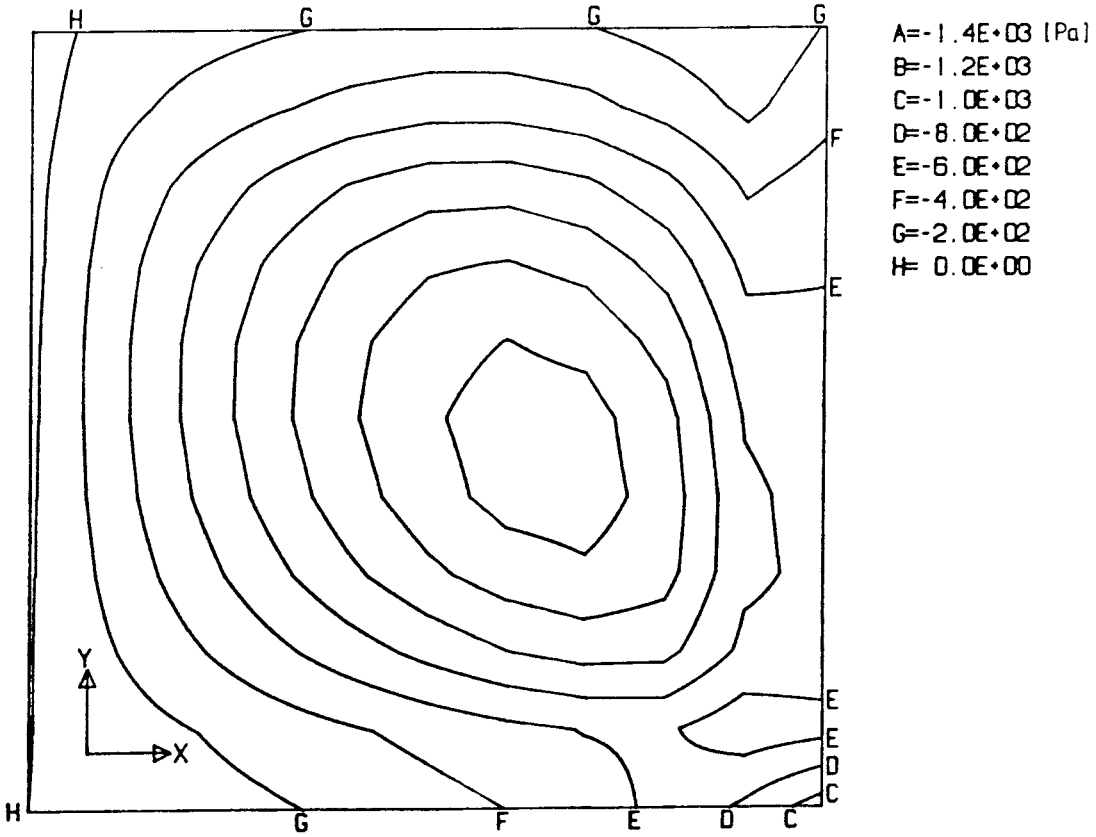

ELASTIC CSM-BLOCK MODEL WITHOUT FAULTS 1.3 : X-DISPLACEMENT

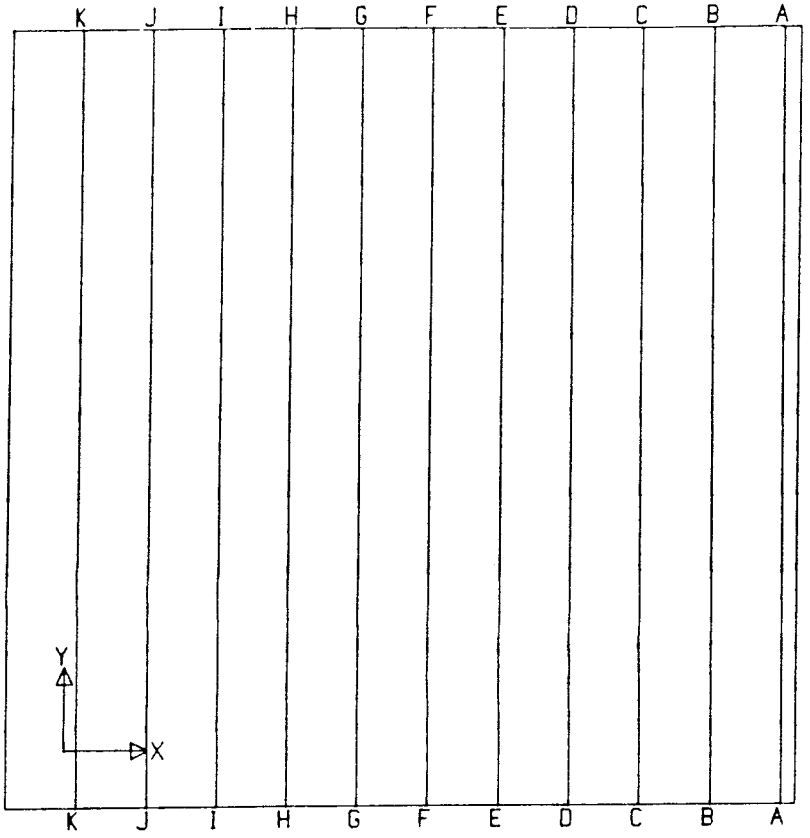

A=-1.1E-04 [m]
B=-1.0E-04
C=-9.0E-05
D=-8.0E-05
E=-7.0E-05
F=-6.0E-05
G=-5.0E-05
H=-4.0E-05
I=-3.0E-05
J=-2.0E-05
K=-1.0E-05
L= 0.0E+00

ELASTIC CSM-BLOCK MODEL WITHOUT FAULTS 1.3 : Y-DISPLACEMENT

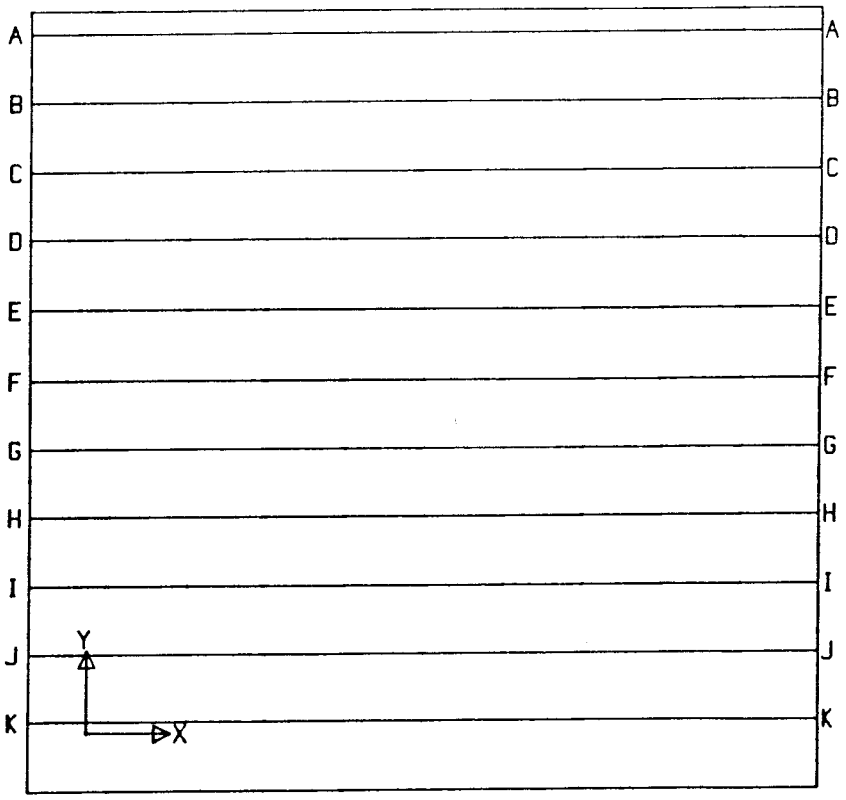

A=-1.1E-04 [m]
B=-1.0E-04
C=-9.0E-05
D=-8.0E-05
E=-7.0E-05
F=-6.0E-05
G=-5.0E-05
H=-4.0E-05
I=-3.0E-05
J=-2.0E-05
K=-1.0E-05
L= 0.0E+00

ELASTIC CSM-BLOCK MODEL WITHOUT FAULTS 1.3 : DISPLACEMENT VECTOR

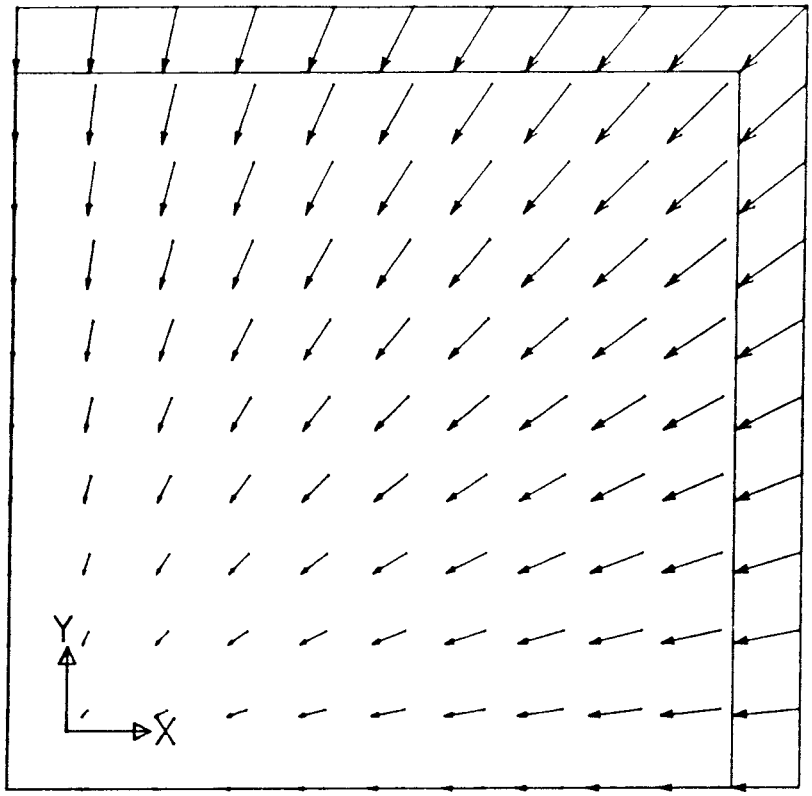

FACTOR
1.0E4

0 0.1 0.2 [mm]

CSM-BLOCK MODEL 2.3 : PRINCIPAL STRESS VECTOR

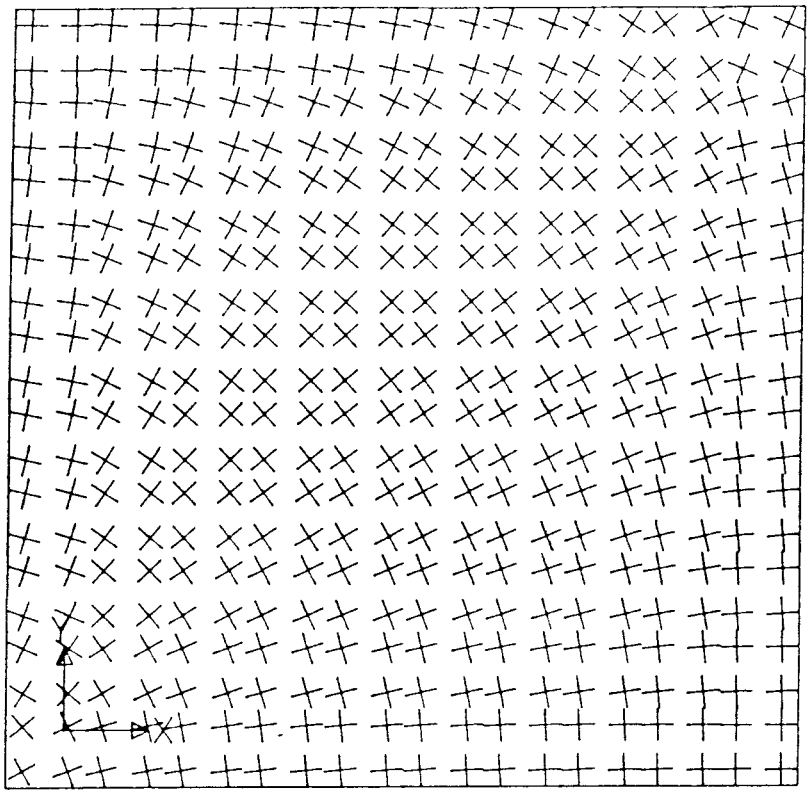

FACTOR
1.0E-7

0 10 [MPa]

CSM-BLOCK MODEL 2.3 : X-STRESS

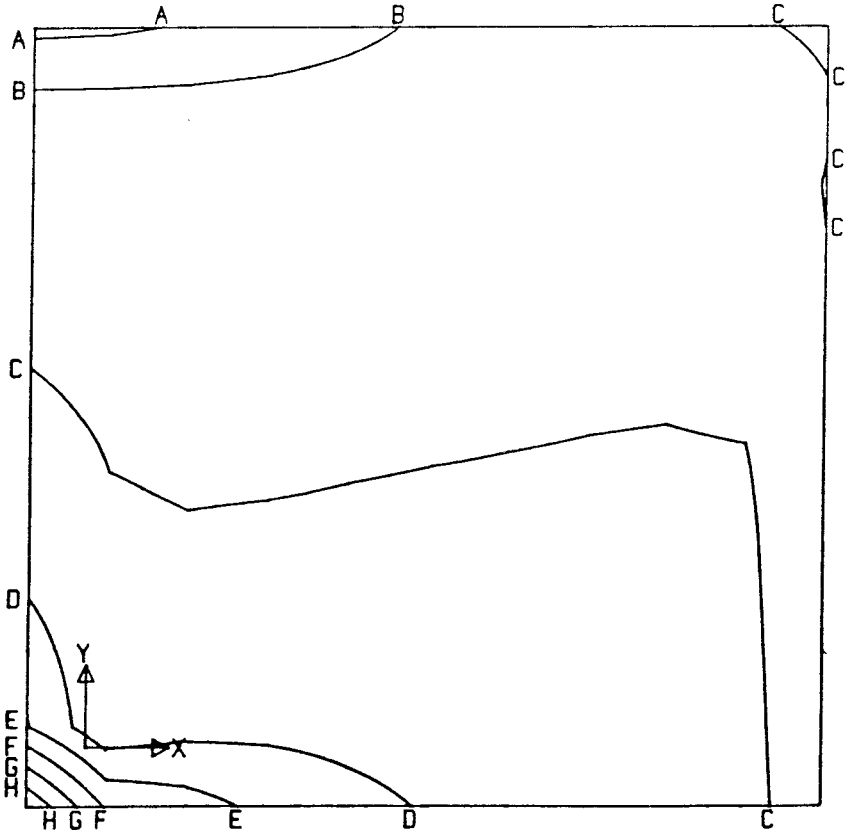

A=-5.6E+06 [Pa]
B=-5.5E+06
C=-5.4E+06
D=-5.3E+06
E=-5.2E+06
F=-5.1E+06
G=-5.0E+06
H=-4.9E+06

CSM-BLOCK MODEL 2.3 : Y-STRESS

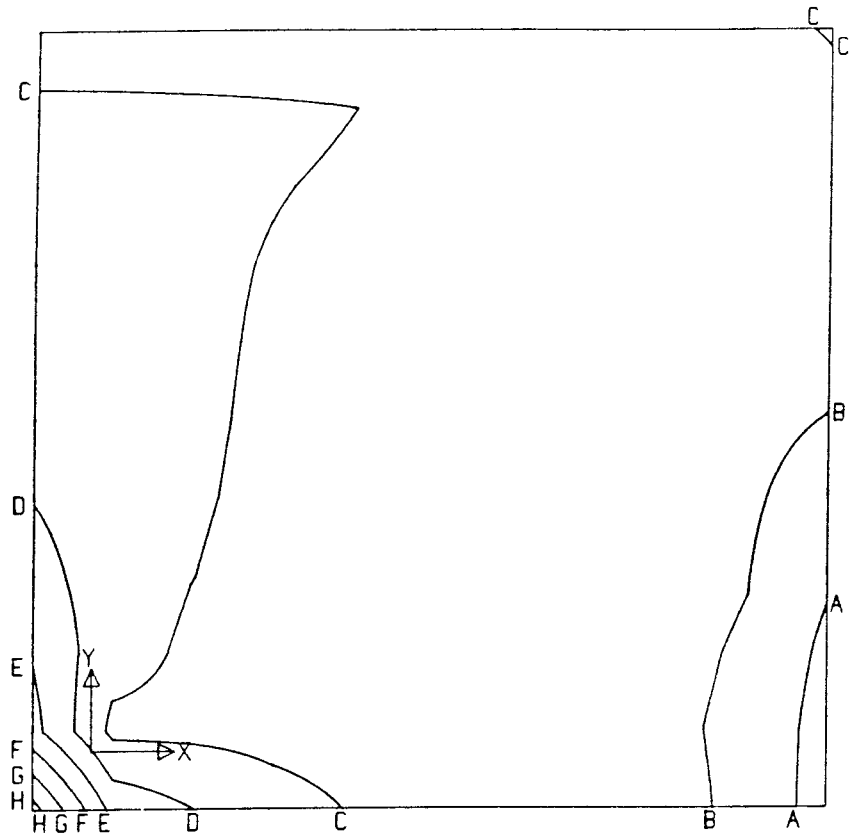

A=-5.6E+06 [Pa]
B=-5.5E+06
C=-5.4E+06
D=-5.3E+06
E=-5.2E+06
F=-5.1E+06
G=-5.0E+06
H=-4.9E+06

CSM-BLOCK MODEL 2.3 : SHEAR STRESS

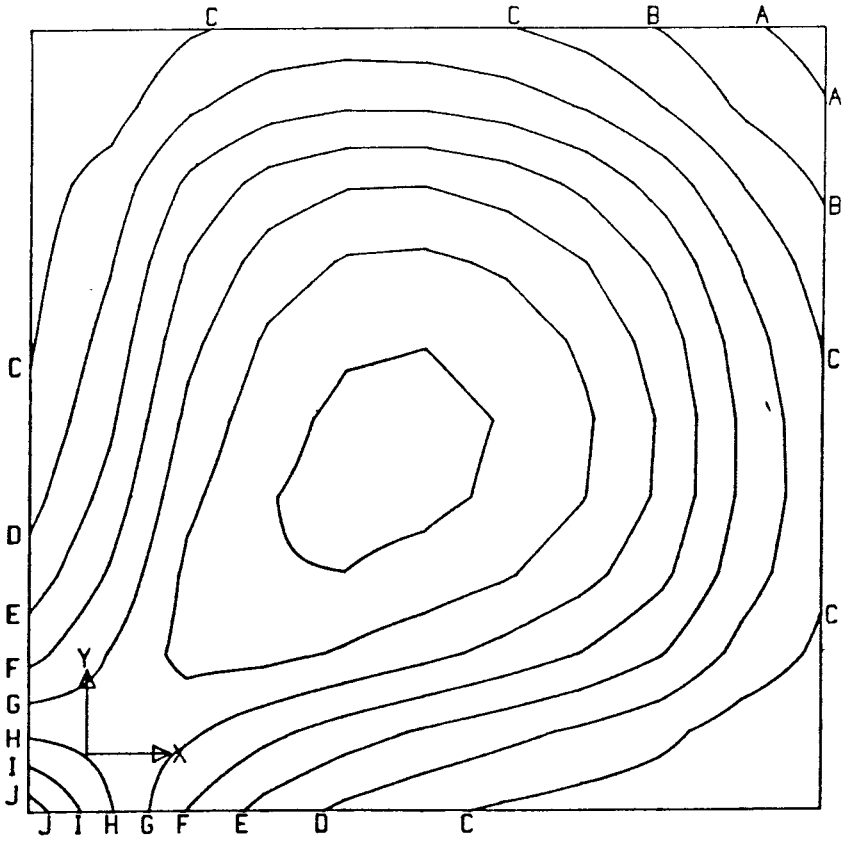

A= 0.0E+00 [Pa]
B= 5.0E+03
C= 1.0E+04
D= 1.5E+04
E= 2.0E+04
F= 2.5E+04
G= 3.0E+04
H= 3.5E+04
I= 4.0E+04
J= 4.5E+04

CSM-BLOCK MODEL 2.3 : X-DISPLACEMENT

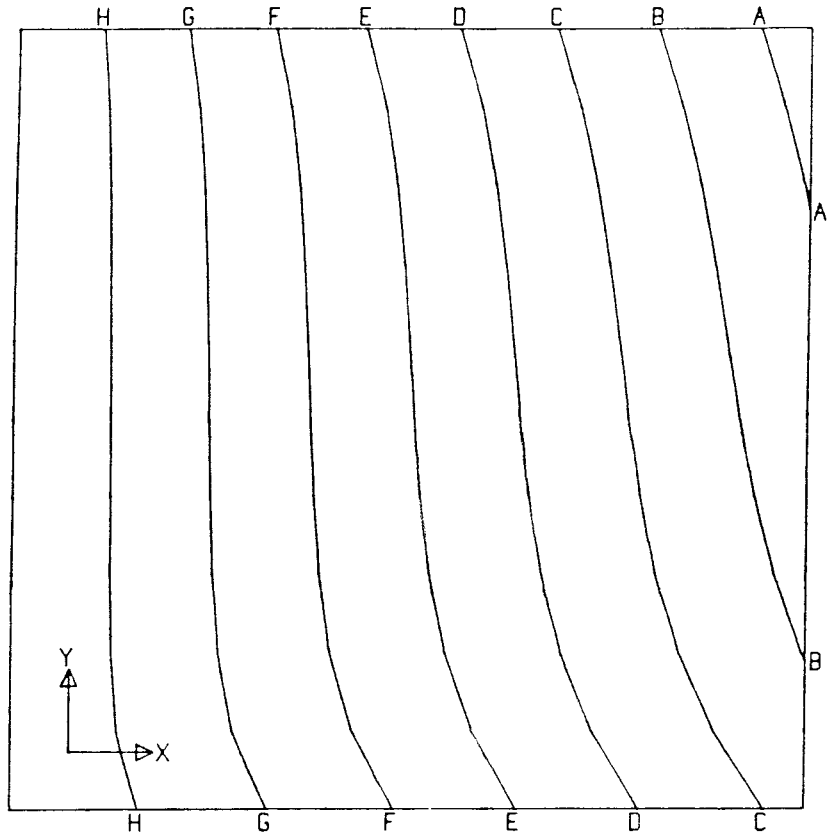

A=-4.0E-04 [m]
B=-3.5E-04
C=-3.0E-04
D=-2.5E-04
E=-2.0E-04
F=-1.5E-04
G=-1.0E-04
H=-5.0E-05
I= 0.0E+00

CSM-BLOCK MODEL 2.3 : Y-DISPLACEMENT

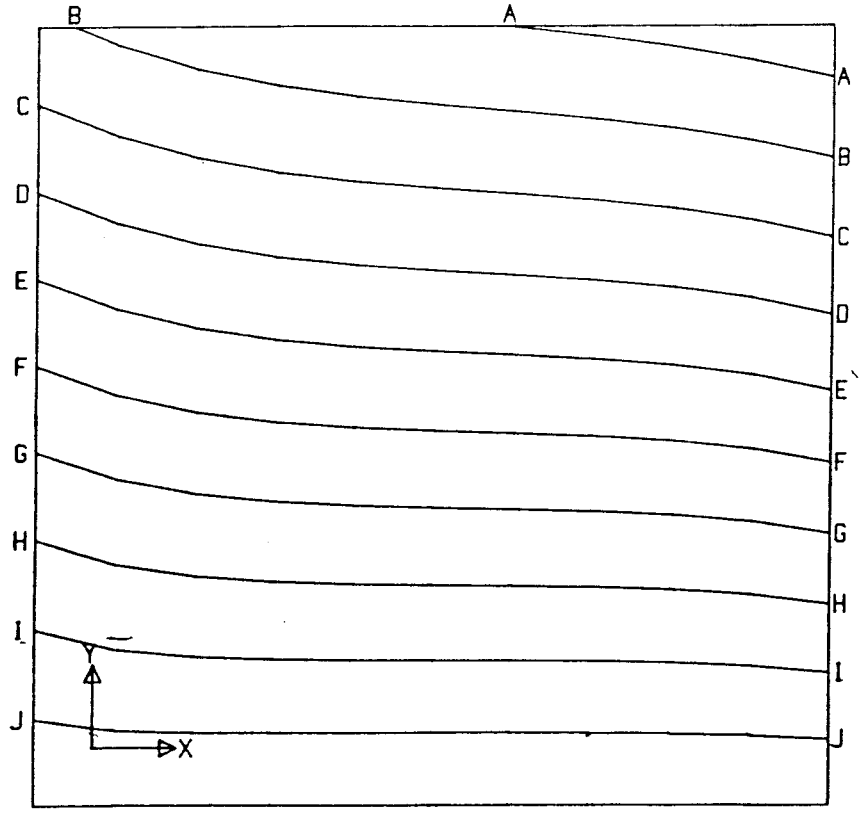

A=-5.0E-04 [m]
B=-4.5E-04
C=-4.0E-04
D=-3.5E-04
E=-3.0E-04
F=-2.5E-04
G=-2.0E-04
H=-1.5E-04
I=-1.0E-04
J=-5.0E-05
K=-1.2E-10

CSM-BLOCK MODEL 2.3 : DISPLACEMENT VECTOR

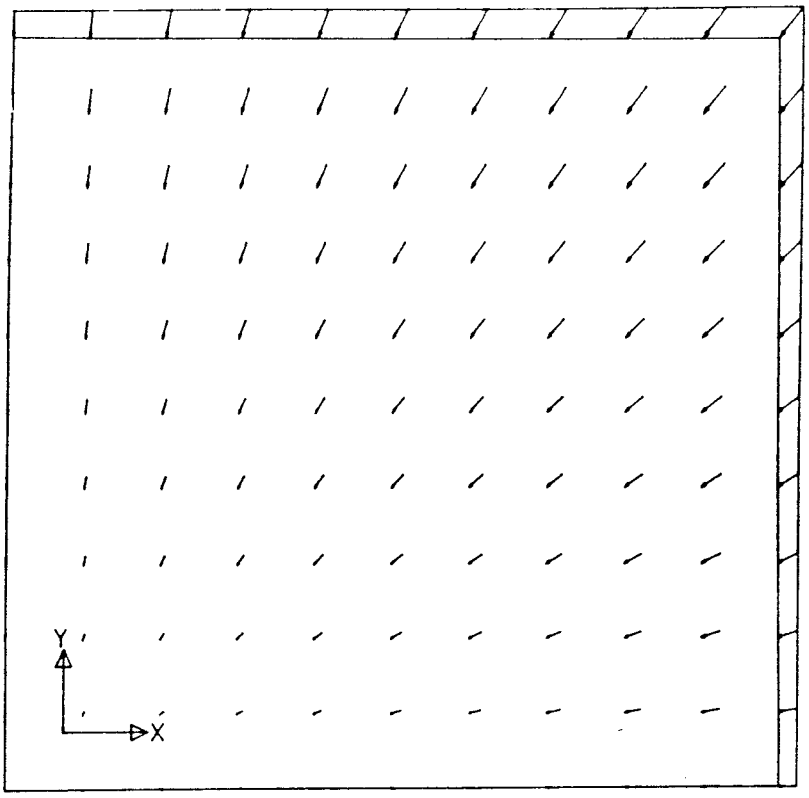

FACTOR

1.0E3

0 1.0 [mm]

CSM-BLOCK MODEL 3.3 : PRINCIPAL STRESS VECTOR

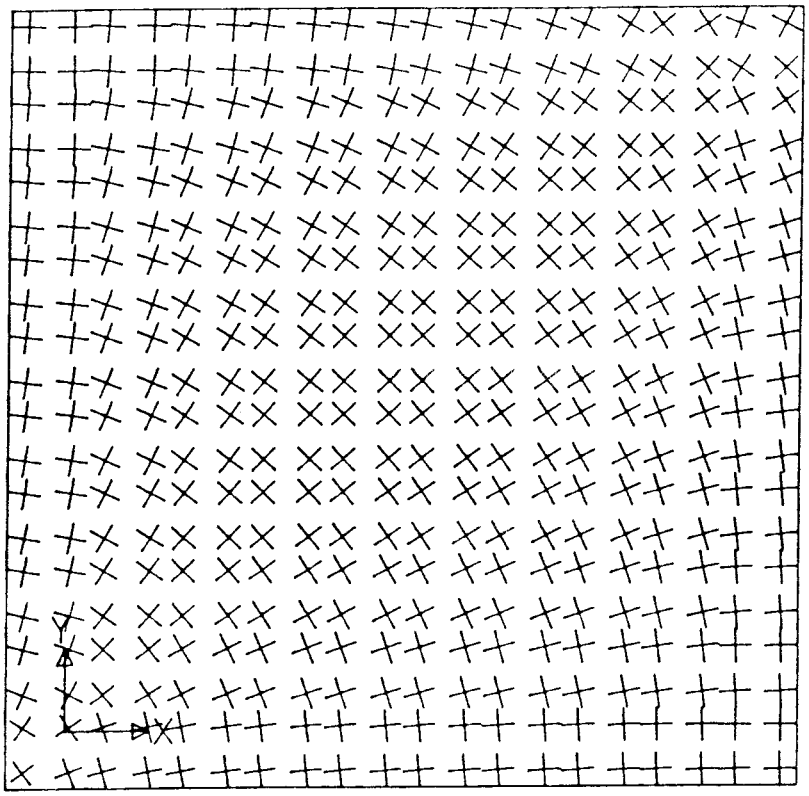

FACTOR
1.0E-7

0 10 [MPa]

CSM-BLOCK MODEL 3.3 : X-STRESS

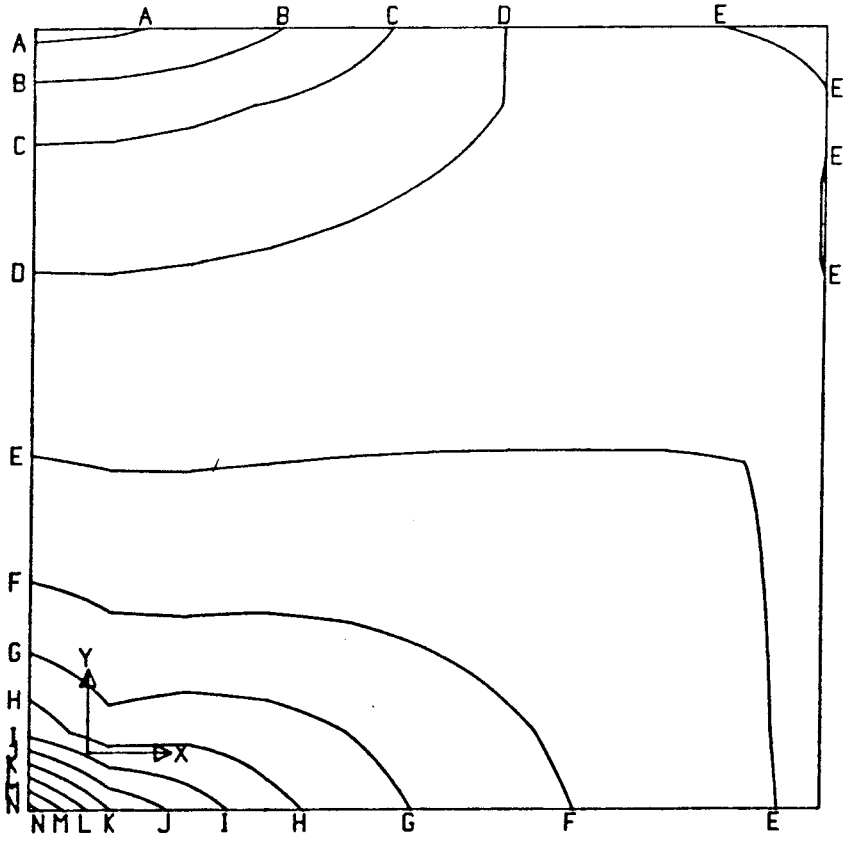

A=-5.8E+06 [Pa]
B=-5.7E+06
C=-5.6E+06
D=-5.5E+06
E=-5.4E+06
F=-5.3E+06
G=-5.2E+06
H=-5.1E+06
I=-5.0E+06
J=-4.9E+06
K=-4.8E+06
L=-4.7E+06
M=-4.6E+06
N=-4.5E+06

CSM-BLOCK MODEL 3.3 : Y-STRESS

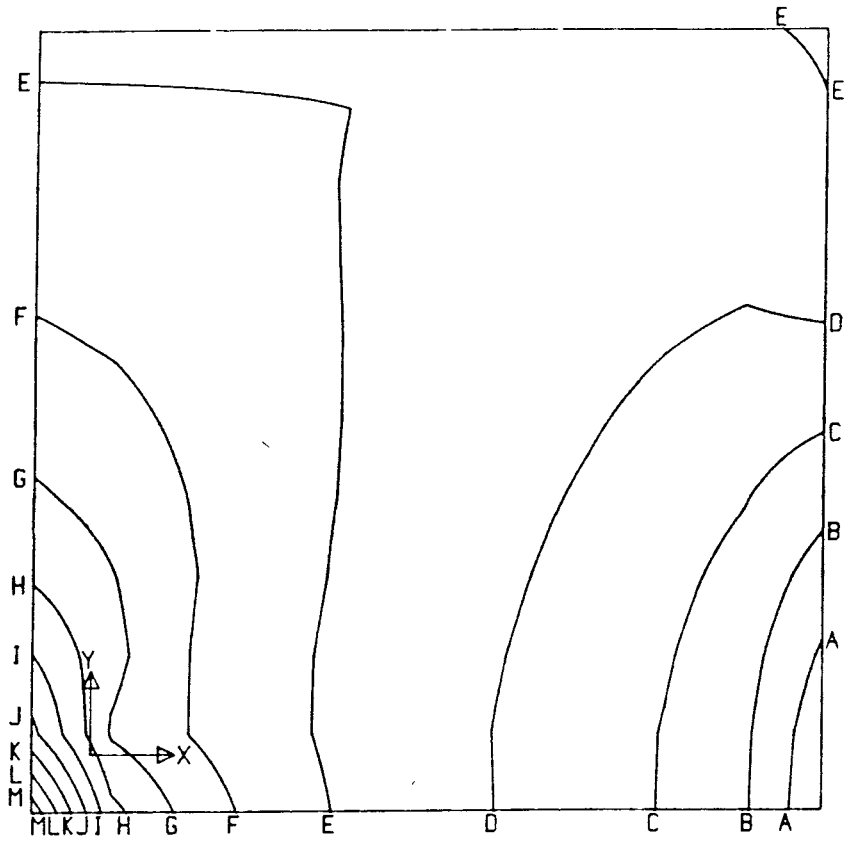

A=-5.8E+06 [Pa]
B=-5.7E+06
C=-5.6E+06
D=-5.5E+06
E=-5.4E+06
F=-5.3E+06
G=-5.2E+06
H=-5.1E+06
I=-5.0E+06
J=-4.9E+06
K=-4.8E+06
L=-4.7E+06
M=-4.6E+06

CSM-BLOCK MODEL 3.3 : SHEAR STRESS

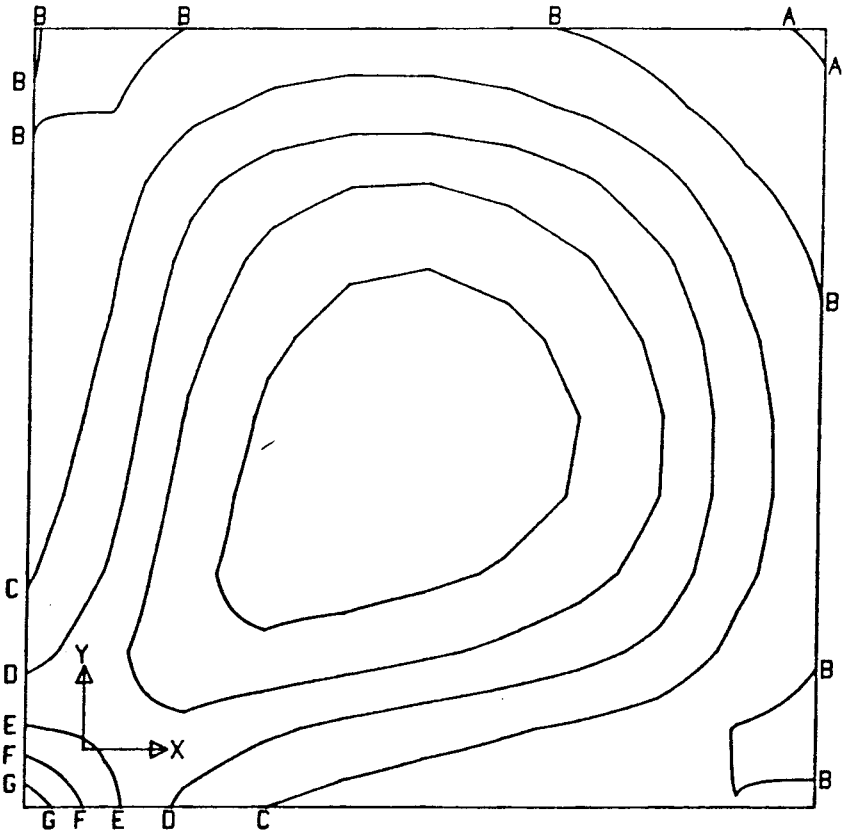

A= 0.0E+00 [Pa]
B= 2.0E+04
C= 4.0E+04
D= 6.0E+04
E= 8.0E+04
F= 1.0E+05
G= 1.2E+05

CSM-BLOCK MODEL 3.3 : X-DISPLACEMENT

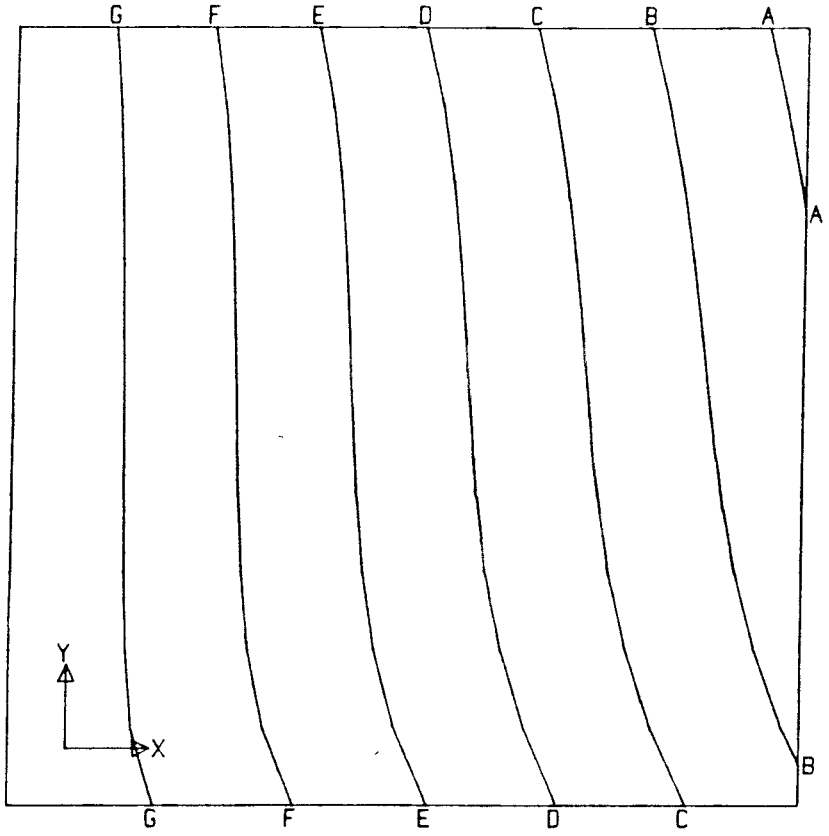

A=-2.8E-04 [m]
B=-2.4E-04
C=-2.0E-04
D=-1.6E-04
E=-1.2E-04
F=-8.0E-05
G=-4.0E-05
H= 0.0E+00

CSM-BLOCK MODEL 3.3 : Y-DISPLACEMENT

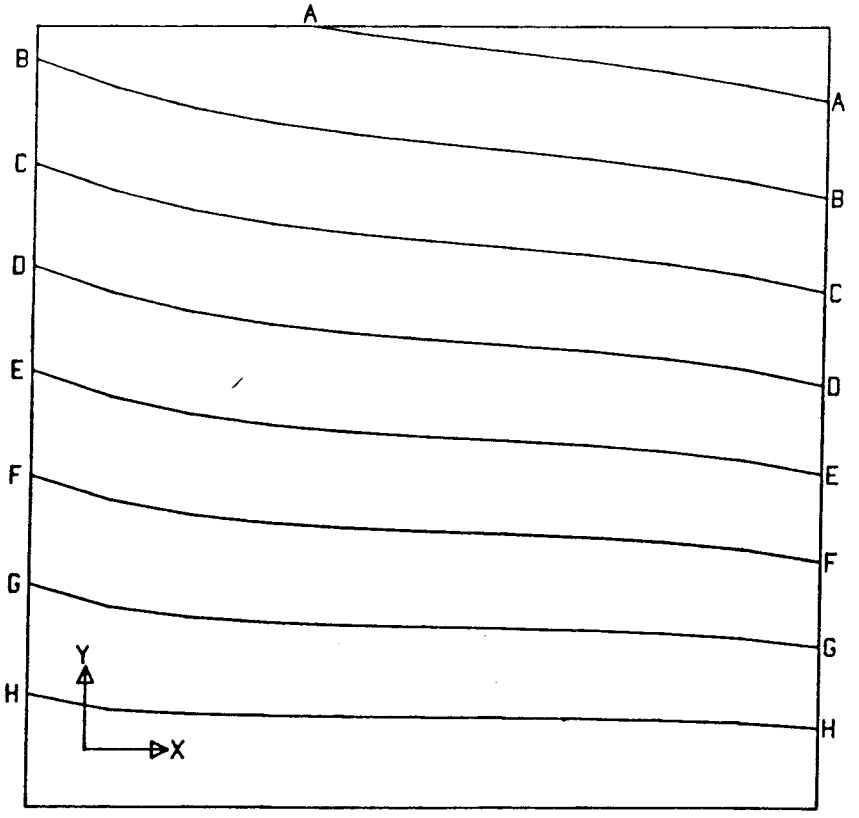

A=-3.2E-04 [m]
B=-2.8E-04
C=-2.4E-04
D=-2.0E-04
E=-1.6E-04
F=-1.2E-04
G=-8.0E-05
H=-4.0E-05
I= 0.0E+00

CSM-BLOCK MODEL 3.3 : DISPLACEMENT VECTOR

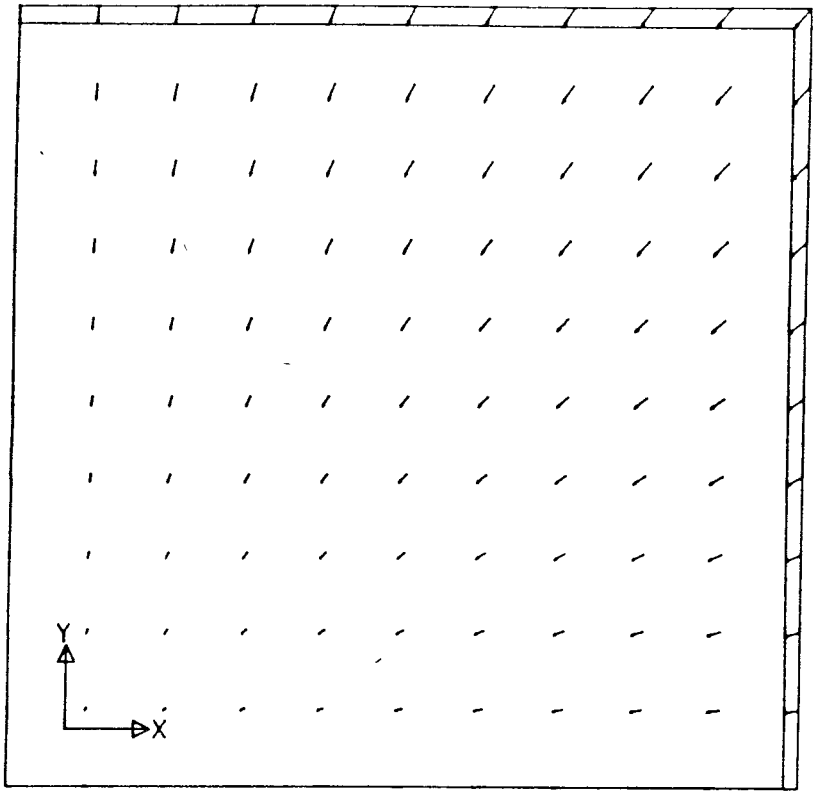

FACTOR
1.0E3

0 1.0 [mm]

CSM-BLOCK MODEL 4.1 : PRINCIPAL STRESS VECTOR

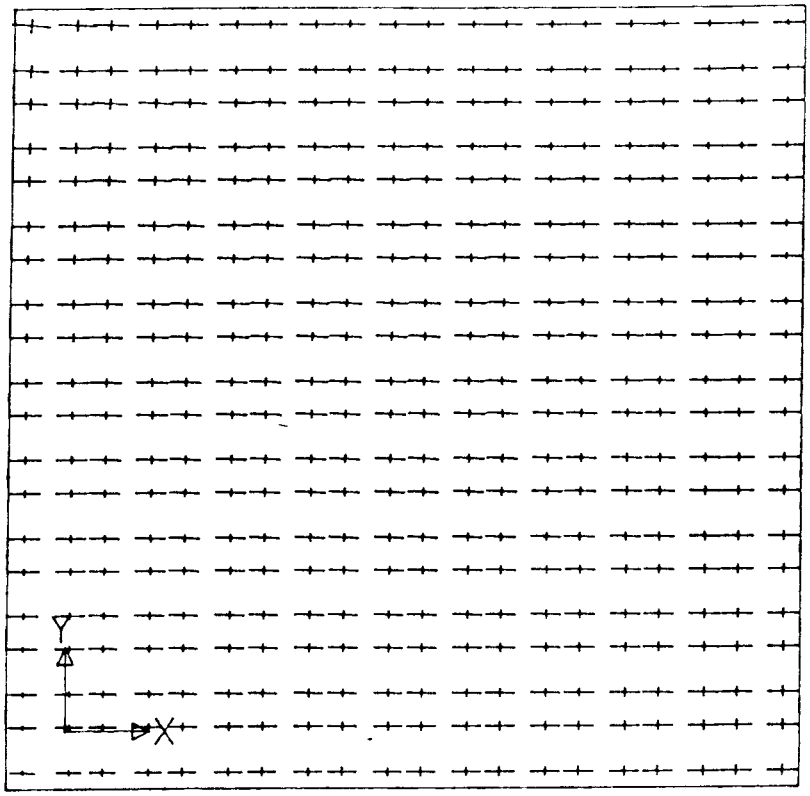

FACTOR
1.0E-7

0 10 [MPa]

CSM-BLOCK MODEL 4.1 : X-STRESS

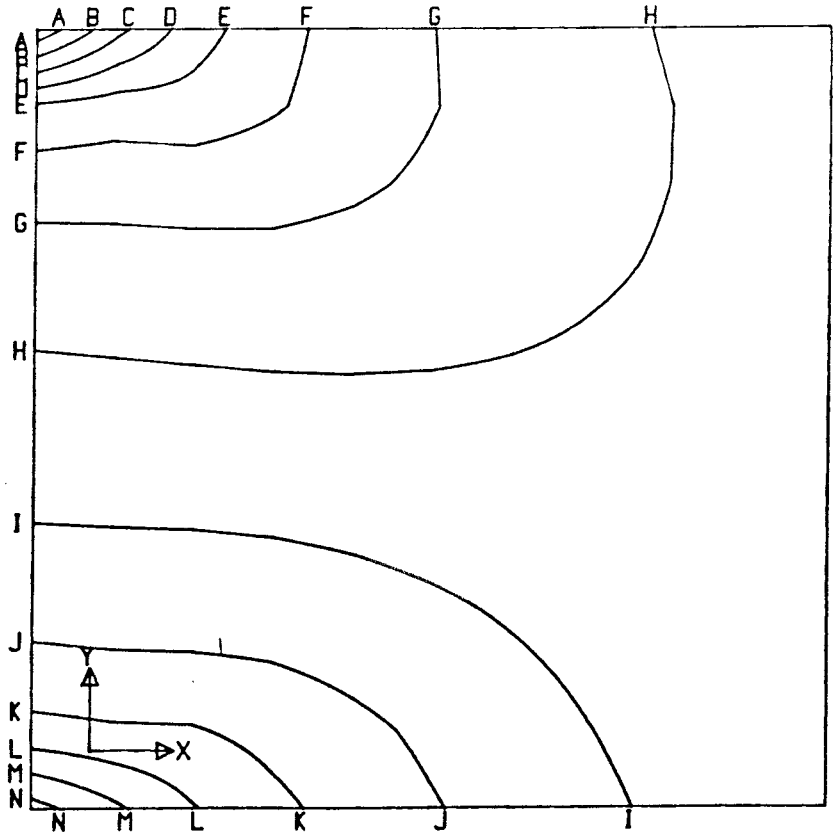

A=-6.6E+06 [Pa]
B=-6.4E+06
C=-6.2E+06
D=-6.0E+06
E=-5.8E+06
F=-5.6E+06
G=-5.4E+06
H=-5.2E+06
I=-5.0E+06
J=-4.8E+06
K=-4.6E+06
L=-4.4E+06
M=-4.2E+06
N=-4.0E+06

CSM-BLOCK MODEL 4.1 : Y-STRESS

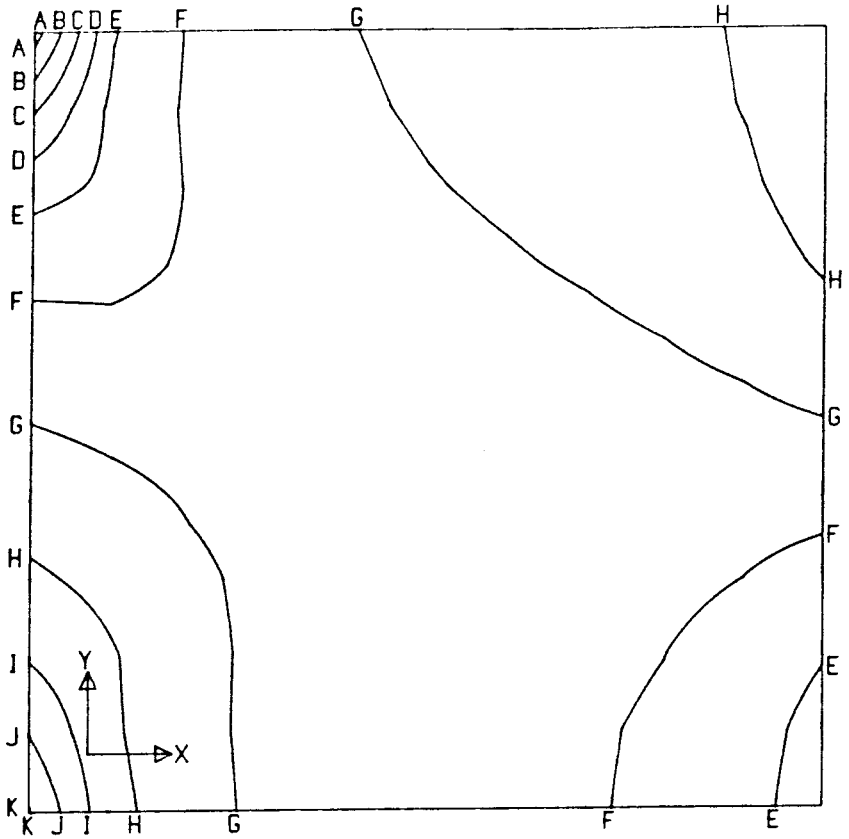

A=-2.4E+06 [Pa]
B=-2.2E+06
C=-2.0E+06
D=-1.8E+06
E=-1.6E+06
F=-1.4E+06
G=-1.2E+06
H=-1.0E+06
I=-8.0E+05
J=-6.0E+05
K=-4.0E+05

CSM-BLOCK MODEL 4.1 : SHEAR STRESS

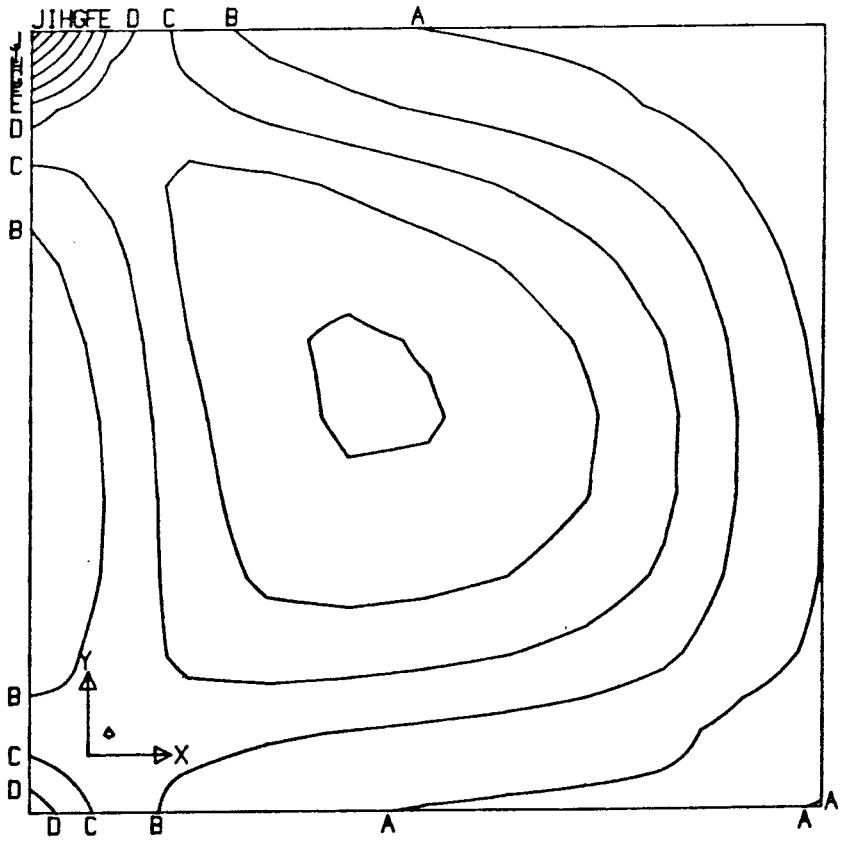

A= 5.0E+04 [Pa]
B= 1.0E+05
C= 1.5E+05
D= 2.0E+05
E= 2.5E+05
F= 3.0E+05
G= 3.5E+05
H= 4.0E+05
I= 4.5E+05
J= 5.0E+05

CSM-BLOCK MODEL 4.1 : X-DISPLACEMENT

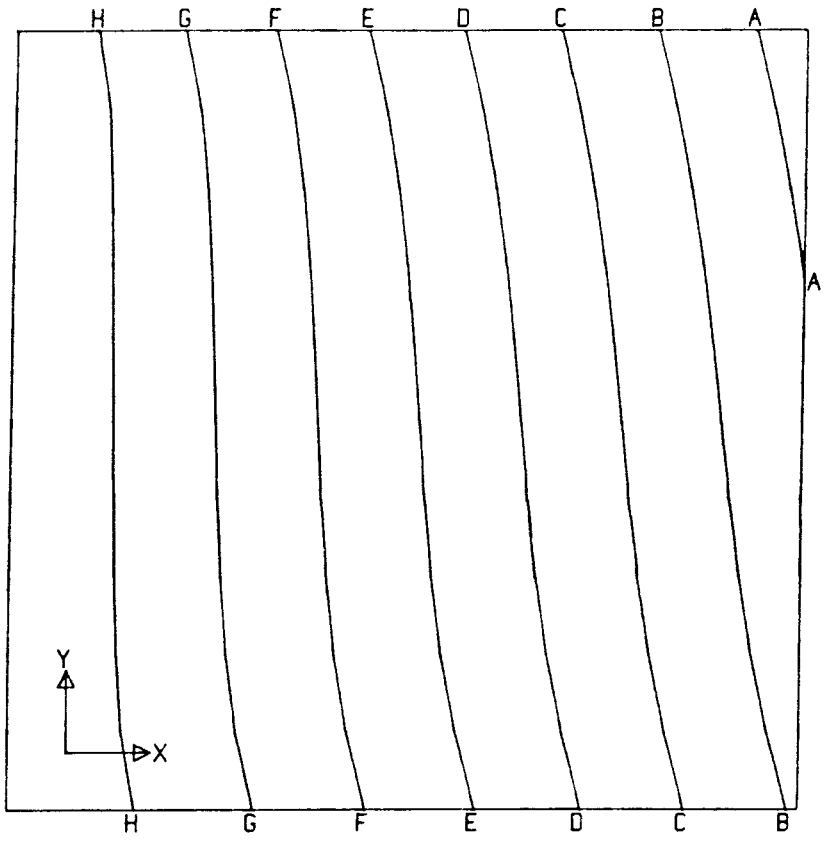

A=-8.0E-04 [m]
B=-7.0E-04
C=-6.0E-04
D=-5.0E-04
E=-4.0E-04
F=-3.0E-04
G=-2.0E-04
H=-1.0E-04
I= 0.0E+00

CSM-BLOCK MODEL 4.1 : Y-DISPLACEMENT

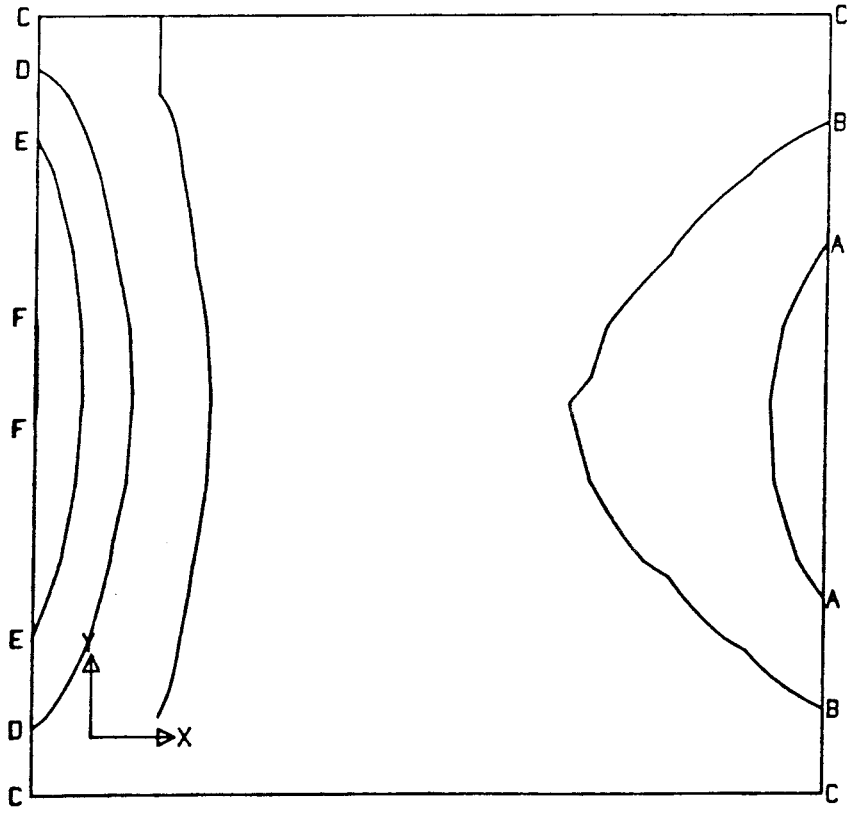

A=-2.0E-05 [m]
B=-1.0E-05
C= 0.0E+00
D= 1.0E-05
E= 2.0E-05
F= 3.0E-05

CSM-BLOCK MODEL 4.1 : DISPLACEMENT VECTOR

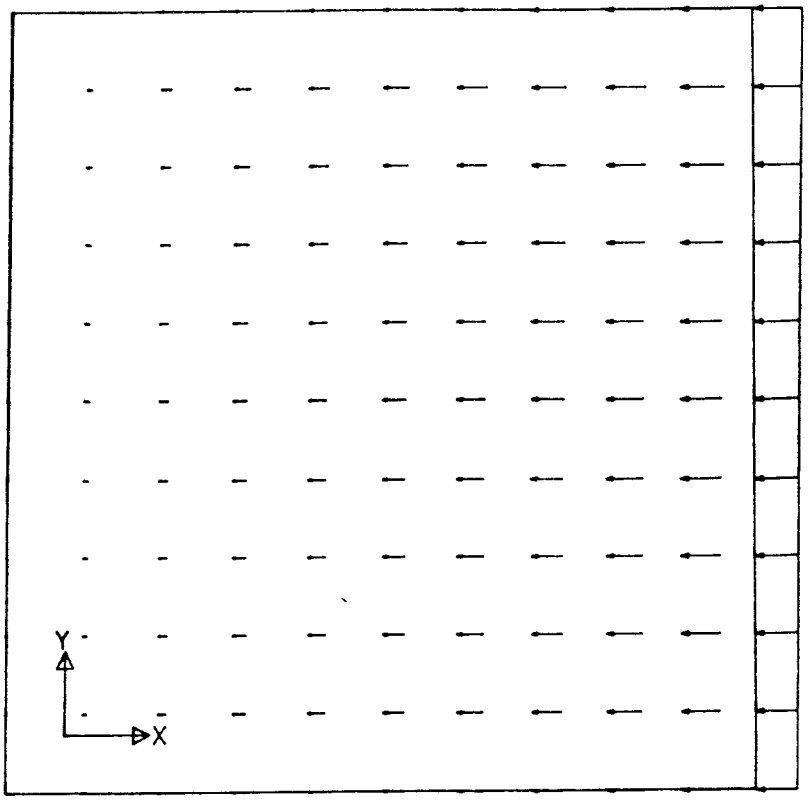

FACTOR

1.0E3

0 1.0 [mm]

CSM-BLOCK MODEL 4.2 : PRINCIPAL STRESS VECTOR

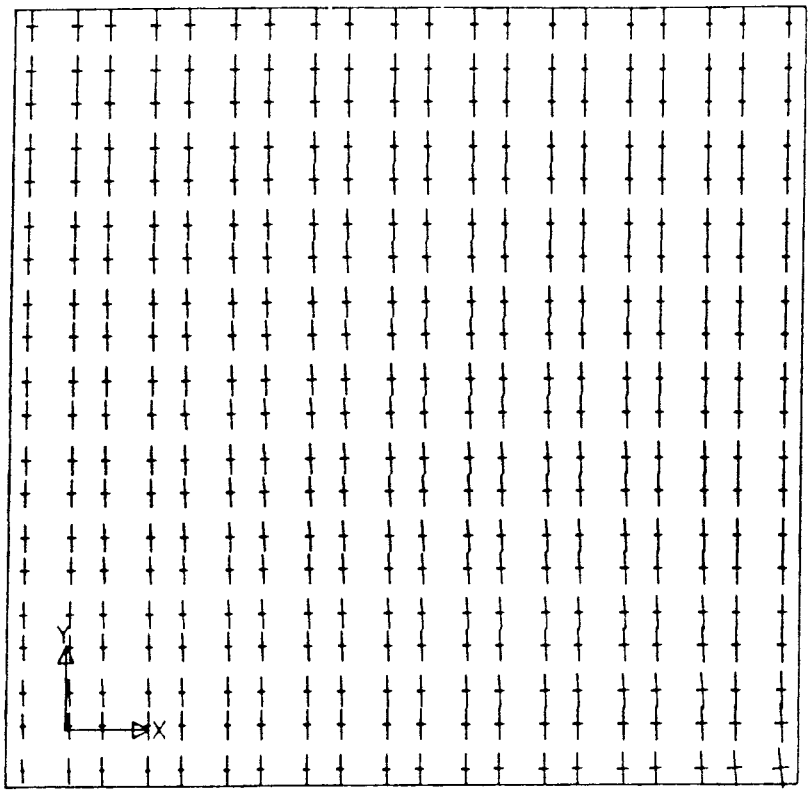

FACTOR
1.0E-7

0 10 [MPa]

CSM-BLOCK MODEL 4.2 : X-STRESS

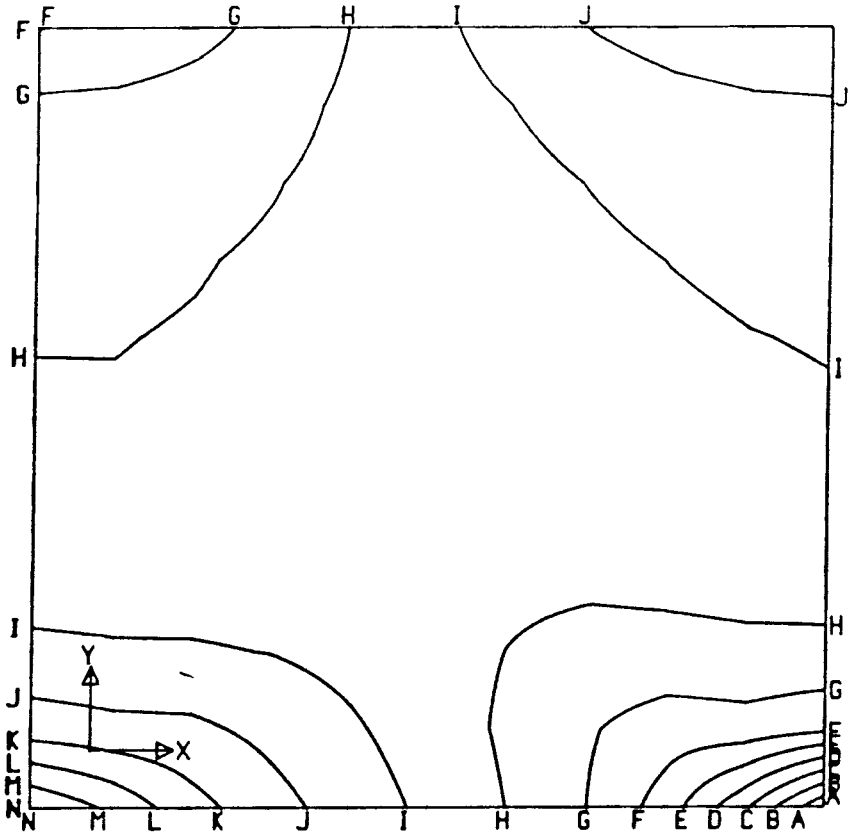

A=-3.0E+06 [Pa]
B=-2.8E+06
C=-2.6E+06
D=-2.4E+06
E=-2.2E+06
F=-2.0E+06
G=-1.8E+06
H=-1.6E+06
I=-1.4E+06
J=-1.2E+06
K=-1.0E+06
L=-8.0E+05
M=-6.0E+05
N=-4.0E+05

CSM-BLOCK MODEL 4.2 : Y-STRESS

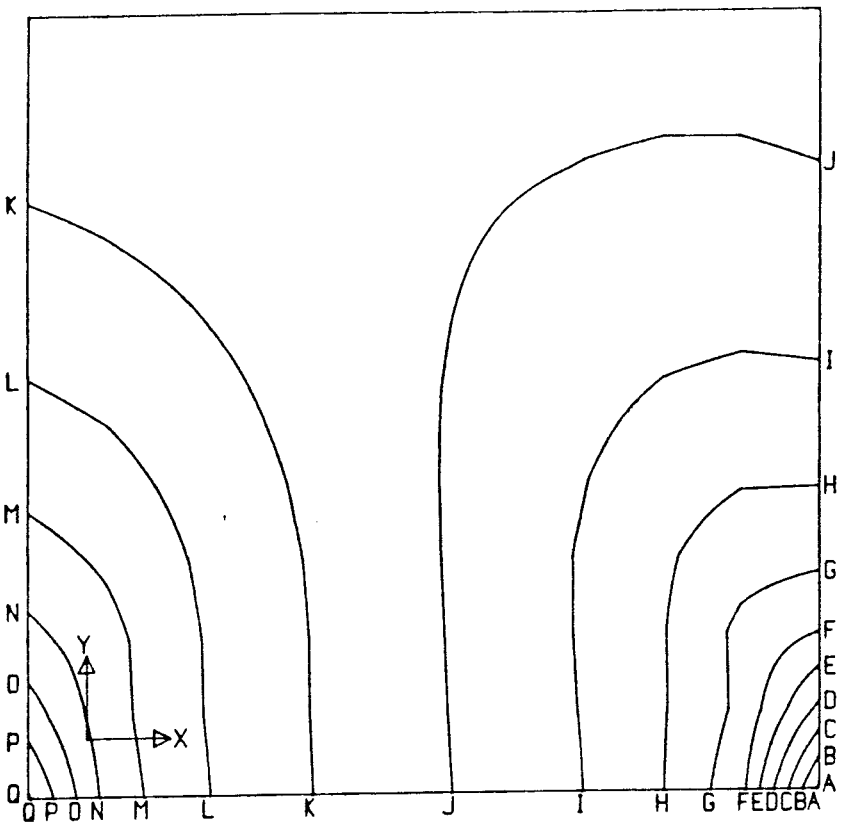

A=-7.0E+06 [Pa]
B=-6.8E+06
C=-6.6E+06
D=-6.4E+06
E=-6.2E+06
F=-6.0E+06
G=-5.8E+06
H=-5.6E+06
I=-5.4E+06
J=-5.2E+06
K=-5.0E+06
L=-4.8E+06
M=-4.6E+06
N=-4.4E+06
O=-4.2E+06
P=-4.0E+06
Q=-3.8E+06

CSM-BLOCK MODEL 4.2 : SHEAR STRESS

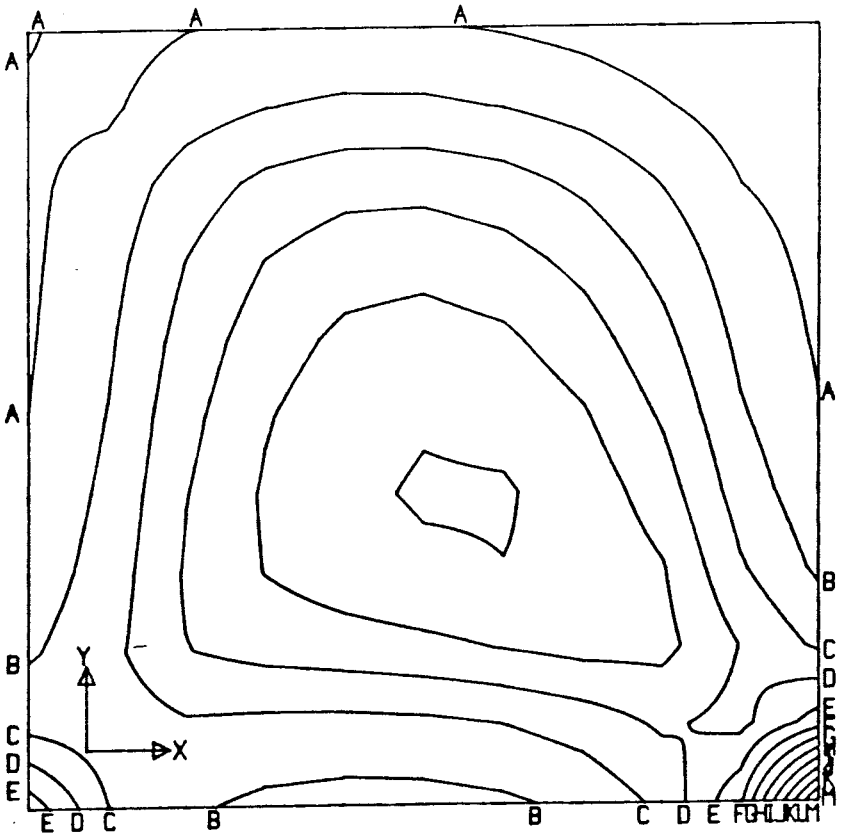

A= 5.0E+04 [Pa]
B= 1.0E+05
C= 1.5E+05
D= 2.0E+05
E= 2.5E+05
F= 3.0E+05
G= 3.5E+05
H= 4.0E+05
I= 4.5E+05
J= 5.0E+05
K= 5.5E+05
L= 6.0E+05
M= 6.5E+05

CSM-BLOCK MODEL 4.2 : Y-DISPLACEMENT

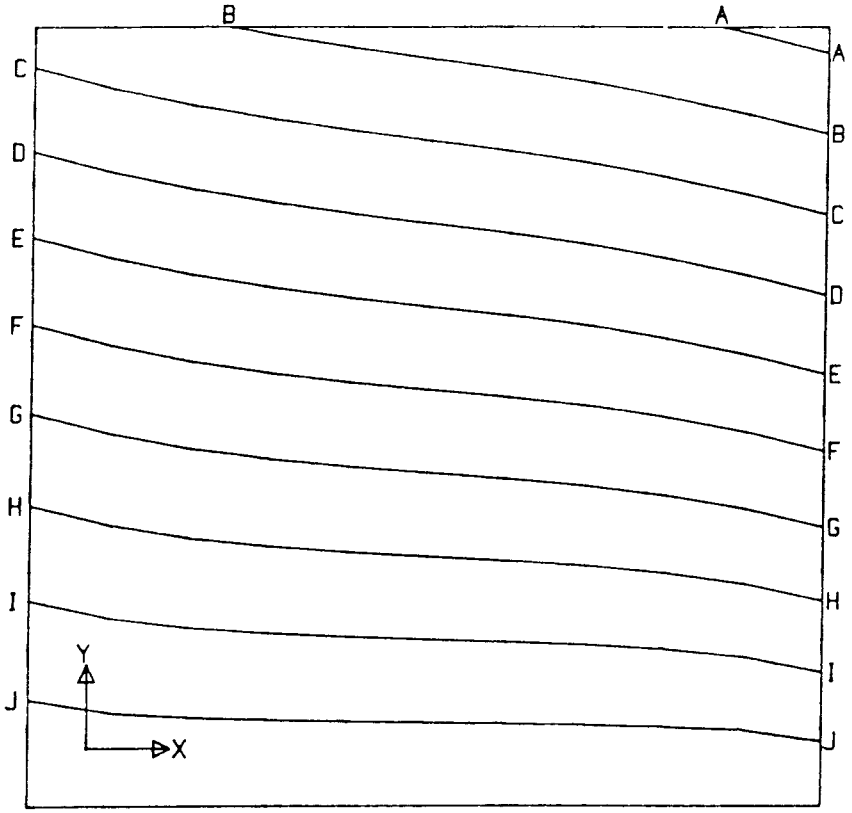

A=-1.0E-03 [m]
B=-9.0E-04
C=-8.0E-04
D=-7.0E-04
E=-6.0E-04
F=-5.0E-04
G=-4.0E-04
H=-3.0E-04
I=-2.0E-04
J=-1.0E-04
K=-2.3E-10

CSM-BLOCK MODEL 4.2 : X-DISPLACEMENT

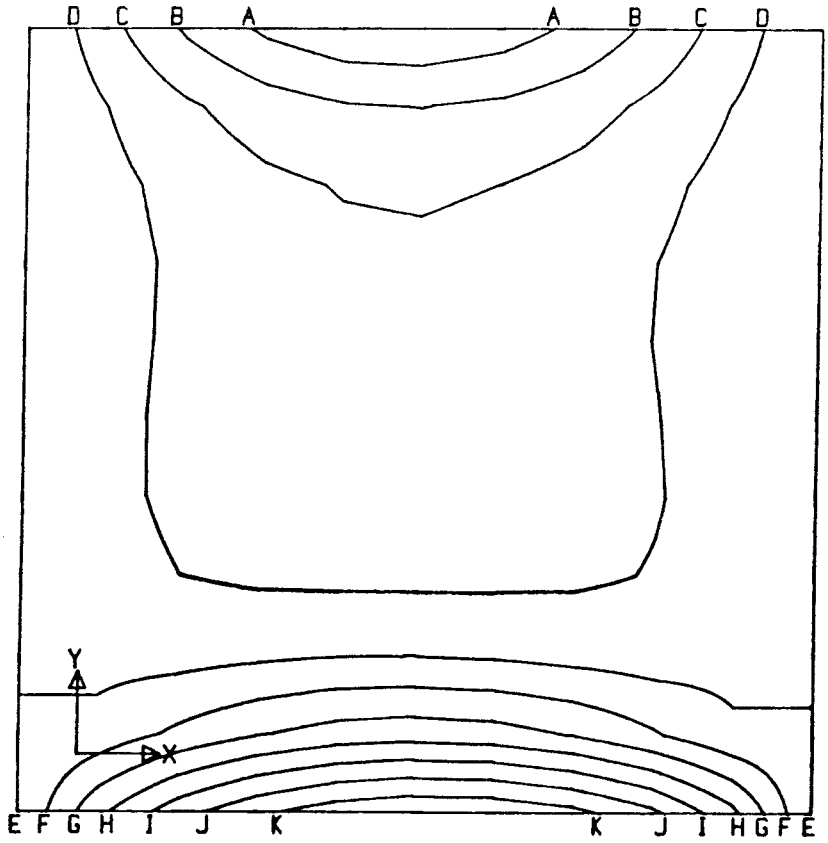

A=-2.0E-05 [m]
B=-1.5E-05
C=-1.0E-05
D=-5.0E-06
E= 0.0E+00
F= 5.0E-06
G= 1.0E-05
H= 1.5E-05
I= 2.0E-05
J= 2.5E-05
K= 3.0E-05

CSM-BLOCK MODEL 4.2 : DISPLACEMENT VECTOR

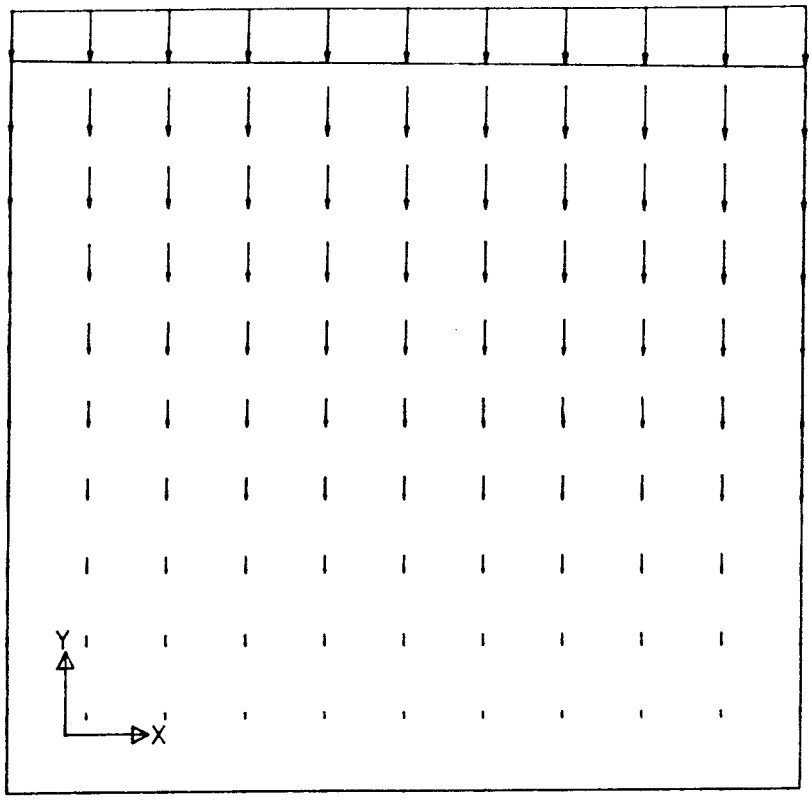

FACTOR

1.0E3

0 1.0 [mm]

CSM-BLOCK MODEL 4.3 : PRINCIPAL STRESS VECTOR

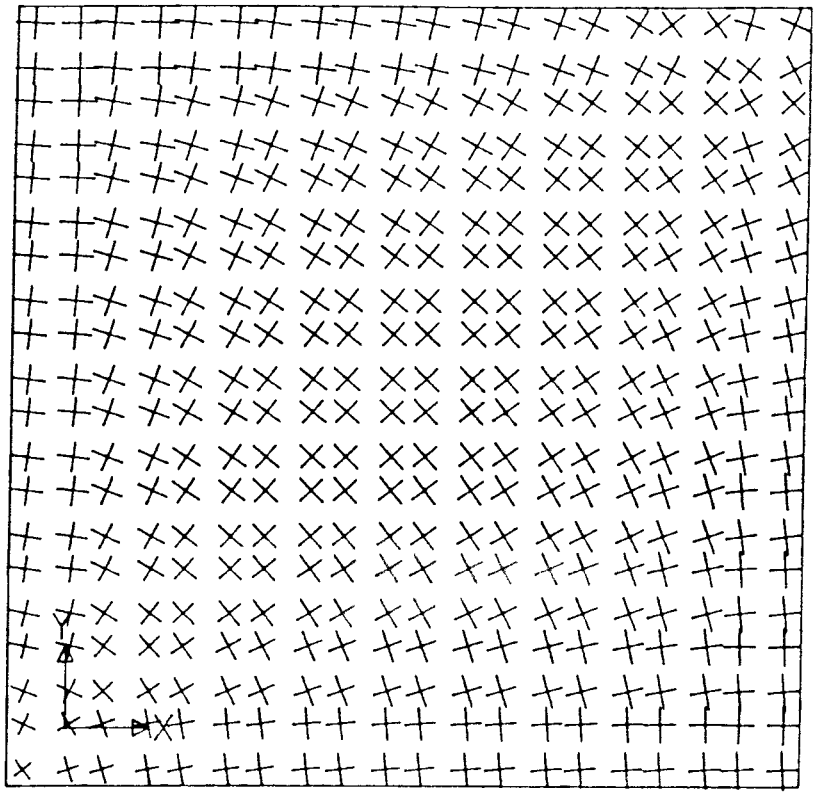

FACTOR
1.0E-7

0 10 [MPa]

CSM-BLOCK MODEL 4.3 : X-STRESS

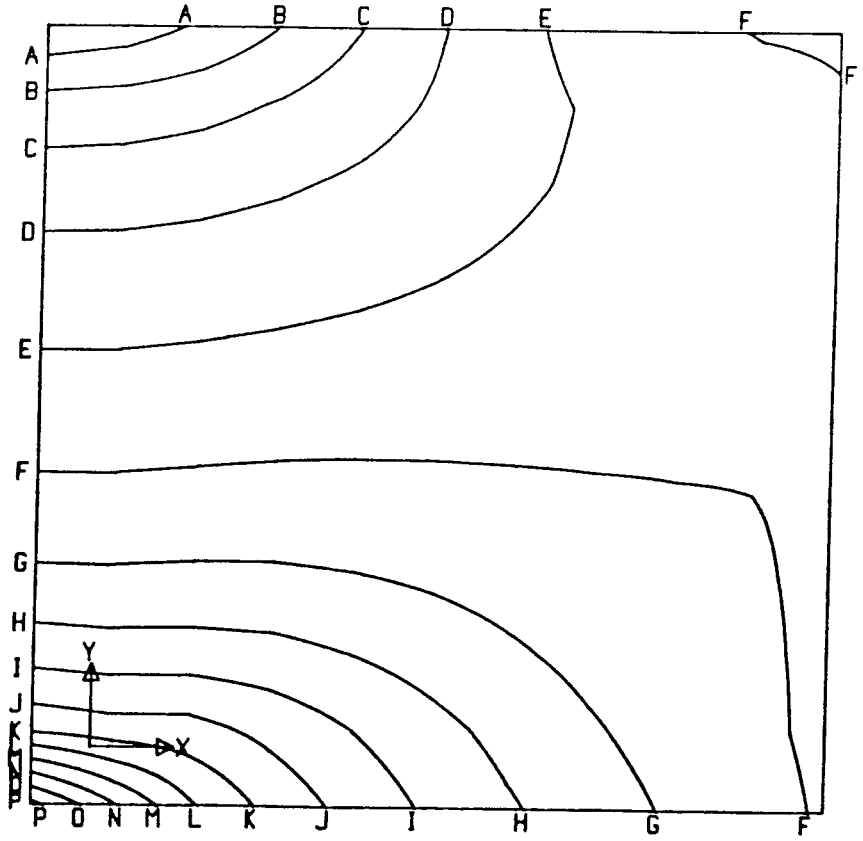

A=-6.4E+06 [Pa]
B=-6.2E+06
C=-6.0E+06
D=-5.8E+06
E=-5.6E+06
F=-5.4E+06
G=-5.2E+06
H=-5.0E+06
I=-4.8E+06
J=-4.6E+06
K=-4.4E+06
L=-4.2E+06
M=-4.0E+06
N=-3.8E+06
O=-3.6E+06
P=-3.4E+06

CSM-BLOCK MODEL 4.3 : Y-STRESS

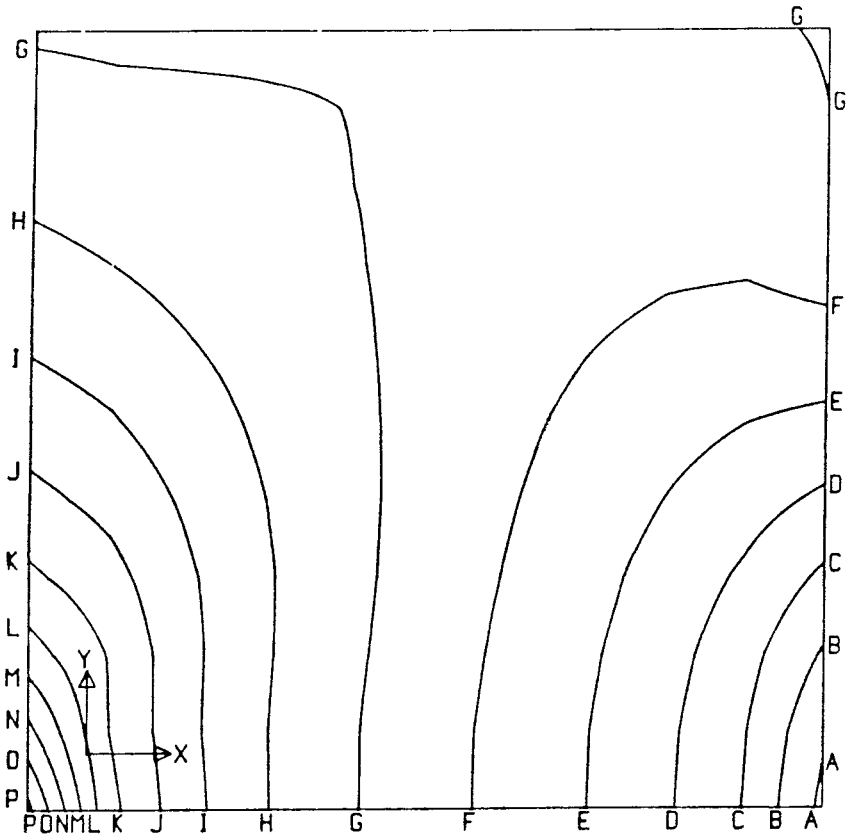

A=-6.6E+06 [Pa]
B=-6.4E+06
C=-6.2E+06
D=-6.0E+06
E=-5.8E+06
F=-5.6E+06
G=-5.4E+06
H=-5.2E+06
I=-5.0E+06
J=-4.8E+06
K=-4.6E+06
L=-4.4E+06
M=-4.2E+06
N=-4.0E+06
O=-3.8E+06
P=-3.6E+06

CSM-BLOCK MODEL 4.3 : SHEAR STRESS

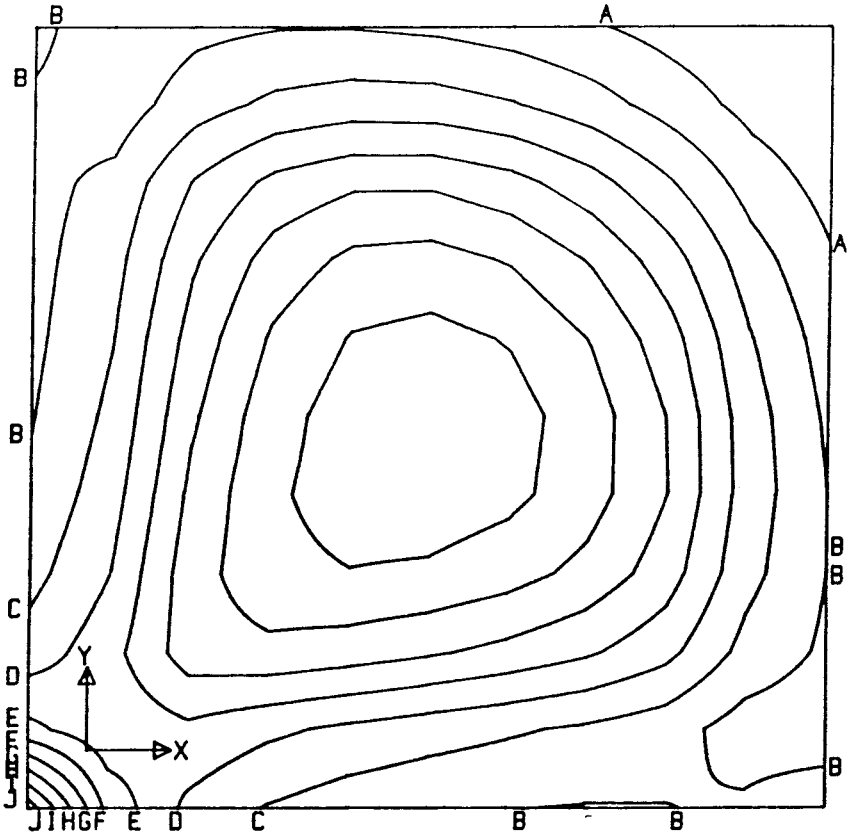

A= 4.0E+04 [Pa]
B= 8.0E+04
C= 1.2E+05
D= 1.6E+05
E= 2.0E+05
F= 2.4E+05
G= 2.8E+05
H= 3.2E+05
I= 3.6E+05
J= 4.0E+05

CSM-BLOCK MODEL 4.3 : X-DISPLACEMENT

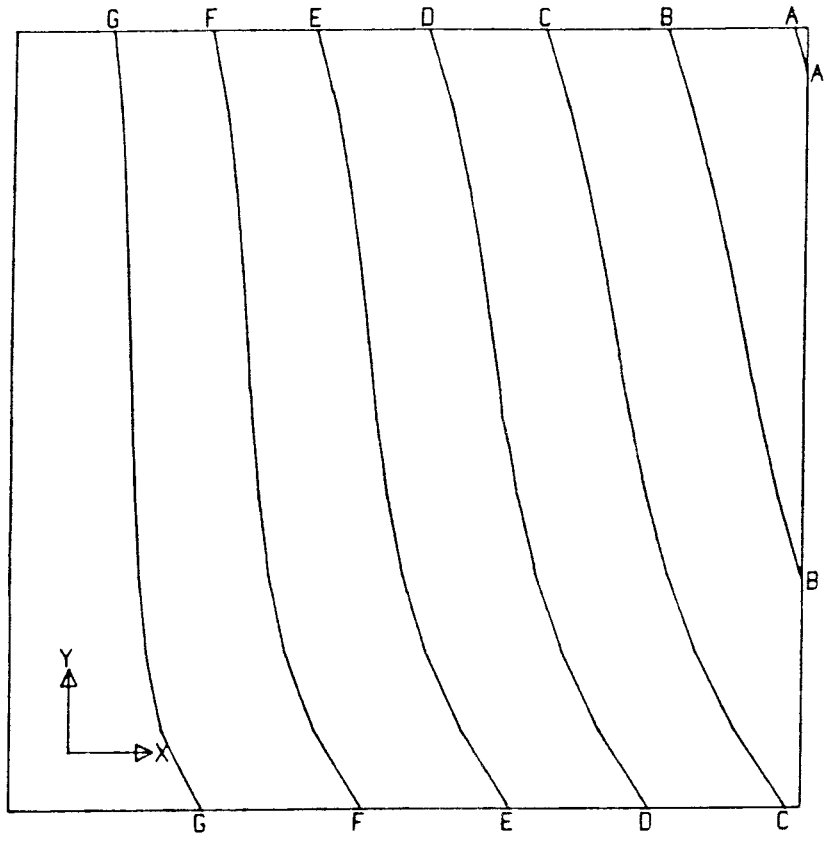

A=-7.0E-04 [m]
B=-6.0E-04
C=-5.0E-04
D=-4.0E-04
E=-3.0E-04
F=-2.0E-04
G=-1.0E-04
H= 0.0E+00

CSM-BLOCK MODEL 4.3 : Y-DISPLACEMENT

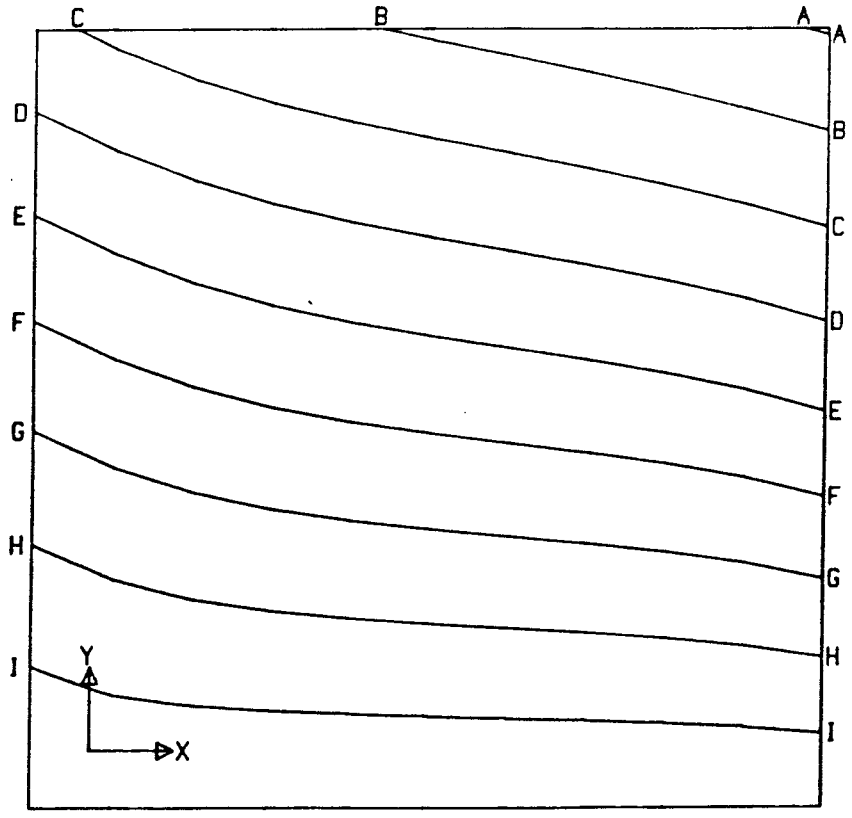

A=-9.0E-04 [m]
B=-8.0E-04
C=-7.0E-04
D=-6.0E-04
E=-5.0E-04
F=-4.0E-04
G=-3.0E-04
H=-2.0E-04
I=-1.0E-04
J= 0.0E+00

CSM-BLOCK MODEL 4.3 ; DISPLACEMENT VECTOR

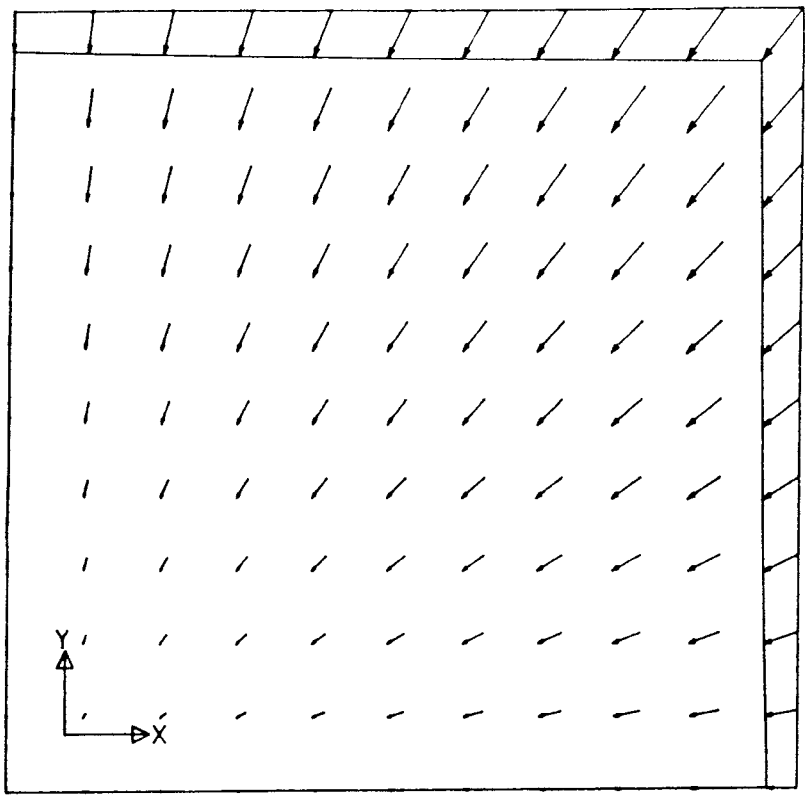

FACTOR

1.0E3

0 1.0 [mm]

List of SKB reports

Annual Reports

1977–78
TR 121
KBS Technical Reports 1 – 120.
Summaries. Stockholm, May 1979.

1979
TR 79–28
The KBS Annual Report 1979.
KBS Technical Reports 79-01 – 79-27.
Summaries. Stockholm, March 1980.

1980
TR 80–26
The KBS Annual Report 1980.
KBS Technical Reports 80-01 – 80-25.
Summaries. Stockholm, March 1981.

1981
TR 81–17
The KBS Annual Report 1981.
KBS Technical Reports 81-01 – 81-16.
Summaries. Stockholm, April 1982.

1982
TR 82–28
The KBS Annual Report 1982.
KBS Technical Reports 82-01 – 82-27.
Summaries. Stockholm, July 1983.

1983
TR 83–77
The KBS Annual Report 1983.
KBS Technical Reports 83-01 – 83-76
Summaries. Stockholm, June 1984.

1984
TR 85–01
Annual Research and Development Report 1984
Including Summaries of Technical Reports Issued during 1984. (Technical Reports 84-01–84-19)
Stockholm June 1985.

1985
TR 85-20
Annual Research and Development Report 1985
Including Summaries of Technical Reports Issued during 1985. (Technical Reports 85-01-85-19)
Stockholm May 1986.

1986
TR 86-31
SKB Annual Report 1986
Including Summaries of Technical Reports Issued during 1986
Stockholm, May 1987

1987
TR 87-33
SKB Annual Report 1987
Including Summaries of Technical Reports Issued during 1987
Stockholm, May 1988

Technical Reports

1988

TR 88-01
Preliminary investigations of deep ground water microbiology in Swedish granitic rocks
Karsten Pedersen
University of Göteborg
December 1987

TR 88-02
Migration of the fission products strontium, technetium, iodine, cesium and the actinides neptunium, plutonium, americium in granitic rock
Thomas Ittner[1], Börje Torstenfelt[1], Bert Allard[2]
[1]Chalmers University of Technology
[2]University of Linköping
January 1988

TR 88-03
Flow and solute transport in a single fracture. A two-dimensional statistical model
Luis Moreno[1], Yvonne Tsang[2], Chin Fu Tsang[2], Ivars Neretnieks[1]
[1]Royal Institute of Technology, Stockholm, Sweden
[2]Lawrence Berkeley Laboratory, Berkeley, CA, USA
January 1988

TR 88-04
Ion binding by humic and fulvic acids: A computational procedure based on functional site heterogeneity and the physical chemistry of polyelectrolyte solutions
J A Marinsky, M M Reddy, J Ephraim, A Mathuthu
US Geological Survey, Lakewood, CA, USA
Linköping University, Linköping
State University of New York at Buffalo, Buffalo, NY, USA
April 1987

TR 88-05
Description of geophysical data on the SKB database GEOTAB
Stefan Sehlstedt
Swedish Geological Co, Luleå
February 1988

TR 88-06
Description of geological data in SKBs database GEOTAB
Tomas Stark
Swedish Geological Co, Luleå
April 1988

TR 88-07
Tectonic studies in the Lansjärv region
Herbert Henkel
Swedish Geological Survey, Uppsala
October 1987

TR 88-08
Diffusion in the matrix of granitic rock. Field test in the Stripa mine. Final report.
Lars Birgersson, Ivars Neretnieks
Royal Institute of Technology, Stockholm
April 1988

TR 88-09
The kinetics of pitting corrosion of carbon steel. Progress report to June 1987
G P Marsh, K J Taylor, Z Sooi
Materials Development Division
Harwell Laboratory
February 1988

TR 88-10
GWHRT – A flow model for coupled groundwater and heat flow
Version 1.0
Roger Thunvik[1], Carol Braester[2]
[1] Royal Institute of Technology, Stockholm
[2] Israel Institute of Technology, Haifa
April 1988

TR 88-11
Groundwater numerical modelling of the Fjällveden study site – Evaluation of parameter variations
A hydrocoin study – Level 3, case 5A
Nils-Åke Larsson[1], Anders Markström[2]
[1] Swedish Geological Company, Uppsala
[2] Kemakta Consultants Co, Stockholm
October 1987

TR 88-12
Near-distance seismological monitoring of the Lansjärv neotectonic fault region
Rutger Wahlström, Sven-Olof Linder,
Conny Holmqvist
Seismological Depertment, Uppsala University,
Uppsala
May 1988